



# PACIFIC EARTHQUAKE ENGINEERING RESEARCH CENTER

## **Test Applications of Advanced Seismic Assessment Guidelines**

**Joe Maffei**

**Karl Telleen**

**Danya Mohr**

**William Holmes**

Rutherford & Chekene, San Francisco

**Yuki Nakayama**

Kajima Corporation, Tokyo

PEER Lifelines Program Task 508

# **Test Applications of Advanced Seismic Assessment Guidelines**

**Joe Maffei  
Karl Telleen  
Danya Mohr  
William Holmes**

Rutherford & Chekene, San Francisco

**and**

**Yuki Nakayama**  
Kajima Corporation, Tokyo

PEER Lifelines Program Task 508

PEER Report 2005/09  
Pacific Earthquake Engineering Research Center  
College of Engineering  
University of California, Berkeley  
August 2006

## ABSTRACT

*Advanced Seismic Assessment Guidelines*, applicable to utility buildings, were developed by Stanford University (Bazzurro et al. 2004) as part of the PEER Lifelines Program, Building Vulnerability Studies (Project Task Number 507). The subject project, Task 508, applies these state-of-the-art guidelines in a detailed fashion to two example buildings, each with differing features and functions within the electric and gas utility network.

The first building studied is a three-story steel moment-frame building. The second building is an older type of utility structure of composite concrete and steel (mill building) construction. Rutherford & Chekene has also used the *Guidelines* to evaluate five additional buildings for Pacific Gas & Electric.

The objectives of the test applications are the following:

- Identify potential difficulties that Structural Engineers would encounter in using the procedures described in the *Advanced Seismic Assessment Guidelines*.
- Recommend possible revisions to the procedure to address any identified difficulties.
- Identify and make recommendations on other issues related to assessing the seismic reliability of utility structures and systems.

The conclusions of this report summarize the applicability of the *Advanced Seismic Assessment Guidelines*, key assumptions in implementation, and specific recommendations for engineers applying the *Guidelines*.

## ACKNOWLEDGMENTS

This project was sponsored by the Pacific Earthquake Engineering Research Center's Program of Applied Earthquake Engineering Research of Lifeline Systems supported by the California Energy Commission, the California Department of Transportation, and the Pacific Gas and Electric Company.

This work made use of the Earthquake Engineering Research Centers Shared Facilities supported by the National Science Foundation under award number EEC-9701568 through the Pacific Earthquake Engineering Research (PEER) Center. Any opinions, findings, and conclusions or recommendations expressed in this material are those of the author(s) and do not necessarily reflect those of the National Science Foundation.

This report was prepared as a result of work sponsored by the California Energy Commission ("the Commission"). It does not necessarily represent the views of the Commission, its employees, or the State of California. The Commission, the State of California, its employees, contractors, and subcontractors make no warranty, express or implied, and assume no legal liability for the information in this report; nor does any party represent that the use of this information will not infringe upon privately owned rights. This report has not been approved or disapproved by the Commission nor has the Commission passed upon the accuracy or adequacy of the information in this report.

Rutherford & Chekene gratefully acknowledges Kent Ferré of PG&E who provided valuable input regarding the practical applicability of the Advanced Seismic Assessment Guidelines, including selecting appropriate buildings for study. Rutherford & Chekene also appreciates the close collaboration with Dr. Paolo Bazzurro, Professor Allin Cornell, and Dr. Nico Luco, who were principal authors of the Guidelines. We are grateful to Professor Graham Powell for discussions with him on the modeling of shear-governed concrete walls, covered in Chapter 5. We gratefully acknowledge the Kajima Corporation, who provided a two-year overseas study fellowship to Mr. Yuki Nakayama, which allowed him to participate in this and other projects at Rutherford & Chekene.

# CONTENTS

<b>ABSTRACT</b> .....	<b>iii</b>
<b>ACKNOWLEDGMENTS</b> .....	<b>iv</b>
<b>TABLE OF CONTENTS</b> .....	<b>v</b>
<b>LIST OF FIGURES</b> .....	<b>ix</b>
<b>LIST OF TABLES</b> .....	<b>xv</b>
<b>NOMENCLATURE</b> .....	<b>xvii</b>
<b>1 INTRODUCTION</b> .....	<b>1</b>
1.1 Background .....	1
1.2 Objectives.....	2
1.3 Scope .....	2
1.4 Outline of the Report.....	3
<b>2 TEST APPLICATION 1: STEEL MOMENT-FRAME BUILDING</b> .....	<b>5</b>
2.1 Description of the Structure .....	5
2.2 Seismic Evaluation of the Intact Structure.....	8
2.2.1 Computer Analysis Model .....	9
2.2.2 Nonlinear Components .....	9
2.2.3 Analysis Results.....	11
2.3 Seismic Evaluation of the Damaged Structure.....	11
2.4 Inferred Dynamic Behavior (SPO2IDA) .....	17
2.5 Post-Earthquake Tagging Limit States .....	24
2.5 Fragility Curves.....	26
2.7 Summary of Steps .....	27
<b>3 STUDY OF ANALYSIS ASSUMPTIONS FOR TEST APPLICATION 1</b> .....	<b>31</b>
3.1 Variation of Assumptions for the Intact Structure .....	31
3.1.1 Foundation Modeling.....	32
3.1.2 Inclusion of Gravity Frame .....	32
3.1.3 Vertical Distribution Pattern of Seismic Forces.....	32
3.2 Variation in Assumptions for the Damaged Structure .....	34
3.2.1 Post-Fracture Plateau Strength.....	35

3.2.2	Effective Residual Drift .....	35
<b>4</b>	<b>TEST APPLICATION 2: MILL BUILDING.....</b>	<b>39</b>
4.1	Description of the Structure .....	39
4.1.1	Steel Framing .....	40
4.1.2	Foundation .....	41
4.1.3	Roof.....	41
4.1.4	Walls .....	41
4.1.5	Connections between Concrete and Steel Elements .....	42
4.1.6	1996 Seismic Retrofit.....	42
4.2	Seismic Evaluation of the Intact Structure.....	45
4.2.1	SAP 2000 Nonlinear Static Analysis Using Sequential Elastic Analyses .....	46
4.2.2	RAM Perform Nonlinear Static Analysis .....	50
4.3	Seismic Evaluation of the Damaged Structure.....	55
4.4	Inferred Dynamic Behavior (SPO2IDA) .....	60
4.5	Post-Earthquake Tagging Limit States .....	65
4.6	Fragility Curves.....	69
<b>5</b>	<b>STUDY OF THE FINITE ELEMENT MODELING ASSUMPTIONS FOR TEST APPLICATION 2 .....</b>	<b>71</b>
5.1	Attempted Calibration of Finite Element Model .....	71
5.1.1	Test Specimen .....	71
5.1.2	Computer Analysis Model .....	72
5.1.3	Results and Recommendations .....	72
<b>6</b>	<b>OTHER APPLICATIONS OF THE GUIDELINES .....</b>	<b>79</b>
6.1	Eight-Story Steel Moment-Frame Building .....	79
6.1.1	Building Description .....	80
6.1.2	Computer Analysis Model .....	81
6.1.3	Incremental Dynamic Analysis .....	84
6.1.4	Results .....	84
6.1.5	Comparison of IDA and SPO2IDA .....	85
6.2	One-Story Mill Building with Two-Story Rear Portion .....	90
6.3	Three-Story Pier-and-Spandrel Building with Concrete Frame.....	92

6.4	One-Story Plus Basement and Mezzanine Concrete and Steel Building.....	94
6.5	One-Story Mill Building with Flat Roof and Skylights.....	96
<b>7</b>	<b>KEY TECHNICAL ISSUES .....</b>	<b>99</b>
7.1	Residual Drift.....	99
7.1.1	Estimating Residual Drift.....	100
7.1.2	Residual Drift Findings from the Evaluation of an Eight-Story Steel Moment Frame .....	102
7.1.3	Effect of Residual Drift on Seismic Performance.....	104
7.2	Tagging Criteria .....	107
<b>8</b>	<b>CONCLUSIONS.....</b>	<b>113</b>
8.1	Overall Findings.....	113
8.2	Specific Recommendations on Implementation.....	114
	<b>REFERENCES.....</b>	<b>117</b>

## LIST OF FIGURES

Figure 2.1	Photo of the building exterior.....	6
Figure 2.2	Typical floor framing showing moment frames included in model.....	7
Figure 2.3	Elevation of moment frames included in model .....	7
Figure 2.4	Analysis model including gravity frames.....	9
Figure 2.5	Generalized force-deformation relation for steel elements or components .....	10
Figure 2.6	Nonlinear static force-displacement curve for the intact structure .....	13
Figure 2.7	Nonlinear static force-displacement curve for DS2 .....	13
Figure 2.8	Nonlinear static force-displacement curve for DS3 .....	14
Figure 2.9	Nonlinear static force-displacement curve for DS4 .....	14
Figure 2.10	Assumed unloading and cyclic behavior of connections whose flanges have not fractured .....	15
Figure 2.11	Assumed unloading and cyclic behavior of connections whose flanges have fractured .....	15
Figure 2.12	Assumed global unloading stiffness from damage state DS <sub>i</sub> .....	16
Figure 2.13	Assumed global reloading of a structure that has been subjected to damage state DS <sub>i</sub> .....	16
Figure 2.14	Example of <i>SPO2IDA</i> spreadsheet.....	18
Figure 2.15	Normalized IDA for intact structure .....	19
Figure 2.16	Normalized IDA for DS2 .....	19
Figure 2.17	Normalized IDA for DS3 .....	20
Figure 2.18	Normalized IDA for DS4 .....	20
Figure 2.19	Intact IDA.....	21
Figure 2.20	DS2 IDA.....	21
Figure 2.21	DS3 IDA.....	22
Figure 2.22	DS4 IDA.....	22
Figure 2.23	Response spectrum of the intact structure and damage states.....	23
Figure 2.24:	IDA, roof drift vs. $S_a/S_{a(10/50)}$ for the intact structure and damage states .....	23
Figure 2.25	Seismic hazard curve for the building site, $S_a$ vs. return period.....	24
Figure 2.26	Main shock vs. aftershock to cause collapse, Tagging Criteria C.....	25
Figure 2.27	Fragility curves.....	27



Figure 3.1	Comparison of intact structure force-displacement curves showing the effect of foundation flexibility.....	33
Figure 3.2	Comparison of intact structure force-displacement curves showing the effect of the gravity frame .....	33
Figure 3.3	Comparison of intact structure force-displacement curves showing the effect of the vertical distribution pattern of lateral forces .....	34
Figure 3.4	Force-displacement curves for damage state DS2, with different estimates of post-fracture plateau strength .....	36
Figure 3.5	Incremental dynamic analysis (IDA) results as influenced by post-fracture plateau strength .....	36
Figure 3.6	Force-displacement curves for damage state DS2, with different estimates of effective residual drift $\Delta_{re}$ .....	37
Figure 3.7	Incremental dynamic analysis (IDA) results as influenced by effective residual drift $\Delta_{re}$ .....	37
Figure 4.1	Roof framing, foundation, and floor plan of the building.....	43
Figure 4.2	Photos of the building: (a) exterior; (b) interior showing existing steel framing, added horizontal steel beam for wall out-of-plane support; and added steel members for roof diaphragm bracing; (c) close up of existing steel column made up of four angles riveted to a web plate .....	44
Figure 4.3	Summary of structural design and dimensions ( <i>RAM Perform</i> model) .....	45
Figure 4.4	<i>SAP 2000</i> computer analysis model .....	46
Figure 4.5	Summary of dead load and strength calculations for the mill-building example.....	47
Figure 4.6	Force-displacement curve developed from the linear <i>SAP 2000</i> model, neglects spandrel degradation .....	48
Figure 4.7	Foundation reaction forces from <i>SAP 2000</i> model .....	49
Figure 4.8	<i>Ram Perform</i> input properties for the intact structure.....	51
Figure 4.9	Nonlinear finite element model using <i>RAM Perform</i> at (a) 0.5% roof drift and (b) 2.0% roof drift .....	52
Figure 4.10	Forces at key structure section cuts, by computer analysis and hand calculation, and points on the force-displacement curve when peak strength of each section is reached.....	53
Figure 4.11	Foundation reaction forces from <i>RAM Perform</i> nonlinear static model .....	54

Figure 4.12	Modeling of each damage state.....	56
Figure 4.13	Force-displacement curves for the intact structure and for damage states DS2 and DS4.....	57
Figure 4.14	Concrete shear strength behavior by FEMA 306.....	58
Figure 4.15	Component material properties in <i>RAM Perform</i> for undamaged and damaged concrete.....	58
Figure 4.16	Spandrel 1 section strength for the intact structure and for damaged structures DS2 and DS4.....	59
Figure 4.17	Spandrel 3 section strength for the intact structure and for damaged structures DS2 and DS4.....	59
Figure 4.18	Pier 5A section strength for the intact structure and for damaged structures DS2 and DS4.....	60
Figure 4.19	Force-displacement curves and linear approximations for the intact structure and damaged structures DS2 and DS4.....	61
Figure 4.20	<i>SPO2IDA</i> intact (R vs. $\mu$ ).....	62
Figure 4.21	<i>SPO2IDA</i> DS2 (R vs. $\mu$ ).....	63
Figure 4.22	<i>SPO2IDA</i> DS4 (R vs. $\mu$ ).....	63
Figure 4.23	<i>SPO2IDA</i> intact ( $S_a$ vs. roof drift).....	64
Figure 4.24	<i>SPO2IDA</i> DS2 ( $S_a$ vs. roof drift).....	64
Figure 4.25	<i>SPO2IDA</i> DS4 ( $S_a$ vs. roof drift).....	65
Figure 4.26	Main shock vs. aftershock to cause collapse, Tagging Criteria C.....	67
Figure 4.27	Main shock vs. aftershock to cause collapse, Tagging Criteria D.....	67
Figure 4.28	Tagging limit states, per Criteria D, on the force-displacement curve of the intact structure.....	68
Figure 4.29	Fragility curves.....	70
Figure 5.1	Calibration to concrete wall test specimen, <i>RAM Perform</i> analysis model.....	73
Figure 5.2	Concrete wall test specimen (Barda 1976) and calibration of <i>RAM Perform</i> cyclic pushover (Run 4).....	74
Figure 5.3	(a) Photo of damaged test specimen (Barda 1976); (b) finite element model (Run 4).....	75
Figure 5.4	<i>RAM Perform</i> input properties for calibration to test specimen (Run 4).....	77

Figure 5.5	Stress-strain curve for concrete confined by rectangular hoops (Park and Paulay 1975).....	78
Figure 6.1	Eight-story moment-frame building (R&C, SGH 2004).....	81
Figure 6.2	Hysteretic behavior of model component (a) and test specimen (b) of beam-column connections (R&C, SGH 2004).....	82
Figure 6.3	Assumed force-deformation relationship for beam-to-column connections (R&C, SGH 2004) (photo courtesy of David Bonowitz and taken from SAC Program UCBN3 test (Popov et al. 1996)) .....	82
Figure 6.4	Selected member rotations for damage state DS4 (FN-L-3x0.75) at 4% roof drift during aftershock +FN-S-2x1.5 (R&C, SGH 2004) .....	83
Figure 6.5	Roof drift vs. time, damage state DS4 main shock + aftershocks (R&C, SGH 2004).....	86
Figure 6.6	IDA from nonlinear response history analyses for intact structure (R&C, SGH 2004).....	87
Figure 6.7	<i>SPO2IDA</i> for intact structure (R&C, SGH 2004) .....	88
Figure 6.8	Main shock vs. aftershock to cause collapse, Tagging Criteria D using <i>SPO2IDA</i> results (R&C, SGH 2004).....	89
Figure 6.9	One-story mill building with two-story rear portion (R&C 2005a).....	90
Figure 6.10	Summary of estimated nonlinear force-displacement behavior at each wall line (R&C 2005a).....	91
Figure 6.11	Three-story pier-and-spandrel building with concrete frame (R&C 2005b).....	93
Figure 6.12	3-D computer structural analysis model (R&C 2005b) .....	93
Figure 6.13	Calibration of frame elements in structural analysis model to match shell element properties (R&C 2005b) .....	93
Figure 6.14	One-story plus basement and mezzanine composite building (R&C 2006a).....	94
Figure 6.15	2-D computer structural analysis model, longitudinal plan direction (R&C 2006a).....	95
Figure 6.16	Median spectral accelerations to cause each tagging limit state; results for two different retrofit schemes overlain on site-specific response spectra (R&C 2006a).....	95
Figure 6.17	One-story mill building with flat roof and skylights (R&C 2006b).....	97
Figure 6.18	2-D computer structural analysis diaphragm model (R&C 2006b) .....	97

Figure 7.1	Comparison of residual roof drift and maximum roof drift (E-W) .....	103
Figure 7.2	Comparison of residual roof drift and maximum roof drift (N-S) .....	103
Figure 7.3	Diagrams of the relationship between displacement capacity and residual displacement.....	106
Figure 7.4	Determining $\alpha_i$ , slope factor effecting residual drift for $DS_i$ . .....	107

## LIST OF TABLES

Table 2.1	Building loads and properties.....	8
Table 2.2	Beam hinge properties, determined using FEMA 356 Table 5-6 .....	11
Table 2.3	Spectral acceleration for damage states .....	18
Table 2.4	Tagging criteria .....	25
Table 2.5	Median roof drifts and median $S_a$ corresponding to structural limit states .....	25
Table 2.6	Uncertainty values.....	26
Table 3.1	Assumptions used in the nonlinear static (pushover) analysis.....	32
Table 4.1	Construction drawings for the mill building of Test Application 2 .....	40
Table 4.2	Expected material strength properties (year of construction =1921) .....	45
Table 4.3	Concrete wall <i>RAM Perform</i> input properties.....	50
Table 4.4	Modeling of each damage state in <i>RAM Perform</i> .....	55
Table 4.5	Assumed fundamental period of vibration .....	56
Table 4.6	<i>SPO2IDA</i> input.....	62
Table 4.7	Spectral acceleration to cause each damage state (from Fig. 4.23).....	65
Table 4.8	Spectral acceleration to collapse the structure in an aftershock.....	65
Table 4.9	$\beta_R$ values taken from the intact structure <i>SPO2IDA</i> results, and $S_{a(cap)}$ values .....	69
Table 4.10	Uncertainty values for fragility curves.....	69
Table 4.11	Spectral acceleration values (g) for fragility curves.....	70
Table 5.1	Concrete wall calibration to test specimen: <i>RAM Perform</i> input properties.....	76
Table 6.1	Applications of the <i>Advanced Seismic Assessment Guidelines</i> .....	80
Table 6.2	Spectral acceleration (g) to cause each damage state, comparison of <i>SPO2IDA</i> and nonlinear response history estimates (R&C, SGH 2004).....	87
Table 6.3	Spectral acceleration (g) to cause collapse in an aftershock, comparison of nonlinear response history and <i>SPO2IDA</i> estimates (R&C, SGH 2004).....	88
Table 6.4	Tagging limit states, comparison of <i>SPO2IDA</i> and nonlinear response history analysis (R&C, SGH 2004).....	89
Table 7.1	Values of $\gamma_1$ , ratio of dynamic to static residual drift.....	101
Table 7.2	Determining $\gamma_2$ .....	107

## NOMENCLATURE

$DS_i$	$i^{th}$ structural damage state
$F_s(S_a)$	Fragility curve, cumulative probability distribution function of an S-state “capacity” measured in ground motion intensity terms
$I$	Moment of inertia of steel member
$K_i$	Global effective initial (elastic) stiffness for the $i^{th}$ damage state
$K_{hi}$	Global hardening stiffness for the $i^{th}$ damage state
$K_{si}$	Global softening stiffness for the $i^{th}$ damage state
$k_i$	Component effective initial (elastic) stiffness for the $i^{th}$ damage state
$k_{hi}$	Component hardening stiffness for the $i^{th}$ damage state
$k_{si}$	Component softening stiffness for the $i^{th}$ damage state
$P$	MAF of exceeding the $S_a(T_i)$ associated with collapse of the damaged structure
$P_o$	MAF of exceeding the $S_a(T_i)$ associated with collapse of the intact structure
$MAF$	Mean annual frequency = $1/RP$
$N_c$	Total number of beam connections
$N_f$	Number of fractured beam connections
$R_i$	Normalized base shear, = $V_i/V_{yi}$
$RP$	Return period
$S_a$	Spectral acceleration, or spectral acceleration to achieve a damage state
$S_{a\ 10/50}$	Spectral acceleration with a 10% probability of exceedance in 50 years
$S_{a\ 5/50}$	Spectral acceleration with a 5% probability of exceedance in 50 years
$S_{a\ 2/50}$	Spectral acceleration with a 2% probability of exceedance in 50 years
$S_{a(cap)i}$	Spectral acceleration to cause collapse of the damaged structure
$S_{a(cap-\phi)i}$	Spectral acceleration at the period of the intact structure that corresponds to $S_{a(cap)i}$ taken at the period of the damaged structure
$S_d$	Spectral displacement
$T_1$	Fundamental period of intact structure.
$T_i$	Fundamental period of structure in the $i^{th}$ damage state
$V$	Base shear
$V_y$	Yield base shear

$\alpha$	Modal participation factor, assumed to be 0.9
$\beta_U$	Dispersion measurement representing epistemic uncertainty
$\beta_R$	Dispersion measurement representing aleatory variability
$\beta$	Dispersion measurement representing uncertainty and variability; equal to the square root sum of the square of $\beta_U$ and $\beta_R$
$\Delta$	Global displacement, typically taken at the roof level
$\Delta_{rs}$	Expected absolute value of the global residual displacement based on a static, monotonic pushover analysis
$\Delta_{rd}$	Expected absolute value of the global residual displacement based on a dynamic nonlinear analysis
$\Delta_{re}$	Effective reduction in global displacement capacity caused by residual displacement.
$\Delta_{yi}$	Yield displacement
$\mu_i$	Global ductility ratio, $\Delta_i/\Delta_{yi}$
IDA	Incremental dynamic analysis
NSP	Nonlinear static procedure of analysis
SPO	Static push-over curve of force versus displacement results from the NSP

# 1 Introduction

## 1.1 BACKGROUND

An important aspect of reducing the potentially costly and destructive impacts of earthquakes to society is to improve the earthquake resistance of utility and transportation networks, or “lifelines.” Protecting these infrastructure networks requires understanding the seismic vulnerability of each of the components of the networks, understanding the most effective ways to reduce their seismic vulnerability, and understanding the interrelated importance of the components.

For many utility and transportation networks, buildings are key components. Predicting the post-earthquake functionality of utility buildings is a crucial step in evaluating the likelihood that a distribution network will be able to provide electricity, gas, water, or communication services to the residents of an earthquake-affected area.

A rational and practical approach to evaluating or reducing the seismic vulnerability of an infrastructure network starts with developing fragility curves for all components of the network. Recent research has led to improved methods of establishing fragility curves for utility buildings.

*Advanced Seismic Assessment Guidelines* were developed by Stanford University (C. Allin Cornell, Paolo Bazzurro, Charles Menun, Maziar Motahari) as part of the PEER Lifelines Program, Building Vulnerability Studies (Project Task Number 507). When the *Guidelines* are applied to a building, the final product is a set of fragility curves for structural limit states directly related to post-earthquake building occupancy status, namely green, yellow, or red tagging.

The subject project, Task 508, applies these guidelines in a detailed fashion to two example buildings. Two utility buildings, with differing properties, are chosen for the test applications.



## 1.2 OBJECTIVES

The objectives of the test applications are the following:

- Identify potential difficulties that Structural Engineers would encounter in using the procedures described in the *Advanced Seismic Assessment Guidelines*.
- Recommend possible revisions to the procedure to address any identified difficulties.
- Identify and make recommendations on other issues related to assessing the seismic reliability of utility structures and systems.

## 1.3 SCOPE

The scope of the project includes test applications, examining two real buildings, of the *Advanced Seismic Assessment Guidelines*. The first building studied is a three-story steel moment-frame building. The second building is an older type of utility structure of composite concrete and steel (mill building) construction. The scope includes developing specific performance predictions for the two structures, and identifying and commenting on, from the practicing engineer's perspective, issues related to the *Advanced Seismic Assessment Guidelines* and the broader objectives of assessing the reliability of lifeline systems affected by building seismic vulnerability.

For each test building the scope includes the following topics:

- Nonlinear static (NSP) analysis of the undamaged building
- NSP analyses of the damaged building
- Conversion of NSP analysis to incremental dynamic analysis (IDA)
- Occupancy status of the damaged building
- Ground motion level associated with each structural limit state
- Computation of fragility curves

The detailed evaluations using the *Guidelines* have also led to study of integral technical issues including the following:

- Computer modeling issues for steel moment-frame and concrete wall structures
- Applicability of analysis approaches ranging from “hand” adjustments on elastic models to fully computerized modeling of damaged structures
- Estimating residual drift and its effect
- Including the effect of building period shift

- Post-earthquake occupancy (tagging) criteria
- Post-earthquake inspection

Throughout the project, Rutherford & Chekene worked closely with the Project 507 researchers to ensure that our interpretations and use of the *Guidelines* were correct, and to ensure that our recommendations complemented the intentions of the *Guidelines*.

#### **1.4 OUTLINE OF THE REPORT**

Section 2 presents the first of two test applications featured in this report: a three-story steel moment-frame building. Section 3 examines the effects of varying several analysis assumptions used in Test Application 1. Section 4 presents the second test application: a one-story mill building. Section 5 examines the finite element modeling assumptions used in Test Application 2. Section 6 briefly describes five additional PG&E buildings for which Rutherford & Chekene has performed seismic evaluations using the *Advanced Seismic Assessment Guidelines*. Section 7 discusses two key technical issues for which R&C determined that further examination and definition of procedures would be useful. Section 8 summarizes the findings and recommendations of this study.

## 2 Test Application 1: Steel Moment-Frame Building

This section presents the first of two test applications of the *Advanced Seismic Assessment Guidelines* featured in this report. It includes a description of the structure in Section 2.1, followed by Sections 2.2–2.6, which discuss the major parts of the Advanced Seismic Assessment process for this building: evaluation of the intact structure, evaluation of the damaged structure, determination of dynamic behavior, definition of post-earthquake tagging limit states, and computation of fragility curves. Section 2.7 presents the assessment in a step-by-step format citing key equations.

### 2.1 DESCRIPTION OF THE STRUCTURE

Test Application 1 examines a service center and operations building designed in 1988. The building is three stories tall with steel moment-resisting frames as the seismic-force-resisting system (Fig. 2.1). The rectangular plan measures 98 feet by 217 feet and the total floor area is 62,600 sq ft. Figure 2.2 shows a plan of typical floor framing for the building.

The floors and roof of the structure consist of lightweight concrete fill over metal deck. Composite steel beams and girders span between steel columns. The columns bear on a foundation consisting of precast concrete piles and reinforced concrete pile caps, which are interconnected by concrete grade beams. Table 2.1 shows the building dead loads, floor masses, and story heights.

As shown in Figure 2.2, the steel moment frames are located around the building perimeter, with an additional two transverse frames bordering a two-story atrium near the building center. Figure 2.3 shows elevations of the moment frames analyzed, including member sizes. Moment-frame beams are Grade 36 steel, while columns are A572 Grade 50 steel. Table

2.1 shows expected yield strengths for each material, based on the recommendations of FEMA 356 (FEMA 2000).

The building has a regular configuration, with no soft or weak stories, nor any other code-identified irregularities. It houses a communications facility that is used during storms and other emergencies. The call center is intended to be operational following an earthquake, so the building was designed as an essential facility, using an importance factor of 1.5. As a result, the structural frame is 50% stiffer and stronger than a typical non-essential steel moment frame from the same era.

The building's steel moment frames are designed and specified to "pre-Northridge" standards, meaning that the beam-column connections may be susceptible to fracture near the welds of beam flanges to columns.

The building is located on a site of high seismicity. The short period design spectral acceleration, for a ground motion with a 5% probability of exceedance in 50 years, is 1.69g, as shown in Table 2.1. The building is on a Type D soil profile. At the building period of 0.78 seconds, the short period plateaus of the design spectra govern design spectral acceleration.



**Figure 2.1 Photo of the building exterior**

**Weight of  
1/2 building  
=2.350k**

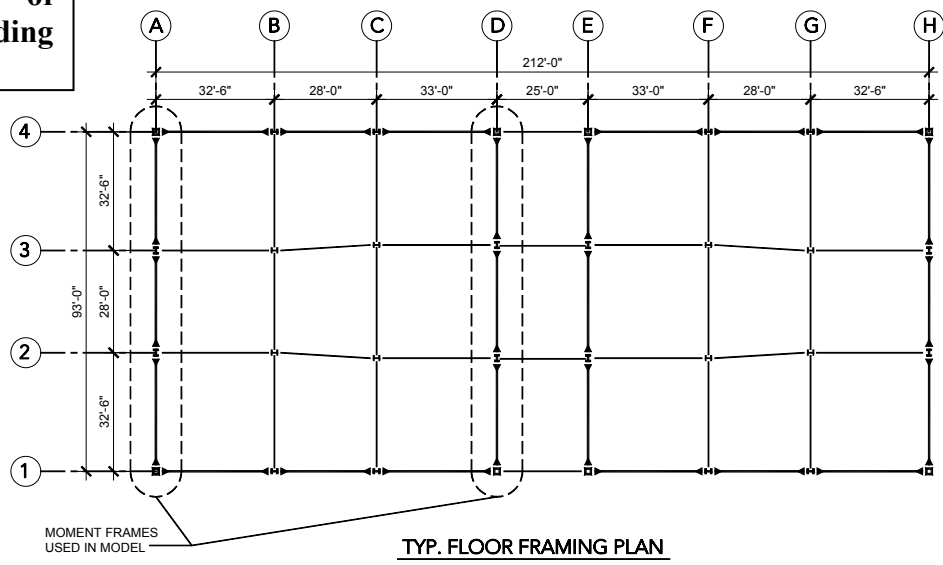


**Figure 2.2 Typical floor framing showing moment frames included in model**

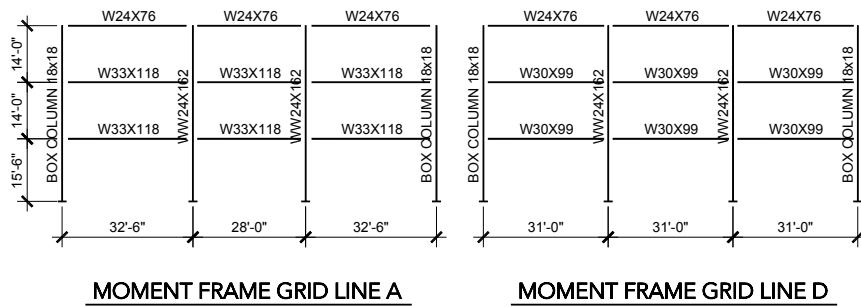


**Figure 2.3 Elevation of moment frames included in model**

**Table 2.1 Building loads and properties**

<b>Building Dead Load</b>	
Ceiling & Mech.	6 psf
Partitions	10 psf
4 ½" LWC over 3" Metal Deck	44 psf
Beams	8 psf
Columns	3 psf
<b>Total</b>	<b>71 psf</b>
<hr/>	
Exterior Walls (2 <sup>nd</sup> & 3 <sup>rd</sup> stories)	15 psf

<b>Floor</b>	<b>Story Ht. (ft)</b>	<b>Area (ft<sup>2</sup>)</b>	<b>Floor DL (K)</b>	<b>Floor Mass (k-s<sup>2</sup>/ft)</b>	<b>Floor LL (K)</b>
Roof	14'	21266	1638	50.9	851
3 <sup>rd</sup>	14'	21266	1638	50.9	2127
2 <sup>nd</sup>	15.5'	20146	1431	44.4	2015
		<b>Totals</b>	<b>4707</b>	<b>146.2</b>	<b>4993</b>

<b>Estimated Material Properties</b>	
Columns	A572 Grade Sc Fy=55ksi
Beams	A36 Fy=51ksi

<b>Site Seismicity Data</b>	From USGS National Seismic Hazard Maps			
	PGA	S <sub>s</sub> (g)	S <sub>1</sub> (g)	S <sub>a</sub> (g) *
10% / 50 yr.	0.61	1.28	0.67	1.28
5% / 50 yr.	0.75	1.69	0.92	1.69
2% / 50 yr.	0.96	2.04	1.25	2.04
MCE				1.50
DBE				1.00
*At building period = 0.78s				
Soil Type D				

## 2.2 SEISMIC EVALUATION OF THE INTACT STRUCTURE

In accordance with the *Guidelines*, the seismic evaluation of the intact structure includes nonlinear static (pushover) analyses. This test application analyzes the building's transverse plan direction using the computer structural analysis program *SAP 2000*. Since a similar lateral-force-resisting system exists in the building's longitudinal direction, the structure is expected to exhibit similar behavior in that direction, so an evaluation of that direction is not included in this study.

### 2.2.1 Computer Analysis Model

The building's regular symmetrical configuration allows a two-dimensional analysis to appropriately capture structural behavior. Half of the building's weight and half of the lateral-force-resisting frames are modeled as indicated in Figures 2.2–2.3. In addition to the moment frames shown in Figure 2.3, the gravity-framing members on building lines B and C are also included in the model.

Figure 2.4 depicts the two-dimensional in-line modeling of parallel moment frames on lines A and D, plus gravity frames on Lines B and C. Foundation springs represent the rotational stiffness of the piles and pile cap foundations beneath each column. Assigned spring constants account for the stiffness of the concrete foundation elements and as well as their expected movement in the supporting soil under seismic forces.

The nonlinear static analysis applies story forces in an inverted triangular pattern proportional to that prescribed in the *Uniform Building Code (UBC)* (ICBO 1997).

A study was carried out on the effects of several of the analysis assumptions using variations of the analysis model. Section 3.1 describes and evaluates variations on the above assumptions.

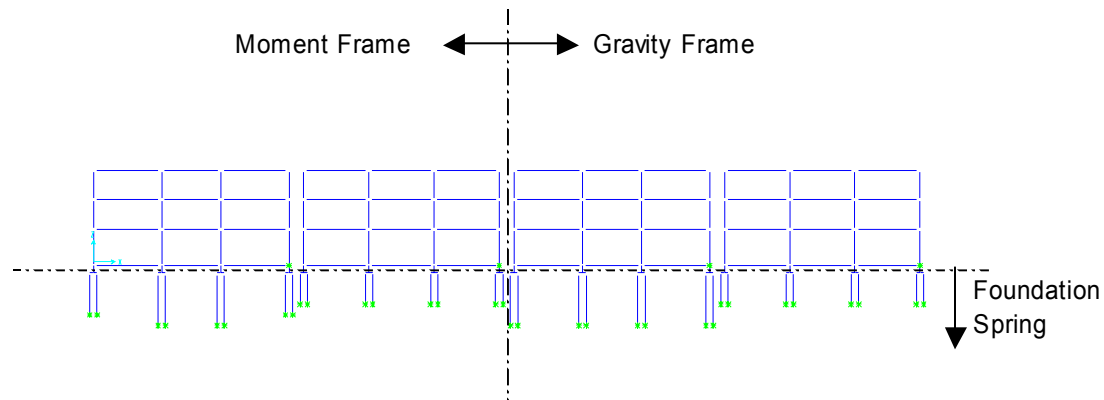


**Figure 2.4 Analysis model including gravity frames**

### 2.2.2 Nonlinear Components

All beams and columns are modeled with potential plastic hinge locations at each end. Plastic hinges in moment-frame beams and columns are assigned flexural strength equal to that of their

steel sections. Plastic hinges in gravity beams are assigned flexural strength equal to that estimated for their shear-tab connections.

Nonlinear force-deformation behavior for steel columns and beams follows the modeling recommendations of FEMA 356. Figure 2.5 depicts a generic force-deformation relationship for steel elements, and Table 2.2 displays the values  $a$ ,  $b$ , and  $c$  which define this relationship for each steel beam. For example, the  $a$  values show that the W33 and W30 floor beams sustain a plastic rotation of 0.8% to 1.3% before flange fracture (the first capacity drop) occurs. Given the length, plastic moment strength, and elastic stiffness of each beam, the yield rotation,  $\theta_B$ , is calculated, which leads to the rotational ductility values at points  $C$  and  $E$ , shown in Table 2.2. These ductility values, along with flexural yield strengths, comprise the input for plastic hinge definitions in the *SAP* model.

A similar procedure computes the expected nonlinear force-deformation behavior for columns. By FEMA 356, columns achieve significantly larger plastic rotations than beams do before the occurrence of flange fracture and strength degradation. At the displacement demands imposed in this evaluation, columns yield but do not degrade.

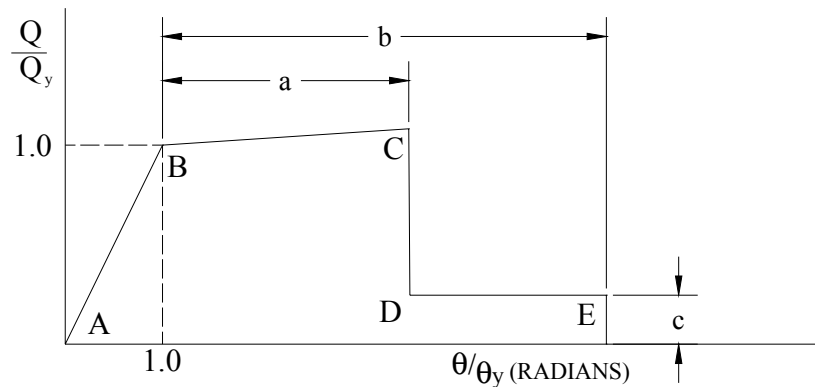


**Figure 2.5 Generalized force-deformation relation for steel elements or components**



**Table 2.2 Beam hinge properties, determined using FEMA 356 Table 5-6**

Size	$L_b$ (ft)	a (radians)	b (radians)	c	$Q_C/Q_B$	$\theta_C/\theta_B$	$\theta_E/\theta_B$
W33x118	30.71	0.008	0.023	0.2	1.036	2.20	4.39
W33x118	25.92	0.008	0.023	0.2	1.043	2.42	5.02
W30x90	29.21	0.013	0.025	0.2	1.052	2.74	4.48
W30x90	28.92	0.013	0.025	0.2	1.053	2.76	4.52
W24x76	30.71	0.020	0.029	0.2	1.064	3.15	4.09
W24x76	29.21	0.020	0.029	0.2	1.068	3.26	4.25
W24x76	28.92	0.020	0.029	0.2	1.068	3.28	4.28
W24x76	25.92	0.020	0.029	0.2	1.076	3.54	4.66

### 2.2.3 Analysis Results

Performing a nonlinear static analysis with the model described above generates the force-displacement response plot of Figure 2.6. The structure reaches a peak base shear of 2000 kips at a roof drift (roof displacement divided by building height) of 1.7%. After this peak, strength degrades as a result of beam flange fracturing. When roof drift reaches 4%, the lateral strength drops to approximately 400 kips.

## 2.3 SEISMIC EVALUATION OF THE DAMAGED STRUCTURE

Using the methodology of the *Guidelines*, damage states are defined at roof drifts where significant losses in lateral-force-resisting capacity occur, labeled “DS1”–“DS4” on the intact structure force-displacement curve of Figure 2.6. Damage states are chosen to capture the range of damage that affects the resulting levels of post-earthquake risk (from green tag to red tag). For each damage state, a “damaged-structure” force-displacement curve characterizes expected behavior in an aftershock (Figs. 2.7–2.9).

Beyond the roof drift that causes each damage state, the corresponding damaged-structure force-displacement curve takes the same shape as that of the intact structure. However, plastic deformations and flange fractures associated with each damage state result in residual roof drift and reloading behavior that differs from that of the intact structure.

The reloading portion of each damaged-structure force-displacement curve is estimated based on the extent of damage and the cyclic moment-rotation behavior of steel moment connections. Figures 2.10–2.11 relate the cyclic moment-rotation behavior of steel moment

connections to the static force-deformation relationship for these connections. From Figure 2.10 as long as flanges do not fracture, the reloading stiffness is the same as the intact initial stiffness; however, from Figure 2.11, after flanges have fractured, stiffness and strength decrease significantly. Also, in both figures the dynamic residual rotation  $\theta_{rd}$  is smaller than the static residual rotation  $\theta_{rs}$ , a result of load reversal.

Relating this element behavior to the damaged-structure behavior (Fig. 2.13), the damaged-structure initial stiffness,  $K_i$  is calculated by modifying the stiffness of elements with fractured flanges in the *SAP* model and then performing an elastic analysis. The damaged-structure hardening stiffness,  $K_{hi}$  is estimated by multiplying the intact structure hardening stiffness by the ratio of remaining unfractured moment connections to total moment connections. The dynamic residual drift  $\Delta_{rd}$  of Figure 2.13 is calculated as 0.3 times the static residual drift  $\Delta_{rs}$  of Figure 2.12. Section 7 of this report provides further discussion and recommendations for estimating dynamic residual drift.

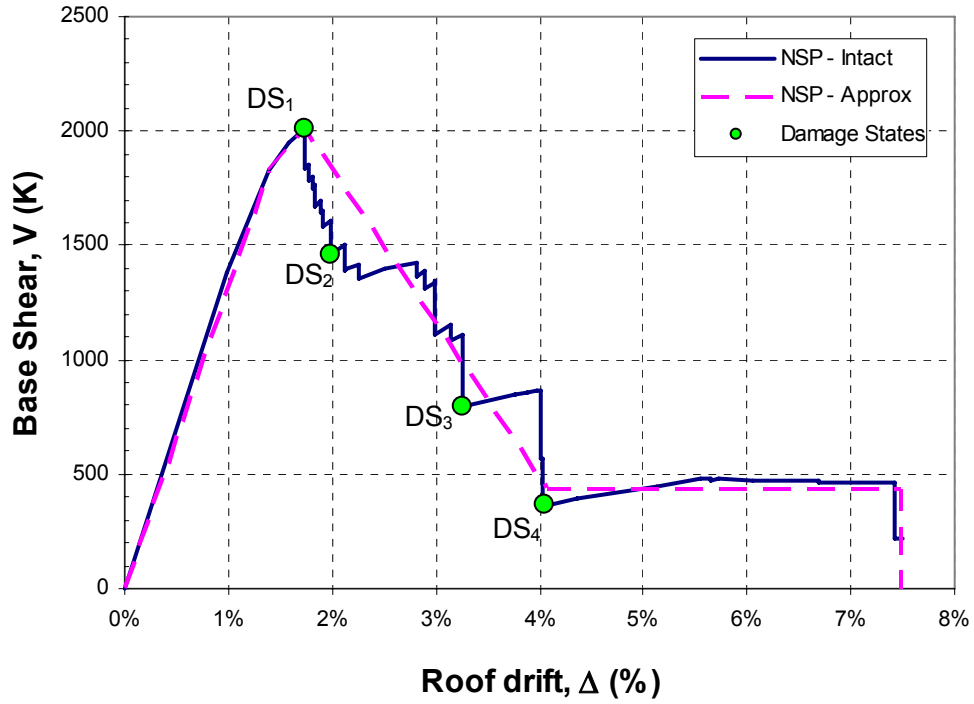


Figure 2.6 Nonlinear static force-displacement curve for the intact structure

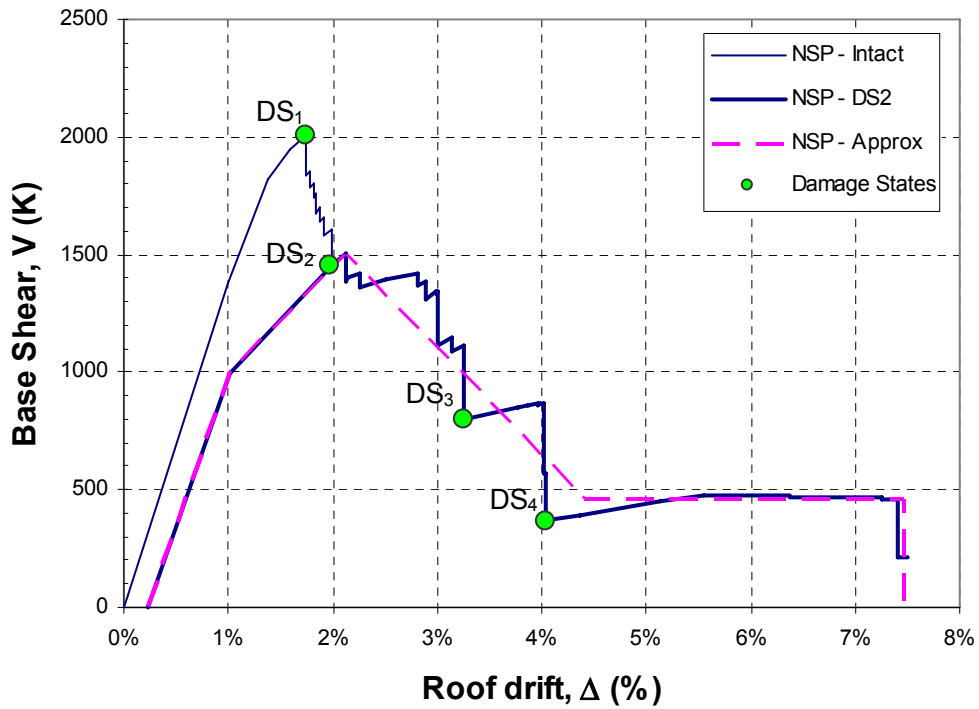


Figure 2.7 Nonlinear static force-displacement curve for DS2

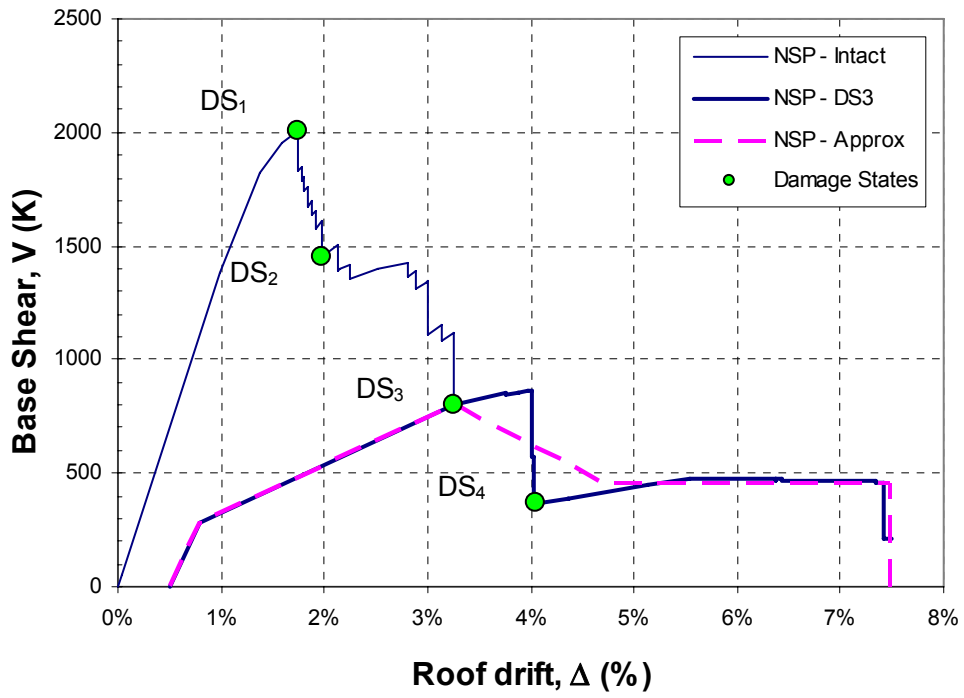


Figure 2.8 Nonlinear static force-displacement curve for DS3

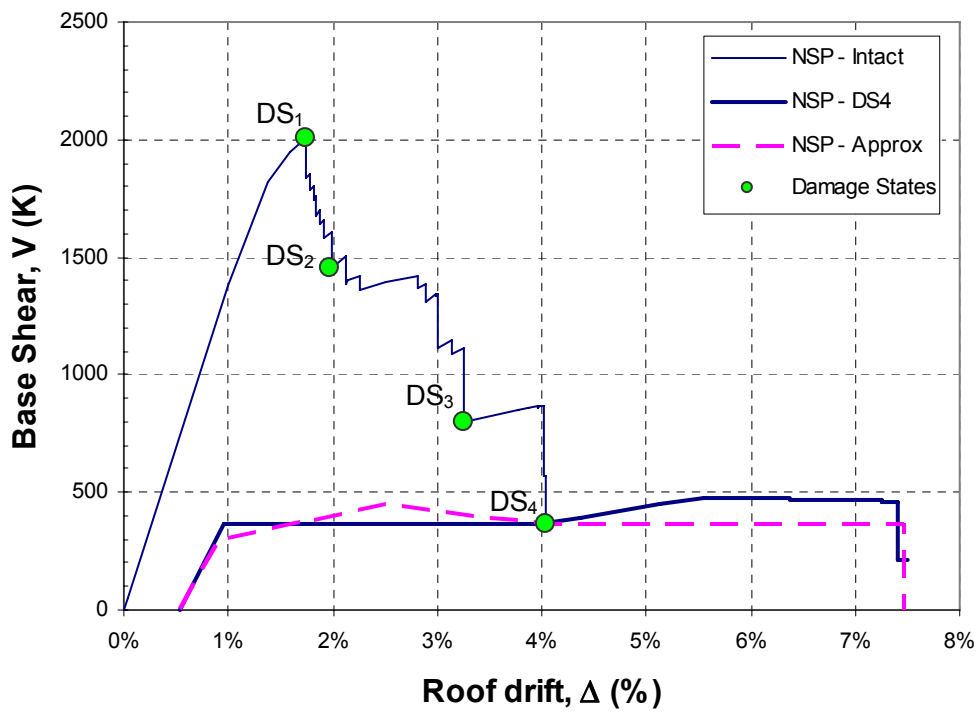
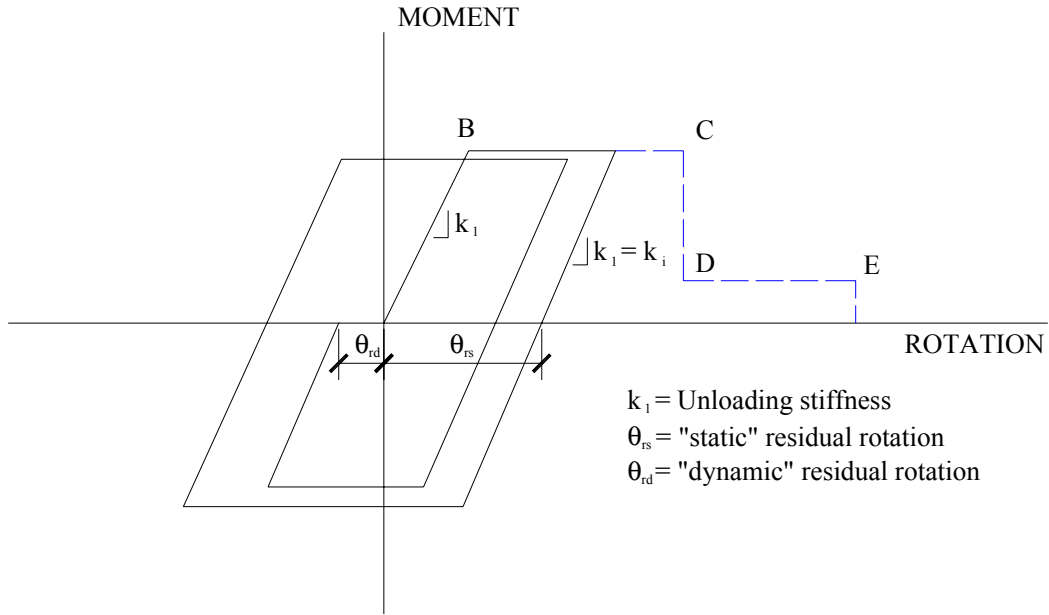
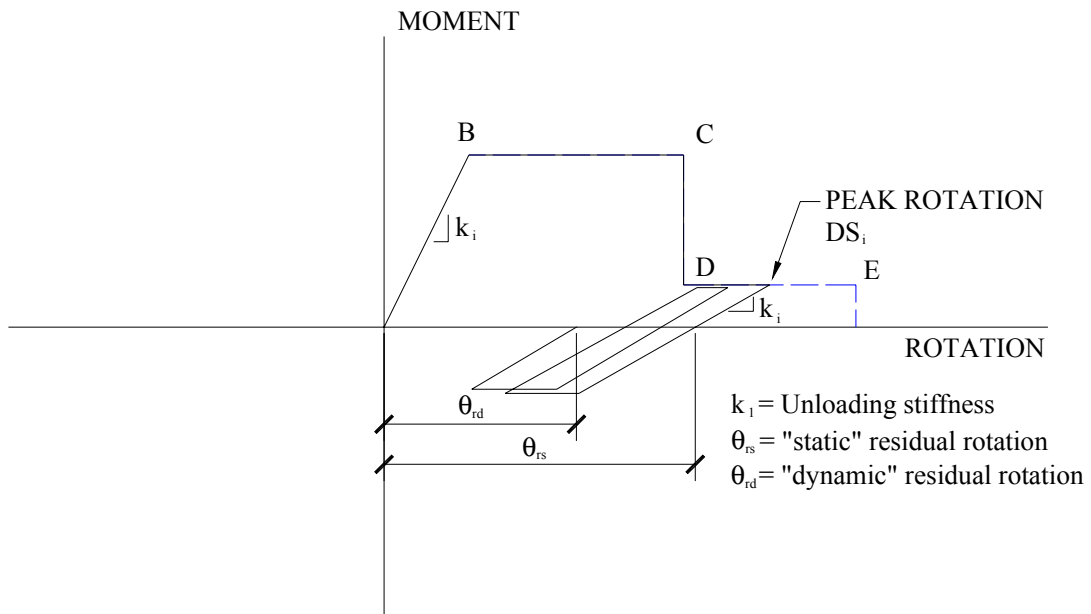


Figure 2.9 Nonlinear static force-displacement curve for DS4



**Figure 2.10 Assumed unloading and cyclic behavior of connections whose flanges have not fractured**



**Figure 2.11 Assumed unloading and cyclic behavior of connections whose flanges have fractured**

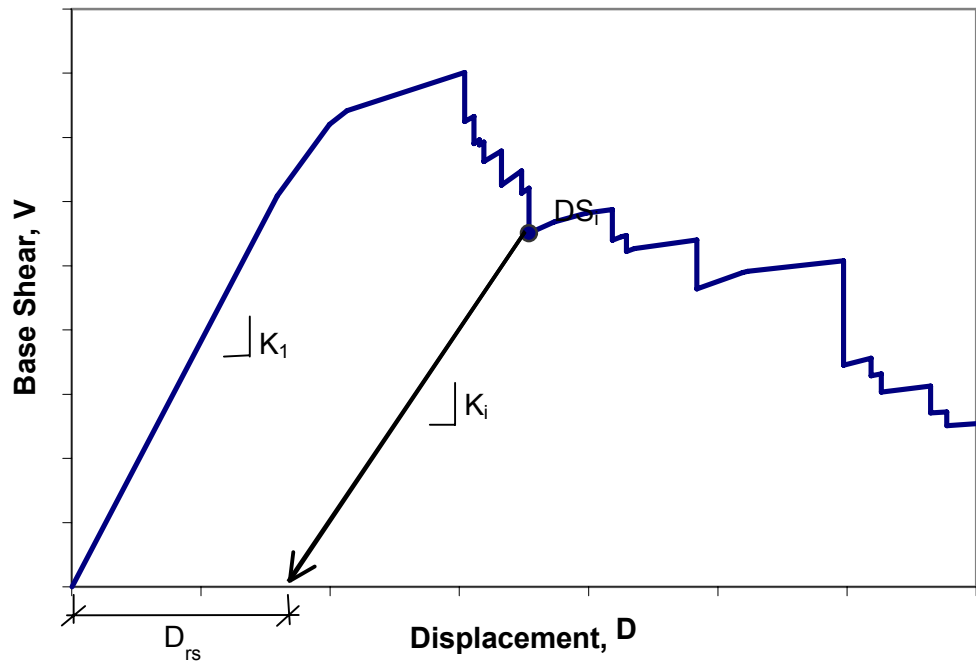


Figure 2.12 Assumed global unloading stiffness from damage state  $DS_i$

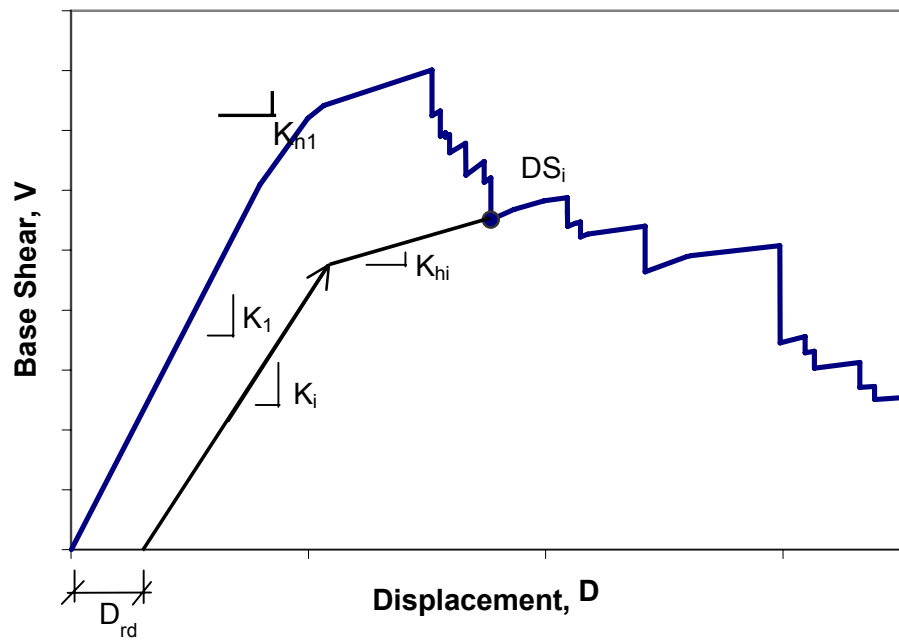


Figure 2.13 Assumed global reloading of a structure that has been subjected to damage state  $DS_i$

## 2.4 INFERRED DYNAMIC BEHAVIOR (SPO2IDA)

From the nonlinear force-displacement plots of Figures 2.6–2.9, the *SPO2IDA* program (Vamvatsikos 2002) is used to compute the relationship between spectral acceleration and global ductility demand for each damage state. Figure 2.14 presents an example *SPO2IDA* spreadsheet with the input interface displayed on the left and the output acceleration-ductility curves graphed on the right.

The *SPO2IDA* program takes as input a fundamental period of vibration and a quadrilinear force-displacement plot. Overlaid on Figures 2.6–2.9 are the quadrilinear approximations of force-displacement response used for input into *SPO2IDA*. Table 2.3 displays the fundamental period of vibration for the structure at each damage state, obtained from the modified *SAP* models mentioned in the previous subsection.

Figures 2.15–2.18 display the normalized graphical output from *SPO2IDA*, and Figures 2.19–2.22 present the same data in terms of spectral acceleration and roof drift. Noted on each of these latter plots are the 10%-in-50-year, 5%-in-50-year, and 2%-in-50-year spectral acceleration values from Table 2.3. Response spectra, fundamental periods, and resulting spectral acceleration values for all damage states are presented graphically in Figure 2.23.

The *SPO2IDA* program accounts for variability in nonlinear displacement response by plotting three different confidence levels of maximum roof drift. For example, for a given peak spectral acceleration, the maximum roof drift will be less than that marked by the IDA-84% line in 84 out of 100 ground motions.

Figure 2.24 plots the median (IDA-50%) curves for each damage state, normalized by the spectral acceleration from the 10%-in-50-year response spectrum at the fundamental period associated with that damage state. This figure indicates that some damage to the structure may actually increase its collapse capacity because the damage lengthens the building's fundamental period of vibration, which in turn reduces spectral acceleration demand. Figure 2.25 shows the seismic hazard curve for the building site, which indicates that the return period for spectral acceleration to collapse the intact or damaged structure ( $S_a/S_{a10/50}$  are all greater than 2.0 from Fig. 2.24) is greater than 2500 years.

From the intact structure *SPO2IDA* plot, the spectral acceleration expected to cause each damage state is determined (Table 2.4). The tabulated acceleration values correspond to points on the median (IDA-50%) curve at which the structure reaches the roof drifts that define each

damage state. Next, from each of the damaged-structure *SPO2IDA* plots, the median spectral acceleration values  $S_{a(cap)}$  expected to cause collapse in an aftershock are determined. The values in Table 2.4 form the basis for defining post-earthquake tagging limit states.

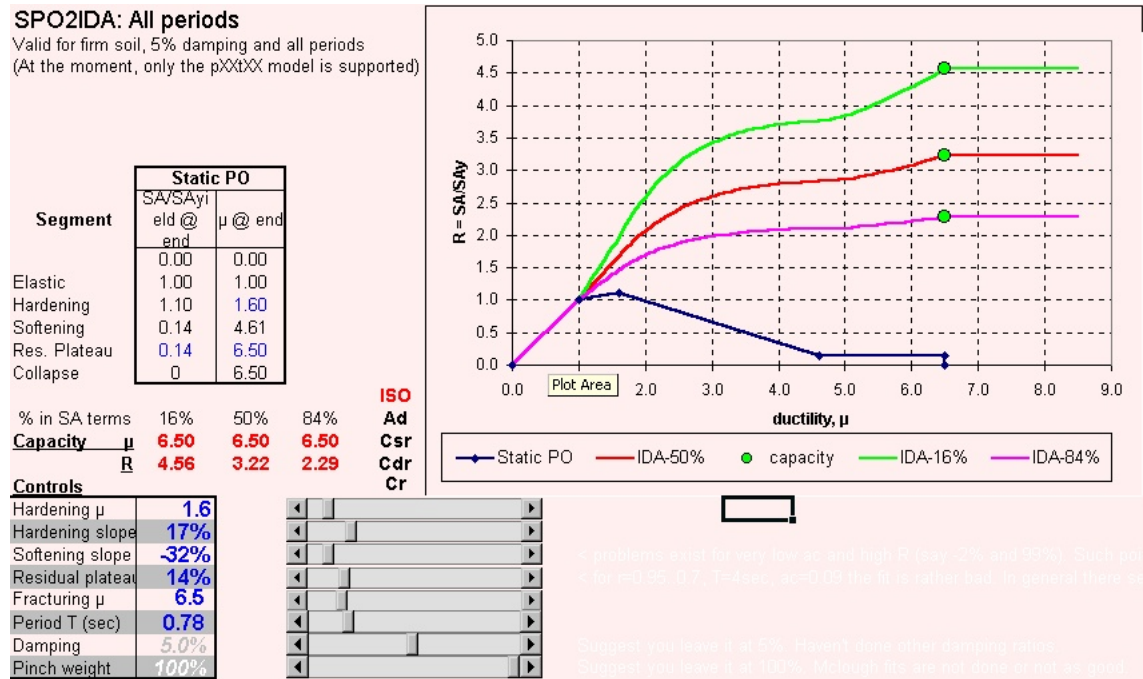


Figure 2.14 Example of *SPO2IDA* spreadsheet

Table 2.3 Spectral acceleration for damage states

$DS_i$	Period(sec)	$S_{a 10/50}$	$S_{a 5/50}$	$S_{a 2/50}$
Intact	0.81	1.25	1.69	2.04
DS2	0.88	1.15	1.58	2.04
DS3	0.99	1.02	1.40	1.90
DS4	1.03	0.98	1.35	1.82



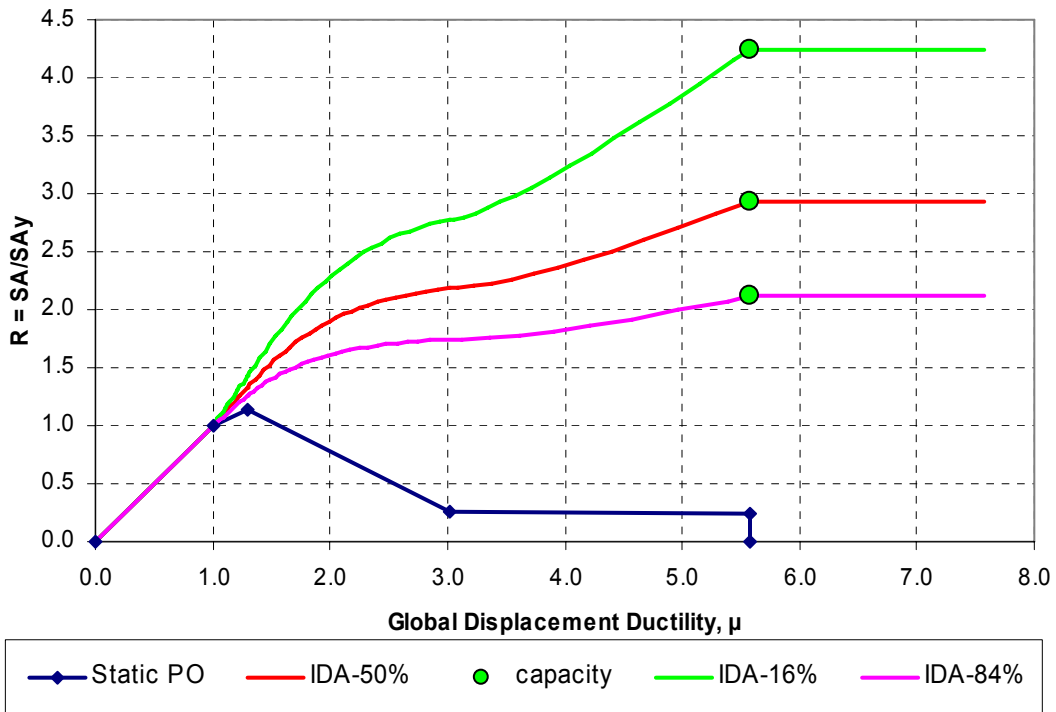


Figure 2.15 Normalized IDA for intact structure

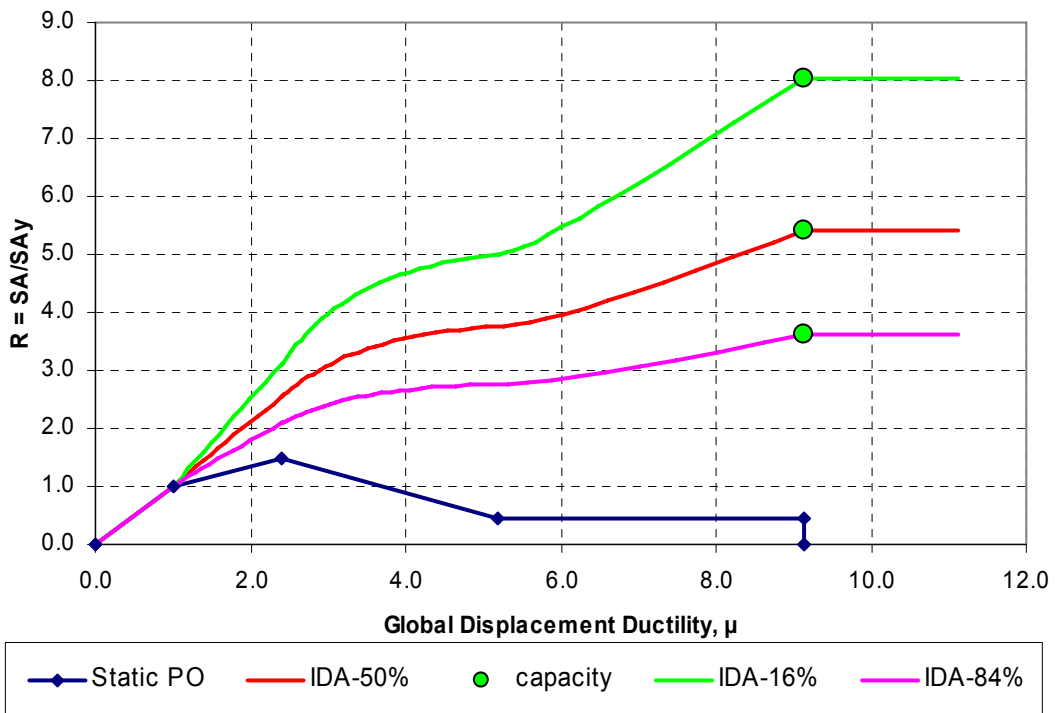


Figure 2.16 Normalized IDA for DS2

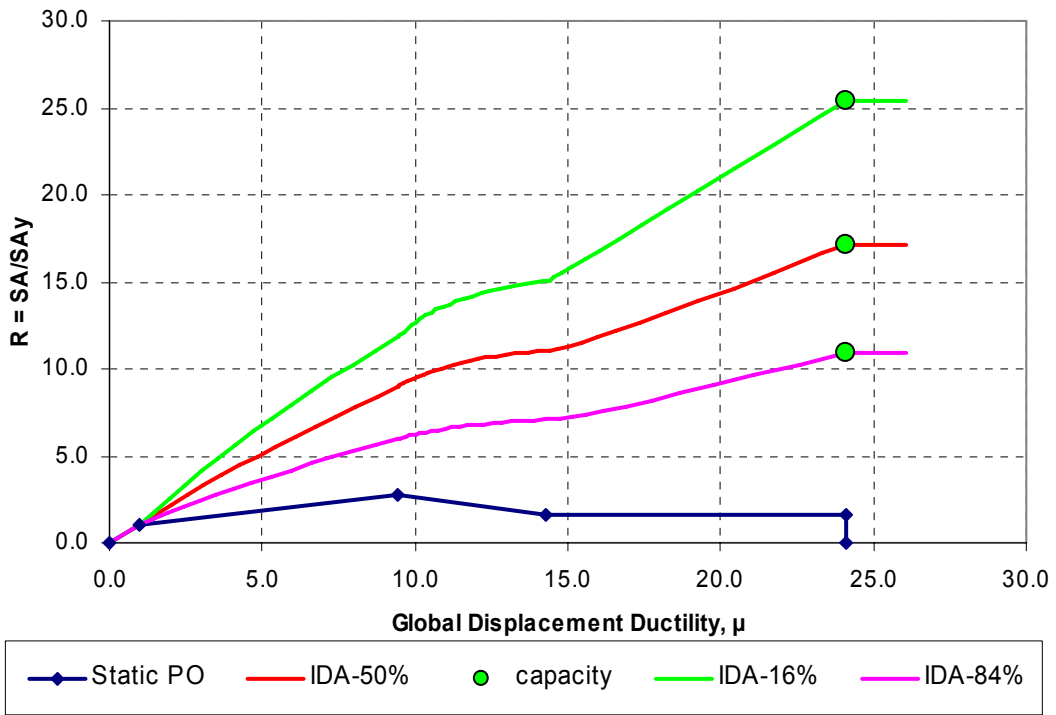


Figure 2.17 Normalized IDA for DS3

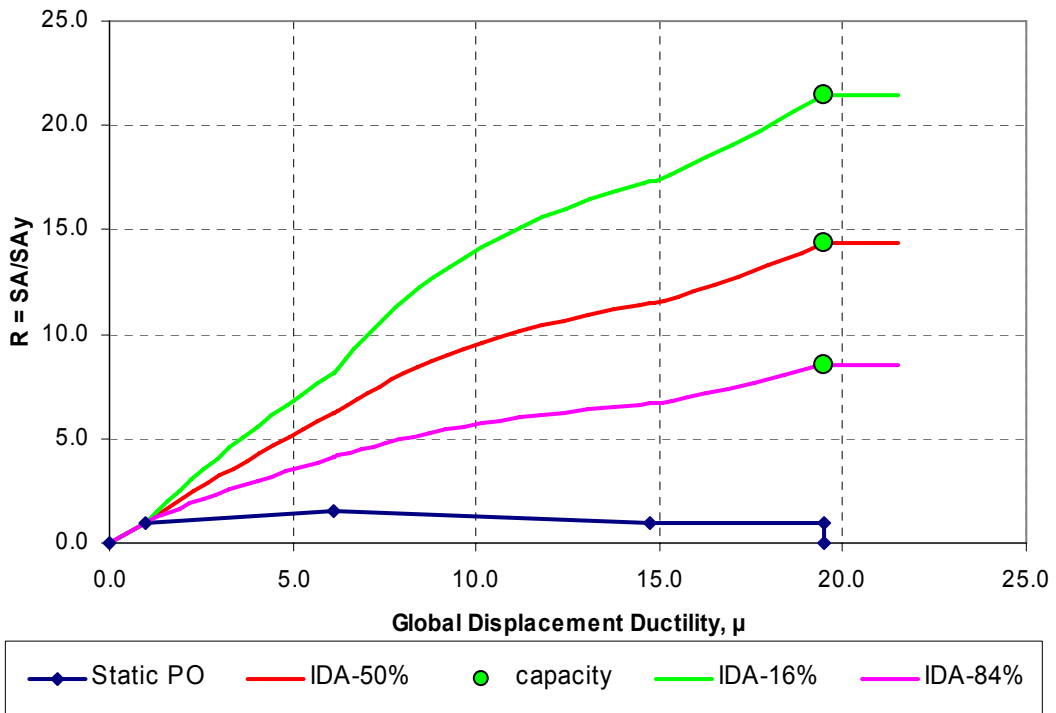


Figure 2.18 Normalized IDA for DS4

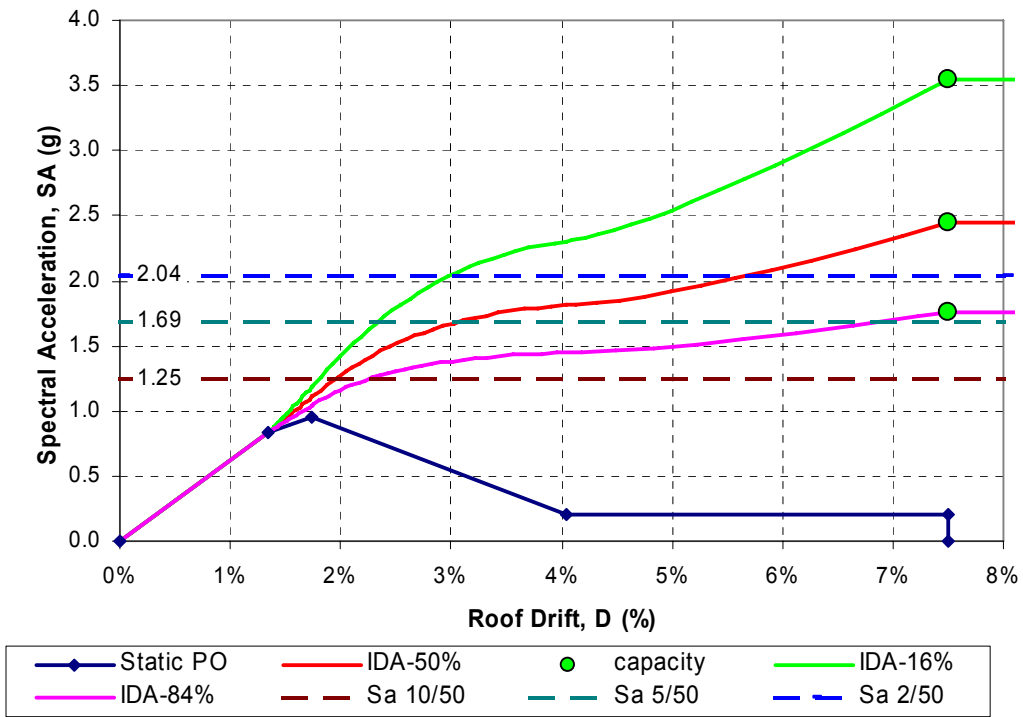


Figure 2.19 Intact IDA

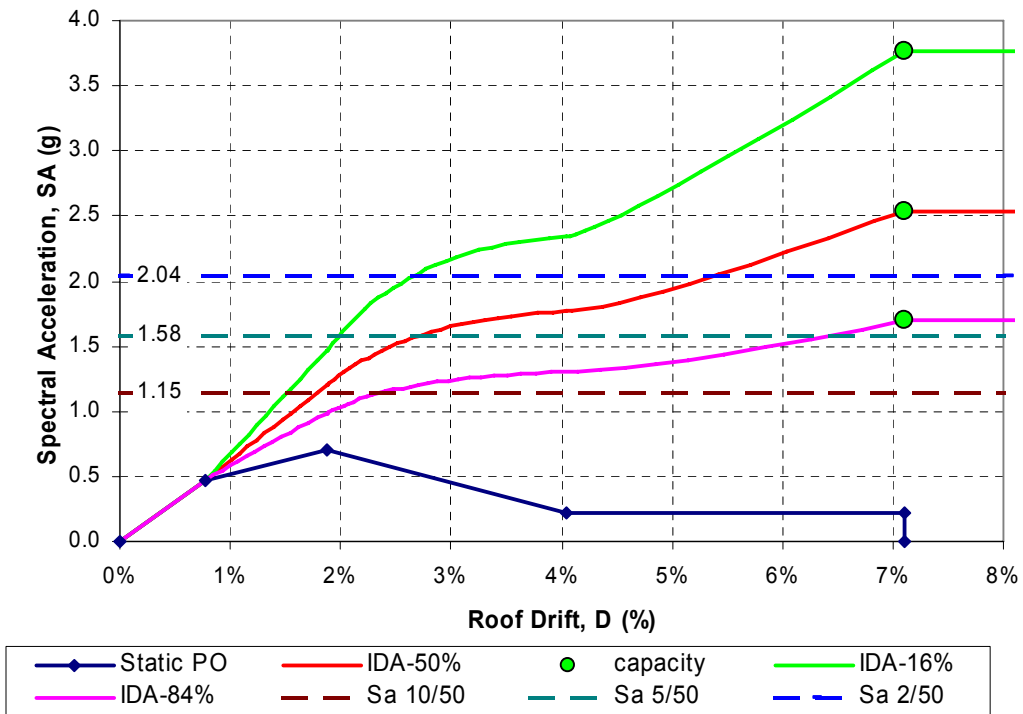


Figure 2.20 DS2 IDA

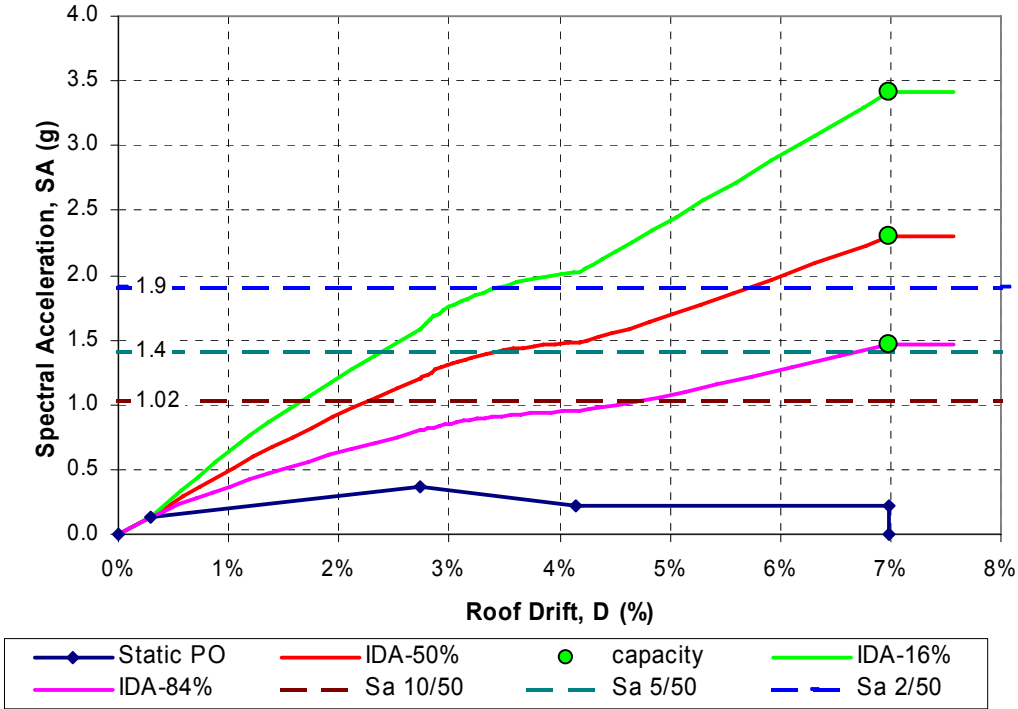


Figure 2.21 DS3 IDA

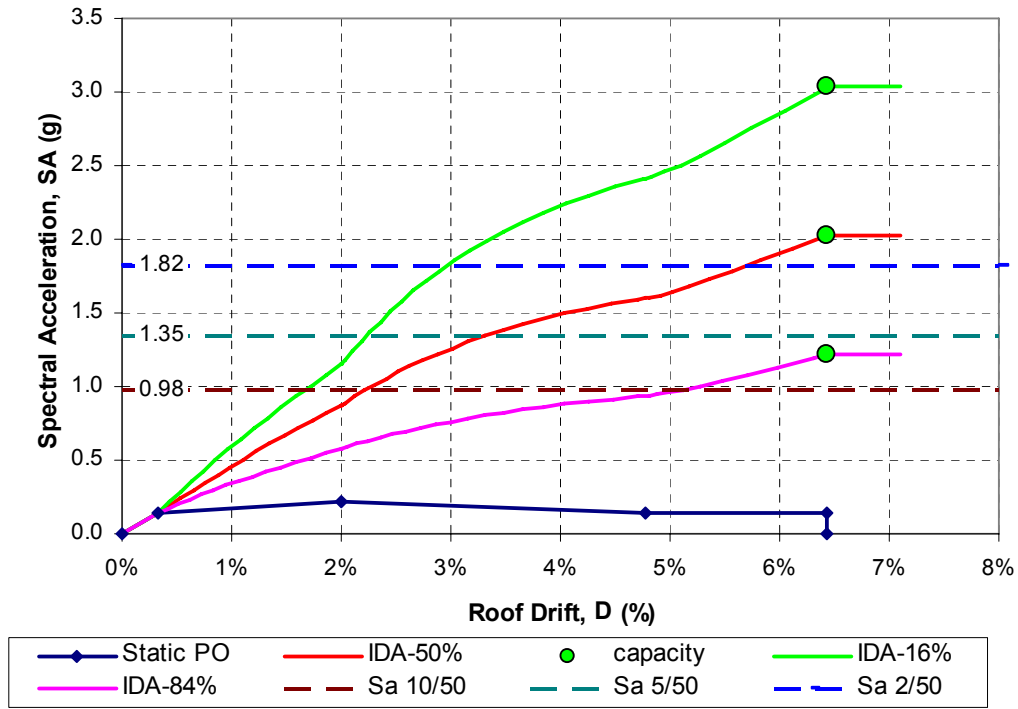


Figure 2.22 DS4 IDA

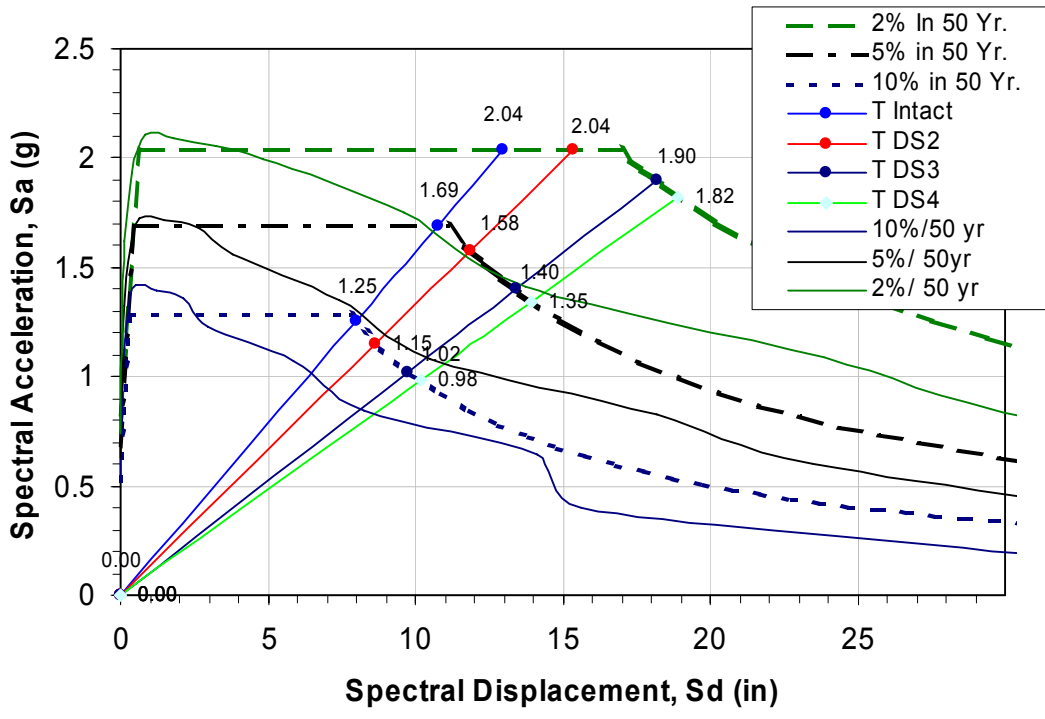


Figure 2.23 Response spectrum of the intact structure and damage states

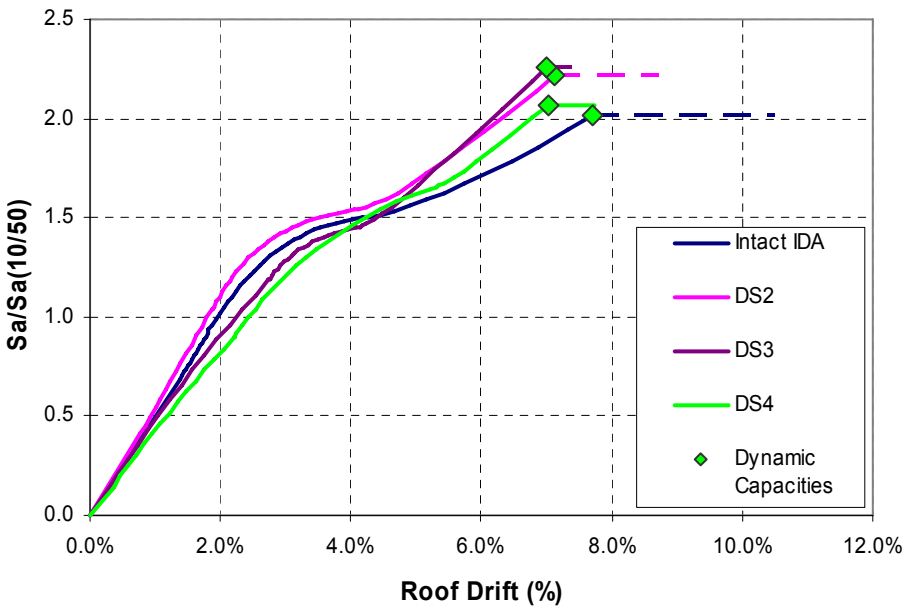
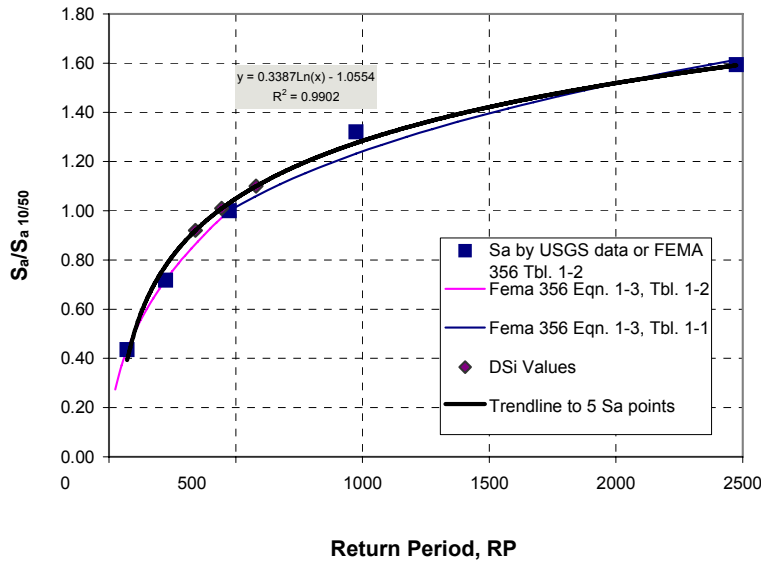


Figure 2.24 IDA, roof drift vs.  $S_a/S_{a(10/50)}$  for the intact structure and damage states



**Figure 2.25 Seismic hazard curve for the building site,  $S_a$  vs. return period**

## 2.5 POST-EARTHQUAKE TAGGING LIMIT STATES

This evaluation uses Tagging Criteria C of the *Guidelines*, which is described in detail in Section 7.2 of this report. Tagging Criteria C defines the onset of yellow tag as the median main-shock acceleration for which an aftershock of the same acceleration will cause collapse in 50 out of 100 ground motions. The onset of red tag is the median main-shock acceleration for which an aftershock having 75% of this acceleration will cause collapse in 50 out of 100 ground motions.

From the data in Table 2.4 the expected tagging for each damage state is determined by plotting  $S_{ai}$ , the spectral acceleration to cause each damage state, versus  $S_{a(cap)}$  the spectral acceleration to collapse the damaged structure. However, first  $S_{a(cap)}$  is normalized to account for the fact that the damaged structure has a longer fundamental period of vibration than does the intact structure. From Table 2.3, the 2%-in-50-year response spectrum plateaus at 2.04g for the intact and DS2 periods, but then it decreases for the periods associated with DS3 and DS4. In order to normalize aftershock accelerations with respect to main-shock accelerations,  $S_{a(cap)}$  values are scaled up by the ratio of the 2%-in-50-year spectral acceleration at the intact structure period to the acceleration at the damaged-structure period. The resulting quantities  $S_{a(cap-\phi)}$  are plotted with respect to  $S_{ai}$  in Figure 2.26.

If  $S_{a(cap-\phi)} / S_{ai}$  is less than 0.75, the damaged structure receives a red tag; if  $S_{a(cap-\phi)} / S_{ai}$  is between 0.75 and 1.0, a yellow tag; if greater than 1.0, a green tag. The main-shock spectral acceleration to cause each tagging limit state is determined by plotting lines with slopes 1.0 and 0.75 that pass through the origin in Figure 2.26. The points A and B, where these lines cross the arc defined by the damage state points, mark the transitions between tagging limit states. The spectral accelerations and corresponding roof displacements at these limit states are listed in Table 2.5.

**Table 2.4 Tagging criteria**

$DS_i$	Roof Drift %	$S_a$ to get to $DS_i$	$S_{a(cap)}$	$S_{a(cap-\phi)}$
Intact	0.00	0.00	2.44	2.44
DS <sub>2</sub>	1.98	1.27	2.55	2.55
DS <sub>3</sub>	3.25	1.76	2.30	2.47
DS <sub>4</sub>	4.04	1.87	2.03	2.28
Collapse	7.50	2.44	0.00	0.00

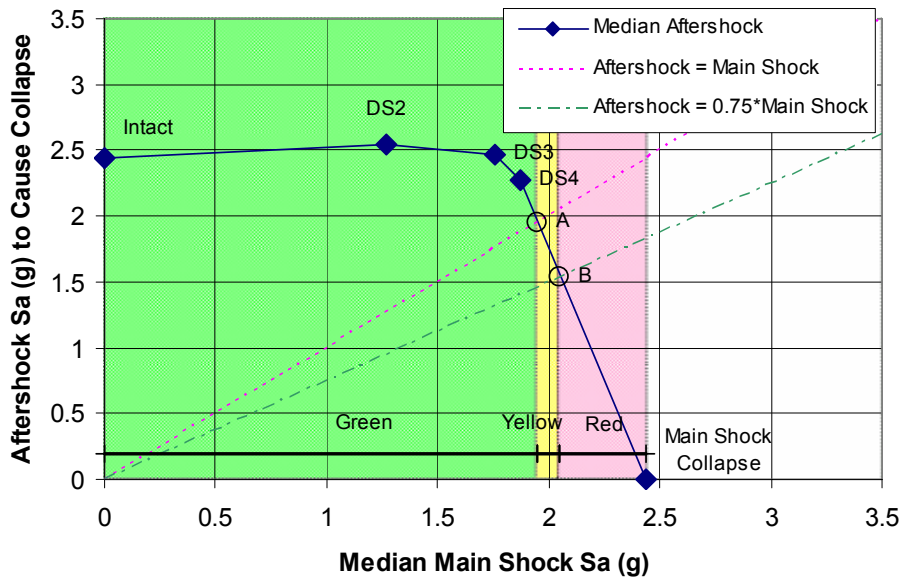


**Figure 2.26 Main shock vs. aftershock to cause collapse, Tagging Criteria C**

**Table 2.5 Median roof drifts and median  $S_a$  corresponding to structural limit states**

Structural Limit State	Onset of Damage	Onset of Yellow	Onset of Red	Collapse
Median Roof Drift	1.38%	5.20%	5.80%	7.50%
Median $S_a$	0.86g	1.95g	2.05g	2.44g

**Table 2.6 Uncertainty values**

<b>Structural Limit State</b>	<b>Onset of Damage</b>	<b>Onset of Yellow</b>	<b>Onset of Red</b>	<b>Collapse</b>
$\beta_u$	0.30	0.60	0.60	0.50
$\beta_r$	0.00	0.25	0.27	0.33
$\beta$	0.30	0.65	0.66	0.60

## 2.6 FRAGILITY CURVES

Based on uncertainty measures for the randomness of nonlinear response in ground motions and the uncertainty of structural capacity ( $\beta_R$  and  $\beta_U$  in Table 2.6), structure fragility curves (Fig. 2.27) provide a probabilistic assessment of spectral acceleration capacity. The quantity  $\beta_R$  measures the variability of nonlinear response in earthquake ground motions and is output by *SPO2IDA* for each roof drift value. As roof drift increases,  $\beta_R$  increases, reflecting the greater uncertainty that is present at large drifts.  $\beta_U$  measures the uncertainty of structural capacity and is dependent on the type of building being analyzed. The uncertainty values  $\beta$  used to compute fragility curves are calculated by taking the square-root sum-of-squares of  $\beta_R$  and  $\beta_U$  for each limit state.

Fragility curves plot probabilities of entering into each tagging state, given a peak spectral acceleration. They assume a lognormal relationship between limit state exceedance probabilities and spectral acceleration. For example, from Figure 2.27, in a ground motion with peak spectral acceleration 2.0g, there is a 52% probability that the building will sustain at least enough damage to receive a yellow tag (48% probability of green tag). For the same peak spectral acceleration, there is a 49% probability that it will reach the onset of red tag, and there is a 38% probability that it will exceed the assumed collapse displacement.



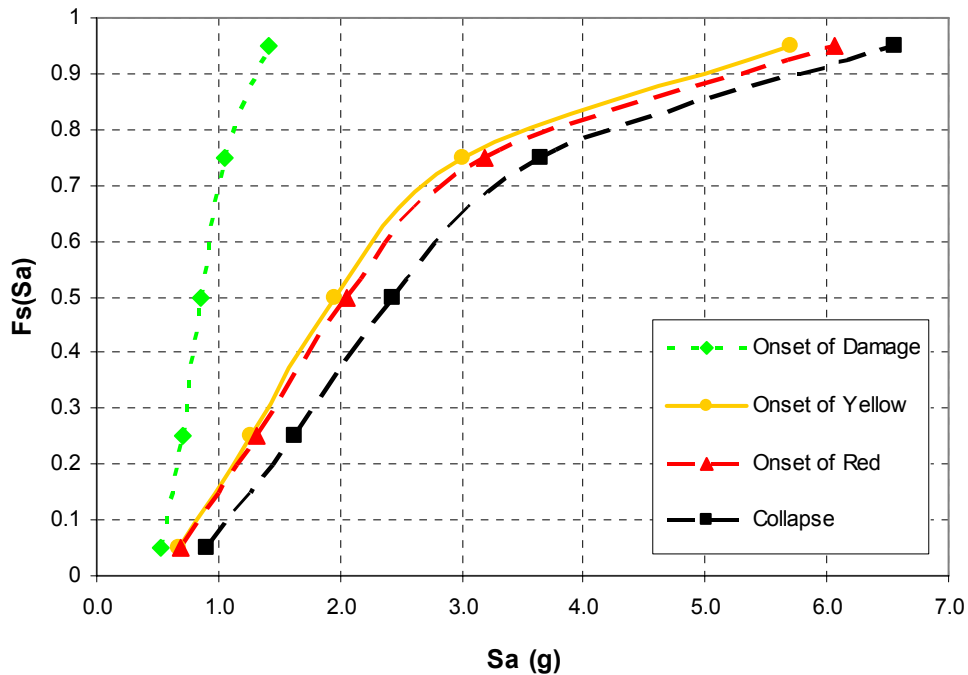


Figure 2.27 Fragility curves

## 2.7 SUMMARY OF STEPS

This section summarizes the steps used in applying the *Guidelines* to the structure of Analysis Run 120. For a description of other analysis runs, see Section 3.1.

### **Step 1: Nonlinear static procedure of the intact building**

- 1.1 Model the structure using *SAP 2000* nonlinear.
- 1.2 Model beam hinges according to FEMA 356 Section 5.5.2.2.2. See Figure 2.5 and Table 2.2 for beam hinge properties.
- 1.3 Obtain SPO for the intact structure.
- 1.4 Define damage states based on points where a significant loss of lateral-force-resisting capacity occurs.

### **Step 2: NSP curves for the damaged building**

- 2.1 Determine the unloading stiffness  $K_i$  using a linear model of the damaged structure in damage state  $DS_i$ . The building is assumed to unload linearly (Fig. 2.12). Construct the

damaged model by reducing the stiffness of damaged beams. For beams whose end connections remain within the elastic or hardening region of the moment-rotation curve (Fig. 2.10), the beam stiffness remains unchanged. For beams whose end connections have “fractured” or gone past point D on the moment-rotation curve (Fig. 2.11), the stiffness decreases to approximate that of a beam with fractured flanges. For a beam that fails on one end, reduce the moment of inertia to  $2/3 I$ ; for a beam that fails on both ends,  $1/3 I$ .

- 2.2 Estimate the dynamic residual displacement  $\Delta_{rd}$ . The residual deformation resulting from SPO unloading is  $\Delta_{rs}$  as shown Figure 2.12. The dynamic residual displacement,  $\Delta_{rd}$ , is estimated to be  $0.3 * \Delta_{rs}$  for this steel moment-frame building.

$$\Delta_{rd} = \gamma_1 * \Delta_{rs}$$

$$(\gamma_1 = 0.3)$$

- 2.3 Determine the effective loss of deformation capacity  $\Delta_{re}$ , which is a function of  $\alpha_i$ . See Table 7.2 for  $\gamma_2$  values for each damage state.

$$\Delta_{re} = \gamma_2 * \Delta_{rd} = \gamma_1 \gamma_2 * \Delta_{rs}$$

- 2.4 Determine the hardening stiffness,  $K_{hi}$ , for the damaged structure based on the ratio of the number of fractured connections to the total number of connections.

$$K_{hi} = (1 - N_f / N_c) * K_{h1}$$

- 2.5 The SPO of the damaged structure meets the SPO of the intact structure at the defined  $DSi$  point and then follows the SPO of the intact structure. Given the two points,  $DSi$  and  $\Delta_{re}$ , and the two slopes  $K_i$  and  $K_{hi}$ , create the SPO curves for the damaged structure (Fig. 2.13).

**Step 3: Inferring dynamic response from static response, SPO2IDA**

- 3.1 Approximate the SPO results from Step 2 into quadrilinear curves (Figs. 2.6–2.9).
- 3.2 Shift the quadrilinear approximation for the damaged structure to account for the effect of residual deformation. Subtract  $\Delta_{re}$  from all deformation capacities on the SPO.
- 3.3 Normalize the SPO by  $\Delta_y$  and  $V_y$ .

$$R = V / V_y \quad \mu = \Delta / \Delta_y$$

- 3.4 Input the SPO approximation into the *SPO2IDA* spreadsheet in terms of  $R$  and  $\mu$ . See (Fig. 2.14) for an example of the *SPO2IDA* spreadsheet interface.

3.5 For the remainder of these steps, use the IDA curves representing the median (50%) for each damage state from *SPO2IDA* output (Figs. 2.15–2.18).

3.6 “De-normalize” the IDA output to plot *Roof Drift* vs.  $S_a$  (Figs. 2.19–2.22).

$$S_a = RV_y/W\alpha \quad \text{Roof Drift} = \mu\Delta_y$$

3.7 To compare the IDA results for the intact structure and each of the damage states on the same graph, normalize the ordinate ( $S_a$ ) values by  $S_{a(10/50)}$  (Fig. 2.24). The SPO for each damage state has a slightly different initial stiffness; therefore it has a different fundamental period of vibration  $T$  and results in different  $S_{a(10/50)}$  values. The  $S_{a(10/50)}$  values are determined for each damage state using the response spectrum for the site. Spectral values for 0.2s and 1.0s are taken from USGS National Seismic Hazard Mapping Project website (<http://geohazards.cr.usgs.gov/eq/index.html>). Soil profile type B is used.  $S_{a(cap)}/S_{a(10/50)}$  is taken as the point on the 50% IDA plot where the curve becomes horizontal.

**Step 4: Occupancy status of the damaged building (Tagging Criteria C)**

4.1 Using the SPO for the intact structure (Fig. 2.6), determine the displacement at which each of the damage states occurs.

4.2 Using the intact IDA curve (Fig. 2.19) and the displacement values from step 4.1, determine the corresponding  $S_{ai}$  for each damage state  $DS_i$ .

4.3 Determine  $S_{a(cap-\phi)_i}$  for each damage state by scaling up  $S_{a(cap)}$  values by the ratio of the 2%-in-50-year spectral acceleration at the intact structure period to the acceleration at the damaged-structure period.

$$S_{a(cap-\phi)_i} = S_{a(cap)_i} (S_{a(2/50)intact} / S_{a(2/50)_i})$$

4.4 Determine tagging states based on the structure’s ability to sustain an aftershock proportional to the main shock.

- Green, if  $S_{a(cap-\phi)_i} / S_{ai} > 1.0$
- Yellow, if  $0.75 < S_{a(cap-\phi)_i} / S_{ai} < 1.0$
- Red, if  $S_{a(cap-\phi)_i} / S_{ai} < 0.75$

4.5 Plot  $S_{a(cap-\phi)}$  vs.  $S_a$  and label tagging limit states (Fig. 2.26).

**Step 5: Ground motion level associated with each structural limit state**

5.1 Onset of damage is taken as the first significant point of yielding.

- 5.2 Determine the  $S_a$  and roof drift levels associated with each structural limit state using the tagging criteria of Figure 2.26 and the intact *SPO2IDA* plot of Figure 2.19.
- 5.3 From the intact *SPO2IDA* spreadsheet, extract the aleatory variability values,  $\beta_r$ , corresponding to the roof drift at each tagging limit state. The epistemic uncertainty values,  $\beta_u$ , are taken from Table 2e of the *Advanced Seismic Assessment Guidelines*. The term  $\beta$  is calculated as the square root sum of the squares of  $\beta_u$  and  $\beta_r$  for each tagging limit state (Table 2.6).

**Step 6: Computation of fragility curves**

- 6.1 Create fragility curves for each tagging limit state using the spectral accelerations and dispersion values  $\beta$  obtained in Step 5 (Fig. 2.27). Fragility curves are plotted for the probability values below, using the relationship described in the *Guidelines*.

$$S_a = S_{at} e^{x\beta}$$

$$x = \{-1.65, -0.67, 0.0, 0.67, 1.65\}$$

$$p = \text{normal distribution}(x) = \{0.05, 0.25, 0.5, 0.75, 0.95\}$$

### 3 Study of Analysis Assumptions for Test Application 1

The evaluation of Test Application 1, reported in Section 2, is based on a series of analysis assumptions considered to be most appropriate. Several variations in analysis assumptions were considered leading up to the selection of assumptions used for the final analysis (identified as Analysis Run 120). The following subsections first examine the effects of varying modeling assumptions in the intact structure, and second examine the effects of varying properties in the damaged structure.

#### 3.1 VARIATION OF ASSUMPTIONS FOR THE INTACT STRUCTURE

For the nonlinear static (pushover) analysis of the intact structure, the evaluation considers variations in foundation stiffness modeling, the vertical distribution of forces used in pushover loading, and the inclusion or exclusion of gravity framing in the analysis model. Table 3.1 summarizes four of the analysis runs used to investigate these variations.

Analysis Runs 120 and 122 are considered the most accurate and appropriate of the variations tested. The remainder of the analysis, described in Section 2, draws on results from Analysis Run 120, which applies story forces in an inverted triangular pattern proportional to that prescribed in the *Uniform Building Code*.

**Table 3.1 Assumptions used in the nonlinear static (pushover) analysis**

<b>Analysis run number</b>	<b>104</b>	<b>110</b>	<b>120*</b>	<b>122</b>
Foundation model:	Fixed	Modeled	Modeled	Modeled
Vertical distribution of forces:	UBC	UBC	UBC	Uniform
Gravity framing included:	No	No	Yes	Yes

\* Used for the final analysis

### **3.1.1 Foundation Modeling**

Analysis Run 104 models moment-frame columns as fixed-base and does not include gravity framing in the model. These simplifying assumptions are appropriate for an initial analysis run.

Analysis Run 110 improves on the fixed-base assumption by including the rotational flexibility of the piles and pile cap foundations underneath each column. Spring elements represent the stiffness of the concrete foundations and their expected movement in the supporting soil under seismic forces.

Figure 3.1 compares the force-displacement response of Analysis Runs 104 and 110. Run 110 exhibits decreased stiffness in the elastic range because it accounts for foundation flexibility. The increase in elastic displacement is 22%. This corresponds to a 10% increase in effective initial period. Strength degradation in the inelastic range tends to occur at a slightly higher displacement for the case where foundation flexibility is modeled. However, as displacement increases, the difference in response for the two cases becomes less pronounced.

### **3.1.2 Inclusion of Gravity Frame**

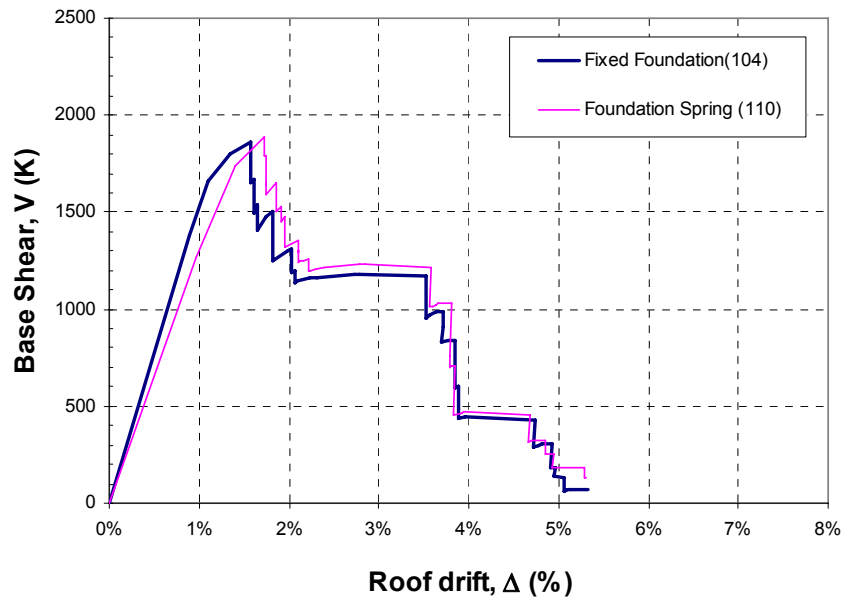
Analysis Run 120 includes gravity framing in the computer analysis model. As mentioned in Section 2.2, plastic hinges modeled in gravity beams have flexural strength equal to that estimated for their shear-tab connections.

Figure 3.2 compares the force-displacement response of Analysis Runs 110 and 120. Run 120 exhibits greater stiffness in the elastic range than Run 110 does. Also, Run 120 exhibits residual strength at high roof drifts because the gravity frames continue to provide lateral force resistance after beam flanges in the moment frames have fractured.

### **3.1.3 Vertical Distribution Pattern of Seismic Forces**

Analysis Run 122 applies a uniform distribution of story forces rather than the UBC's inverted triangular pattern applied in previous runs. Typically in a nonlinear static analysis, the uniform distribution is more likely to concentrate deformations in the lower stories of the structure because it applies relatively smaller lateral forces to the upper levels of the structure.

Figure 3.3 compares the force-displacement response of Analysis Runs 120 and 122. Run 122 exhibits smaller roof drifts than does Run 120 because the uniform force distribution causes smaller story drifts in the upper stories. Columns are sufficiently strong with respect to beams that neither force distribution results in a concentration of nonlinear deformation in a single story.



**Figure 3.1 Comparison of intact structure force-displacement curves showing the effect of foundation flexibility**

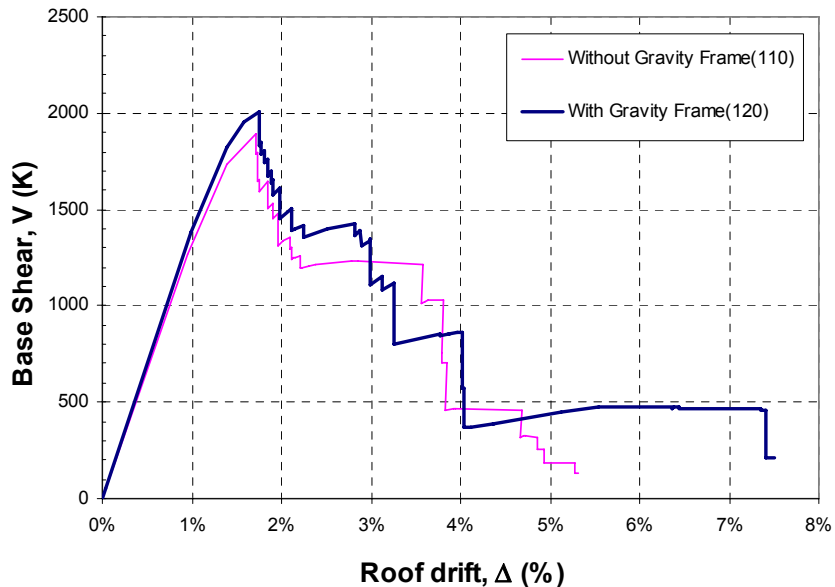


**Figure 3.2 Comparison of intact structure force-displacement curves showing the effect of the gravity frame**

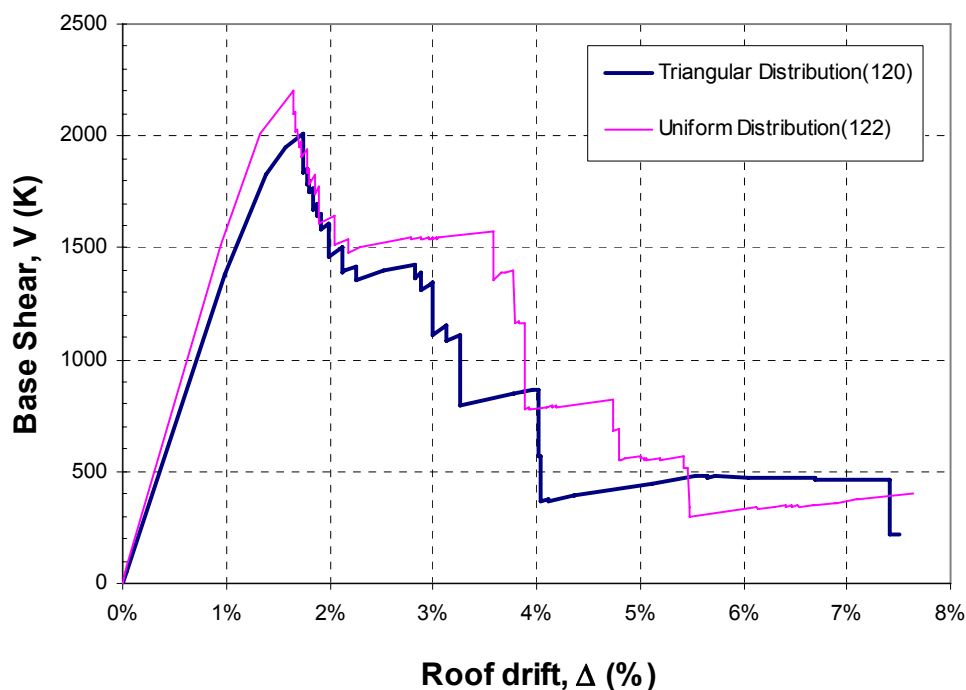


**Figure 3.3 Comparison of intact structure force-displacement curves showing the effect of the vertical distribution pattern of lateral forces**

### 3.2 VARIATION IN ASSUMPTIONS FOR THE DAMAGED STRUCTURE

The analysis of the damaged structure reported in Section 2 assumes, from FEMA 356 component properties and the nonlinear static analyses, that the post-fracture plateau strength of the structure at large displacements is 46% of the yield strength (Figs. 2.6–2.9). Limited test data on steel moment frames at large displacements make it difficult to judge the accuracy of this assumption. The analysis further assumes that the effective residual drift is equal to 0.3 times the static residual drift — that which results from unloading the structure statically from its peak drift. The randomness of earthquake ground motions make this quantity difficult to predict. (See Section 7.1 for further discussion of residual drift.) To assess the significance of these assumptions, analyses are carried out with varying values of post-fracture plateau strength and effective residual drift. The following parameter studies assess the effects and significance of each quantity on the building’s inferred dynamic behavior.



### 3.2.1 Post-Fracture Plateau Strength

Little scientific testing data exist to document structural performance at very large drifts. In this analysis, the residual plateau strength depends on whether or not gravity frames are modeled, the modeled strength of gravity frame components, and the post-fracture strength assigned to moment-frame connections.

Based on Analysis Run 120, the analysis predicts a post-fracture plateau strength equal to 46% of the DS2 yield strength (Fig. 3.4). Also plotted in Figure 3.4 are three alternative force-displacement curves with post-fracture plateau strengths of 60%, 20%, and 10% of the DS2 yield strength.

Figure 3.5 compares the inferred dynamic behavior from *SPO2IDA* for each input force-displacement relationship from Figure 3.4. As expected, greater values of post-fracture plateau strength require greater spectral acceleration to cause collapse. For example, changing the post-fracture plateau strength from 10% to 60% of the structure yield strength increases the spectral acceleration required to cause collapse by 24%.

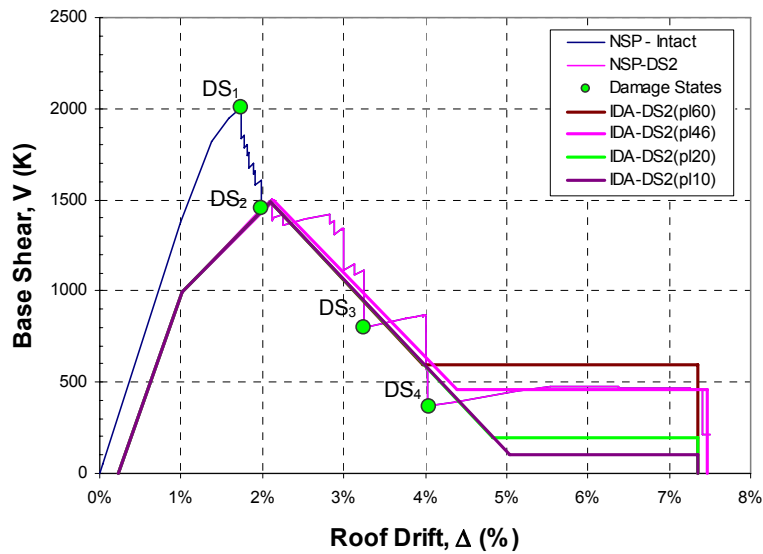
### 3.2.2 Effective Residual Drift

Residual drift and its effect on damaged-structure performance depend on the randomness of earthquake ground motions and whether or not aftershock accelerations act in the same direction as the structure's residual drift from the main shock. Since earthquakes shake structures back and forth rather than applying force in only one direction, dynamic residual drifts tend to be smaller than static residual drifts for the same peak base shear. Section 7.1 discusses residual drift in further detail.

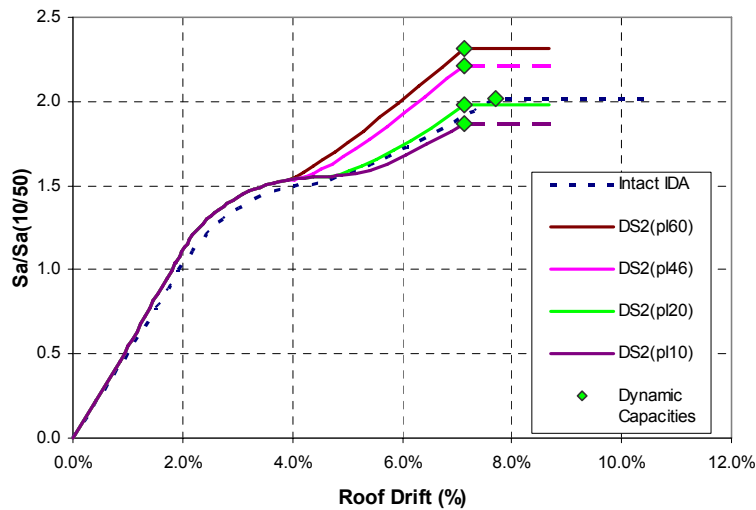
The analysis presented in Section 2 assumes that the structure's effective dynamic residual drift is 0.3 times the static residual drift. Figure 3.6 plots the DS2 force-displacement curve used in Section 2 along with three alternative curves that assume effective dynamic residual drifts of 0.1, 0.5, and 0.7 times the static residual drift.

Figure 3.7 compares the inferred dynamic behavior from *SPO2IDA* for each input force-displacement relationship from Figure 3.6. The output does not exhibit a clear trend relating effective residual drift to collapse potential in an aftershock. This result arises because, following the methodology described in Section 2.3, decreasing the assumed residual drift also

decreases the assumed yield base shear of the damaged structure as shown in Figure 3.6. Increasing the total displacement capacity is expected to increase the spectral acceleration required to cause collapse, while decreasing the yield base shear will decrease the spectral acceleration required to cause collapse. Therefore, when both of these two variables change, their effects on spectral acceleration capacity partially offset one another. Within the range of effective residual drifts examined, the resulting spectral acceleration capacities are all within 10% of one another.



**Figure 3.4 Force-displacement curves for damage state DS2, with different estimates of post-fracture plateau strength**



**Figure 3.5 Incremental dynamic analysis (IDA) results as influenced by post-fracture plateau strength**

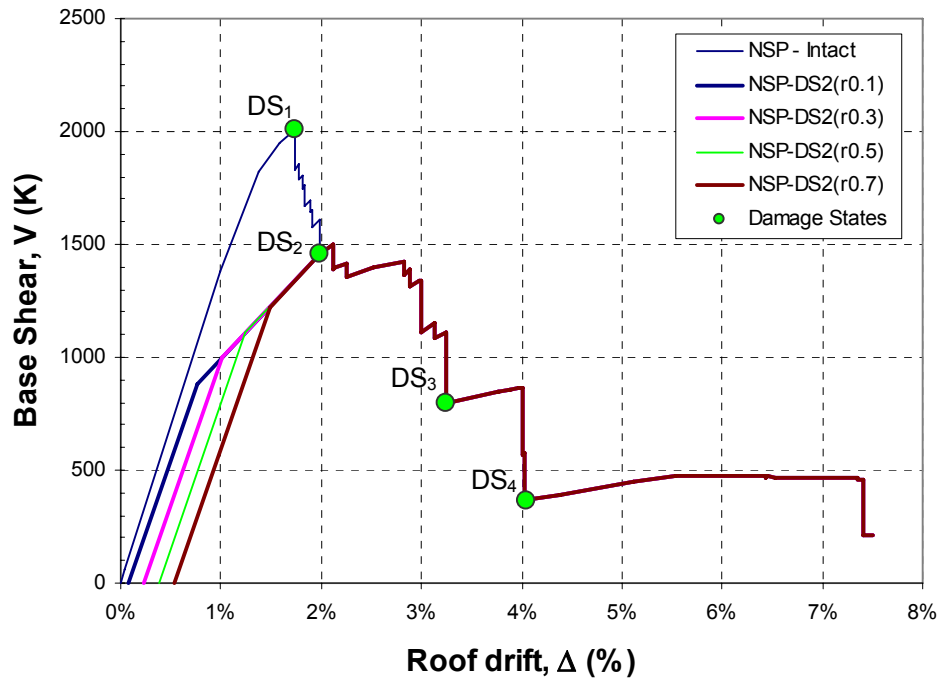


Figure 3.6 Force-displacement curves for damage state DS2, with different estimates of effective residual drift  $\Delta_{re}$

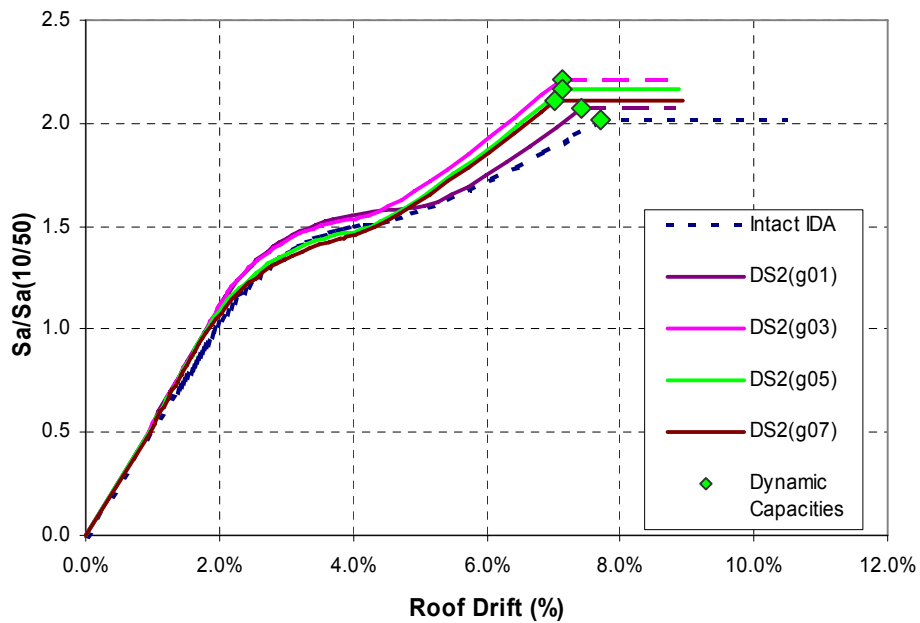


Figure 3.7 Incremental dynamic analysis (IDA) results as influenced by effective residual drift  $\Delta_{re}$

## 4 Test Application 2: Mill Building

This section presents the second of the two test applications of the *Advanced Seismic Assessment Guidelines* featured in this report. Similar to Section 2, this section includes a description of the structure (4.1), followed by subsections (4.2–4.6) that discuss the major parts of the Advanced Seismic Assessment process for this building: evaluation of the intact structure, evaluation of the damaged structure, determination of dynamic behavior, definition of post-earthquake tagging limit states, and computation of fragility curves.

Because the structural system assessed in Test Application 2 is different from that of Test Application 1, the analysis methods applied here differ from those used for Test Application 1. Both cases illustrate compatibility between the methodology of the *Guidelines*, the building types being assessed, and the analysis methods used.

### 4.1 DESCRIPTION OF THE STRUCTURE

The second example is a substation building, designed in 1921, of a type referred to as a mill building. The building has an open interior framed with exposed steel columns and trusses, which provide gravity support. The exterior walls of the building are cast-in-place concrete and provide the building's resistance to seismic forces.

The drawings that describe the original building, provided by PG&E, are listed in Table 4.1. The building has a regular configuration with a rectangular plan measuring 94 feet by 42 feet, as shown in Figure 4.1. The building was designed so that a 37-foot-long addition could be constructed at each end, which would have increased the building size to 168 feet by 42 feet. The additions were never built. (New equipment at the substation has generally been added outdoors, so new building space was not needed.) Figure 4.2 shows the exterior and part of the interior of the building.

**Table 4.1 Construction drawings for the mill building of Test Application 2**

Topic	Drawing Numbers	Date
Structural steel framing plans and details	34768, 34769	8 October 1920
Foundation plan	34697	23 August 1921
Plans, elevations, sections, and details	34746–34754	17 September 1921
Reinforcement plan for walls	41179	24 September 1921

#### 4.1.1 Steel Framing

The left half of Figure 4.1 shows the steel framing that forms a hip roof. Roof trusses span across the short direction of the building and support hip trusses and 8-inch I-beam purlins. The truss members are typically double angles connected with gusset plates, stitch plates, and rivets. The rivets are  $\frac{3}{4}$ " diameter installed in  $\frac{13}{16}$ " diameter holes. Most of the rivets are shop installed, which the drawings indicate with open circles. At the field splices of the steel assemblies, the drawings show filled circles to indicate field rivets.

The roof framing allows an open interior, with columns on the building perimeter. Twelve main columns support the roof trusses. The columns are built-up sections approximately 10 inches square, consisting of a 10" x  $\frac{5}{16}$ " web plate riveted to four 5" x  $3\frac{1}{2}$ " x  $\frac{5}{16}$ " angles. See Figure 4.2(c). Each column is has four anchor bolts at the base, 1" diameter by 2'-6" long. Three additional columns, 8" wide-flange sections, support the 15" deep I-beams at the north and south eaves of the building. Two columns are at the south end and one column is at the north end. These columns have two anchor bolts each.

At the east and west eaves, in the building longitudinal direction, trusses span between the columns forming "sway frames." The end bays in the longitudinal direction also have angle bracing in a chevron configuration, with  $2\frac{1}{2}$ " x 2" x  $\frac{1}{4}$ " single angles, as shown in Figure 4.3. Along the ridge of the building, a "ridge sway frame" is created with trusses connecting between the building transverse trusses.

#### **4.1.2 Foundation**

The building foundation consists of spread footings under each column, connected by a continuous 12" x 18" grade beam around the building perimeter. The grade beam has longitudinal reinforcement consisting of four 7/8" square bars. The footings have tapered sides so that they form a truncated pyramid shape. No reinforcement is shown for the footings. There is a 4" slab on grade, presumably unreinforced and not connected to the foundation.

#### **4.1.3 Roof**

The steel roof purlins support a 5" thick concrete roof slab reinforced with 4" x 16" #6/10 "Clinton Fabric" (i.e., welded wire reinforcement.) For gravity loads, the roof slab spans one way between purlins, apparently with 6-gage wires (area 0.029 in<sup>2</sup>) at a 4-inch spacing parallel to the span, and 10 gage wires (area 0.014 in<sup>2</sup>) at a 16-inch spacing perpendicular to the span. The roof is topped with clay tile, and two skylights in the western slope of the roof penetrate the 5" slab.

#### **4.1.4 Walls**

The building's exterior walls are 6-inch-thick reinforced concrete. The reinforcement is specified as square "corrugated bars." The walls are typically reinforced with a single curtain of 3/8" square bars at a spacing of 12 inches in each direction. The walls connect to the perimeter grade beam with 1/2" x 3'-0" dowels at a 2'-0" spacing.

The concrete mix is specified as "1-2-4" apparently specifying the relative amounts of cement to sand to gravel. This indicates that cement represents 1/7, or 14%, of the total volume of dry ingredients. For comparison, in current construction a typical 5-sack mix with design strength 3000 psi contains cementitious material (cement plus fly ash) that represents 9% of the total dry volume.

#### **4.1.5 Connections between Concrete and Steel Elements**

The apparent construction sequence of the structure was to first build the foundation, then erect steel framing, and then construct the concrete walls and roof. Portions of the steel framing, including the outer column flanges are embedded in the concrete walls. The inside face of the concrete wall is approximately flush with the inside of the outer column flange. The longitudinal trusses connect to each column at this outer flange, and thus one angle of each double-angle member is embedded in the concrete wall. The single-angle chevron braces are also embedded in the concrete wall. Because of the embedded steel members, full composite action between the steel framing and the concrete walls is expected, meaning that the steel members can be assumed to act like reinforcement in the walls.

#### **4.1.6 1996 Seismic Retrofit**

The building was retrofitted in 1996 with the following items:

- steel bracing members at the roof that strengthen the roof diaphragm
- steel braced frames at the two short walls of the building, which provide lateral force resistance for earthquake shaking in the building transverse direction
- horizontal steel members between columns that support the existing concrete walls out of plane

The retrofitting addressed the principal seismic deficiencies of the building, which were generally related to transverse direction earthquake forces. The evaluation described in this document assesses the seismic performance for longitudinal direction seismic forces. This performance is governed by the in-plane behavior of the longitudinal walls, which was not affected by the 1996 retrofit work. (As indicated in Section 4.6, the results of this evaluation verify that retrofit work for the building longitudinal direction is not required.)

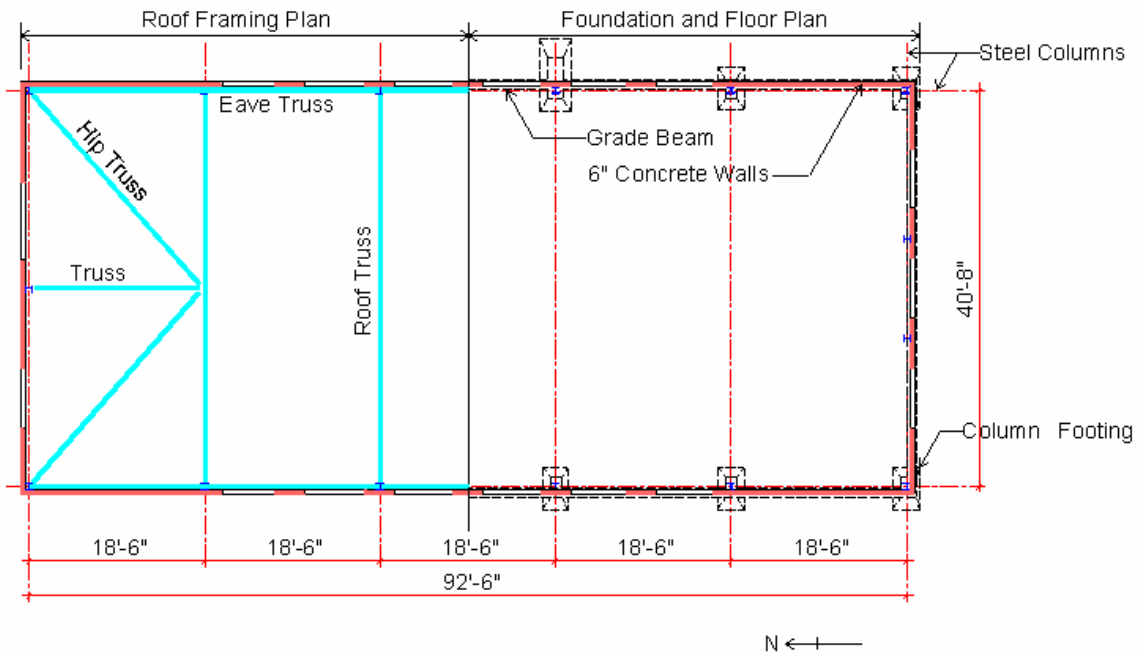


**Figure 4.1 Roof framing, foundation, and floor plan of the building**



(a)



(b)



(c)



**Figure 4.2 Photos of the building: (a) exterior; (b) interior showing existing steel framing, added horizontal steel beam for wall out-of-plane support, and added steel members for roof diaphragm bracing; (c) close up of existing steel column made up of four angles riveted to a web plate.**

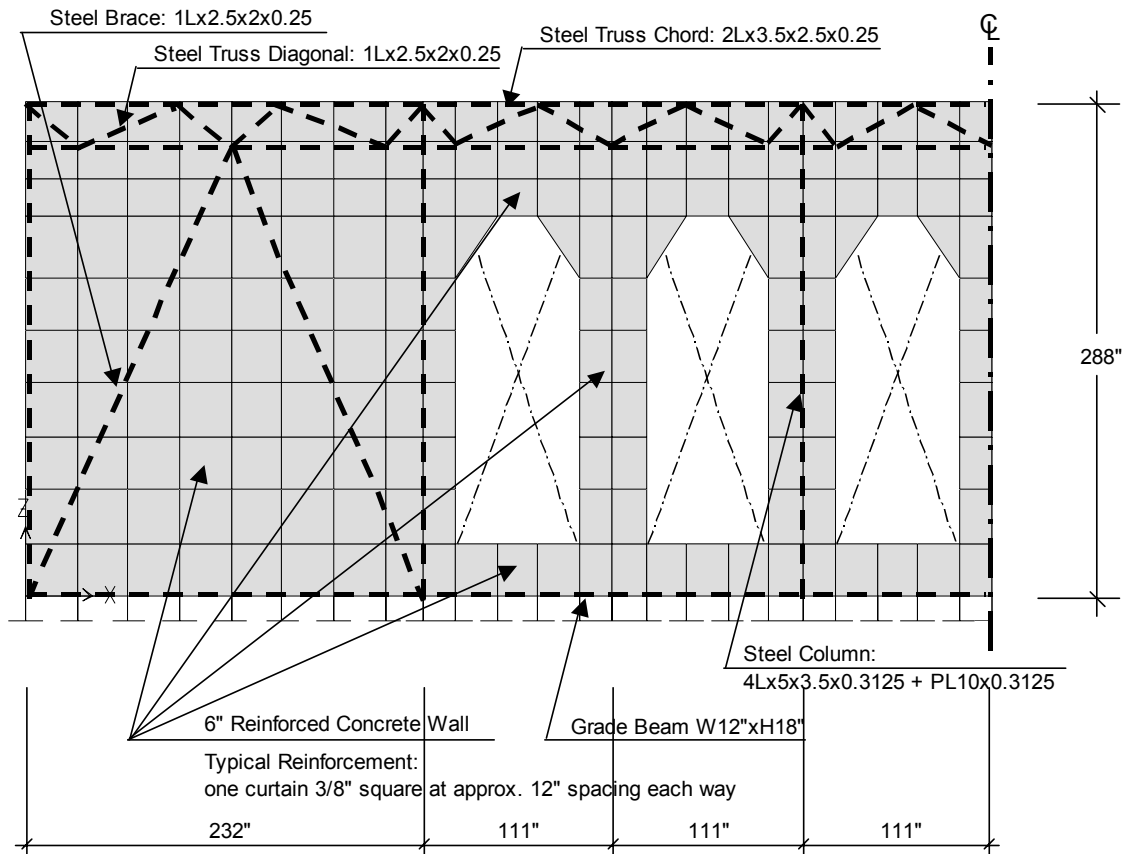


**Figure 4.3 Summary of structural design and dimensions (*RAM Perform* model)**

**Table 4.2 Expected material strength properties (year of construction =1921)**

Material	Expected Strength	Basis
Structural Steel	$f_y = 30.8$ ksi	From FEMA 356 tables 5-2 and 5-3: 28ksi*1.1
Concrete	$f'_c = 3750$ psi	From FEMA 356 tables 6-3 and 6-4: 2500psi*1.5
Reinforcing Steel	$f_y = 41.3$ ksi	From FEMA 356 tables 6-1 and 6-4: 33ksi*1.25

## 4.2 SEISMIC EVALUATION OF THE INTACT STRUCTURE

For simplicity in this example, the analysis examines the building's resistance to seismic shaking only in the longitudinal (north-south) direction. In a complete seismic evaluation, a similar procedure would be applied to the transverse (east-west) direction.

The building's rectangular plan and symmetrical wall configuration allow us to capture the structure's global performance in the longitudinal direction by analyzing the lateral-force-resisting behavior of one wall line, loaded with half of the building's suspended mass. Two

different two-dimensional computer analysis models were used (programs *SAP 2000* and *RAM Perform*) to evaluate the structure's expected behavior under seismic forces.

#### 4.2.1 SAP 2000 Nonlinear Static Analysis Using Sequential Elastic Analyses

A series of elastic analyses were carried out using the program *SAP 2000* to produce an initial estimate of the sequence of yielding under lateral forces. The *SAP* model, shown in Figure 4.4, consists of shell elements representing the concrete wall, and frame elements representing the steel columns and braces. The model sits on no-tension foundation springs. Figure 4.5 summarizes the loads and element properties that are input into the model as well as the calculated strengths of each concrete element. Shear strength calculations follow the methodology described in FEMA 306 (ATC 1999a), which, based on the work of Priestley et al., considers the degradation of shear strength as a function of ductility and includes the beneficial effect of axial compression on shear strength. For sliding shear, the ACI 318 (ACI 2005) equations for shear friction are used.

To determine a yielding sequence, lateral force is increased on the elastic model until an element reaches its yield strength or the foundation begins to uplift. When one of these events occurs, the lateral force and displacement is noted. The stiffness properties of the yielding element are then modified and the process is repeated until a plastic mechanism forms. Figures 4.6–4.7 document the results of this procedure. This type of analysis was performed only for the intact structure.

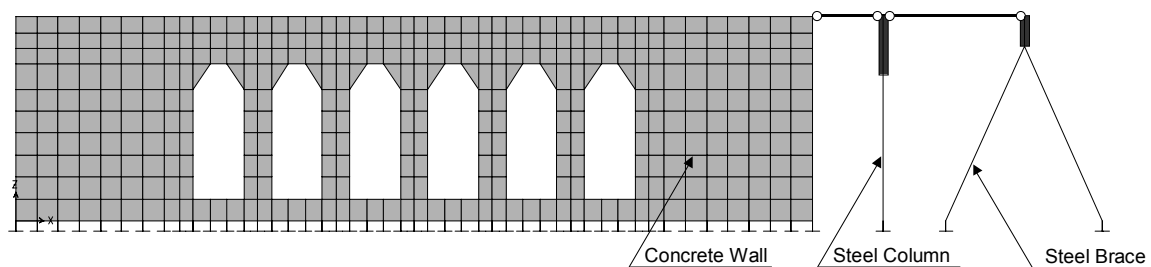
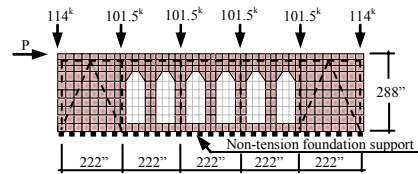


**Figure 4.4** *SAP 2000* computer analysis model

Model: SAP Planar shell element model on non-tension foundation  
 Weight (1/2 of bldg): 360(k)  
 Roof displacement(1g): 0.054(in)  
 Stiffness: 6679(k/in)  
 Period: 0.074(sec)  
 f'c: 3750(psi)  
 fy: 30.8(ksi)



**-Hand Calculations for strength-**

- A) Concrete wall pier without steel column (3 total):
- DL assuming concrete wall pier taken roof load = 23.0(k)
  - $M_{CR}$ (cracking strength) = 715(k-in)
  - Mn(flexural strength at DL=23.0k) = 59(k-ft)= 710(k-in)
  - V\*(shear corresponding to Mn) = 28.1(k)
  - Shear strength in diagonal tension (DL=33.8k):
    - Low ductility = 38.0(k)
    - High ductility = 20.4(k)
  - Sliding shear strength = 23.4(k)
  - $(Ec)_{eff} = (EI)_{eff} / I_{gross} = 589(ksi) \rightarrow 0.3EcIg$
- B) Concrete wall pier with steel column (2 total):
- DL assuming concrete wall pier taken roof load = 50.0(k)
  - Mn(flexural strength at DL=50.0k) = 307(k-ft)= 3680(k-in)
  - V\*(shear corresponding to Mn) = 45.5(k)
  - Shear strength in diagonal tension (DL=33.8k):
    - Low ductility = 82.0(k)
    - High ductility = 25.8(k)
  - Sliding shear strength = 152(k) (limit 650psi)
  - $(Ec)_{eff} = (EI)_{eff} / I_{gross} = 1880(ksi) \rightarrow 0.6EcIg$

- C) Concrete wall segment 20'-long with steel column and brace:
- DL assuming concrete wall pier taken roof load = 81.4(k)
  - Mn(flexural strength at DL=81.4k) = 9320(k-ft)= 112000(k-in)
  - V\*(shear corresponding to Mn) = 1380(k)
  - Shear strength in diagonal tension (DL=81.4k):
    - Low ductility = 535(k)
    - High ductility = 248(k)
  - Shear strength in diagonal tension (Ne=146k ):
    - Low ductility = 650(k)
    - High ductility = 364(k)
  - Shear strength in diagonal tension (Ne=-117k ):
    - Low ductility = 443(k)
    - High ductility = 156(k)
  - Sliding shear strength = 936(k) (limit 650psi)
  - $(Ec)_{eff} = (EI)_{eff} / I_{gross} = 0.6EcIg$
  - First foundation uplift = 48.6(k)
  - Uplift of entire end wall = 113, 369(k)

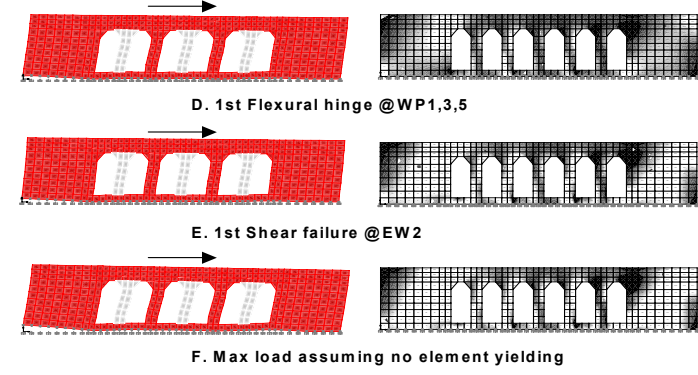
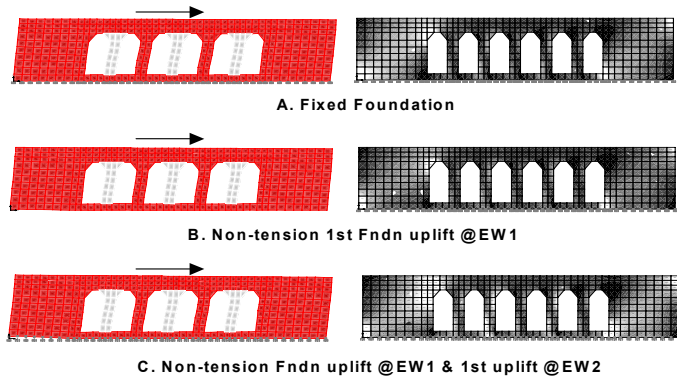
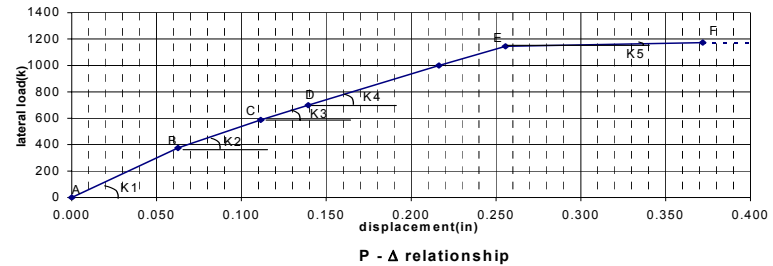
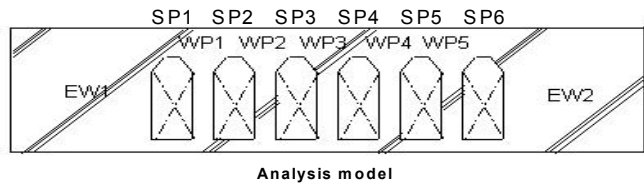
- D) Concrete roof diaphragm (5''):
- At a section through skylights
- Shear strength in diagonal tension:
    - Low ductility = 580(k)
    - High ductility = 177(k)
  - Sliding shear strength = 679(k)
  - Diaphragm shear demand at 1g lateral force = 116(k)
- At Wall
- Shear strength in diagonal tension:
    - Low ductility = 1090(k)
    - High ductility = 331(k)
  - Sliding shear strength = 1272(k)
  - Diaphragm shear demand at 1g lateral force = 296(k)

- E) Concrete spandrel (6''):
- Shear strength in diagonal tension:
    - Low ductility = 130(k)
    - High ductility = 55.5(k)
  - Sliding shear strength = 257(k) (limit 650psi)
  - Flexural strength(Mu) = 14840, 5770(k-in)
  - $V_{Mu}$  = 286(k)

**Figure 4.5 Summary of dead load and strength calculations for the mill-building example**

**Force Distribution on Non-tension foundations**

Case	Lateral load at zero uplift	$\Delta$ (in) Kn(k/in)	Force distribution(kip)					Shear force(kip)							
			EW1	EW2	WP1	WP2	WP3	WP4	WP5	SP1	SP2	SP3	SP4	SP5	
A	Fixed Foundation	360k(1.0g) (100%)	0.054 (6679)	169 (47%)	169 (47%)	3.4 (0.9%)	6.1 (1.7%)	3.4 (0.9%)	6.1 (1.7%)	3.4 (0.9%)	34.8	9.7	8.0	8.0	9.7
B	Non-tension 1st Fndn uplift @EW 1	376k (100%)	0.063 (5997)	168 (44%)	183 (47%)	4.0 (1.8%)	6.3 (1.7%)	3.9 (1.7%)	6.5 (1.7%)	4.0 (1.8%)	37.1	9.7	9.5	8.4	11.4
C	Non-tension Fndn uplift @EW 1 & 1st uplift @EW 2	587k (100%)	0.111 (4340)	233 (40%)	311 (53%)	7.1 (1.2%)	10.9 (1.9%)	6.7 (1.1%)	10.9 (1.9%)	7.1 (1.2%)	57.1	15.0	17.7	13.4	20.5
D	1st Flexural hinge @WP1,3,5	700k (100%)	0.139 (4026)	271 (39%)	375 (54%)	8.9 (1.3%)	13.6 (1.9%)	8.3 (1.2%)	13.6 (1.9%)	9.1 (1.3%)	68.7	17.9	22.6	16.2	26.4
E	1st Shear failure @EW 2	1146k (100%)	0.256 (3835)	416 (36%)	632 (55%)	17.0 (1.5%)	24.6 (2.2%)	14.1 (1.2%)	24.4 (2.1%)	17.6 (1.5%)	116.7	34.5	38.4	25.5	51.1
F	Max load assuming no element yielding	1174k (100%)	0.372 (242)	421 (36%)	653 (56%)	17.6 (1.5%)	24.9 (2.1%)	14.2 (1.2%)	24.7 (2.1%)	18.2 (1.5%)	151.3	20.3	38.2	5.1	21.5



Deformation and stress

Figure 4.6 Force-displacement curve developed from the linear *SAP 2000* model neglects spandrel degradation

**Reaction force of Non-tension foundations**

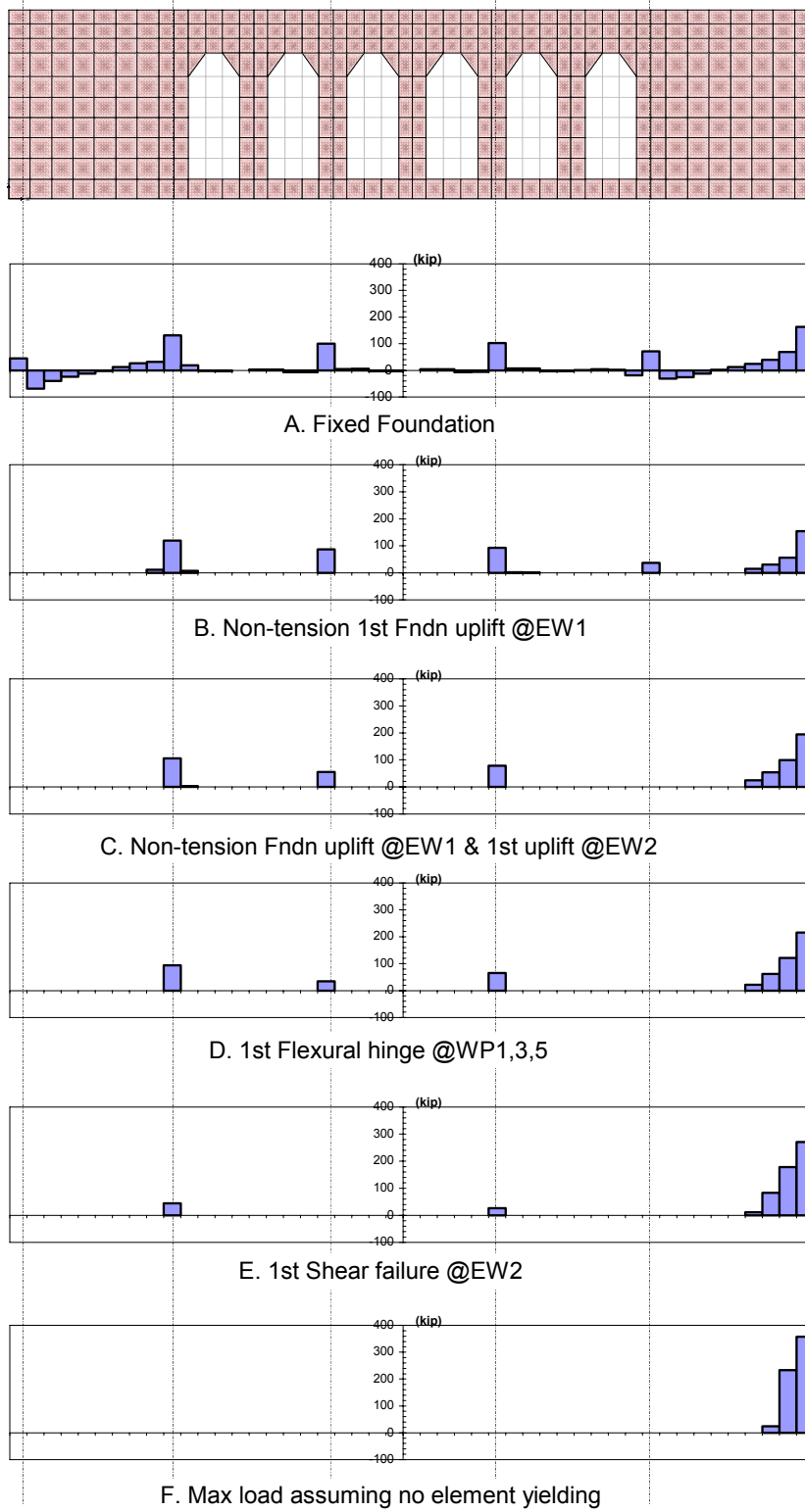


**Figure 4.7 Foundation reaction forces from *SAP 2000* model**

## 4.2.2 RAM Perform Nonlinear Static Analysis

As a more sophisticated alternative to the analysis described above, a nonlinear static analysis using the program *RAM Perform* generates a nonlinear force-displacement response (pushover) plot for the structure. The *RAM Perform* model consists of finite elements representing the concrete wall, and frame elements representing the steel columns and braces. Unlike the *SAP* model's shell elements, finite elements in the *RAM Perform* model have the capability of modeling nonlinear stress-strain behavior. Table 4.3 summarizes the element properties input into the model, and Figure 4.8 depicts the nonlinear stress-strain "backbone" curves assigned to each structural material. Shear strength calculations again follow FEMA 306, and no-tension foundation springs again represent soil stiffness while allowing for uplift.

Performing a nonlinear static analysis with this model generates the deflected shapes for the structure as shown in Figure 4.9. Figure 4.10 displays the nonlinear force-displacement curve from the analysis, along with a comparison of hand-calculated element strengths to peak values obtained from computer analysis. Figure 4.11 graphs the foundation reaction forces corresponding to several different roof drifts. The foundation forces shown in this diagram indicate that foundation rocking of the solid end walls ultimately governs the wall behavior.

**Table 4.3 Concrete wall *RAM Perform* input properties**

Reinforcing Steel	$K_0 = 29,000 \text{ ksi} (= E_s)$ $F_U = 41.3 \text{ ksi} (= f_y)$
Inelastic Concrete Material	$K_0 = 3,491 \text{ ksi} (= E_c)$ $F_U = 3.75 \text{ ksi} (= f'_c)$ $D_L = 0.003$ $D_R = 0.006$ $F_R/F_U = 0.2$
Inelastic Shear Material	$K_0 = 580 \text{ ksi} (= G_{eff} = 0.17E_c = 10\rho E_s)$ $F_U = 0.75 \text{ ksi} (= 12.2\sqrt{f'_c})$ $D_L = 0.0075 (\mu = 5.8)$ $D_R = 0.0085 (\mu = 6.6)$ $F_R/F_U = 0.4$
Diagonal Compression Material	Same as inelastic concrete material

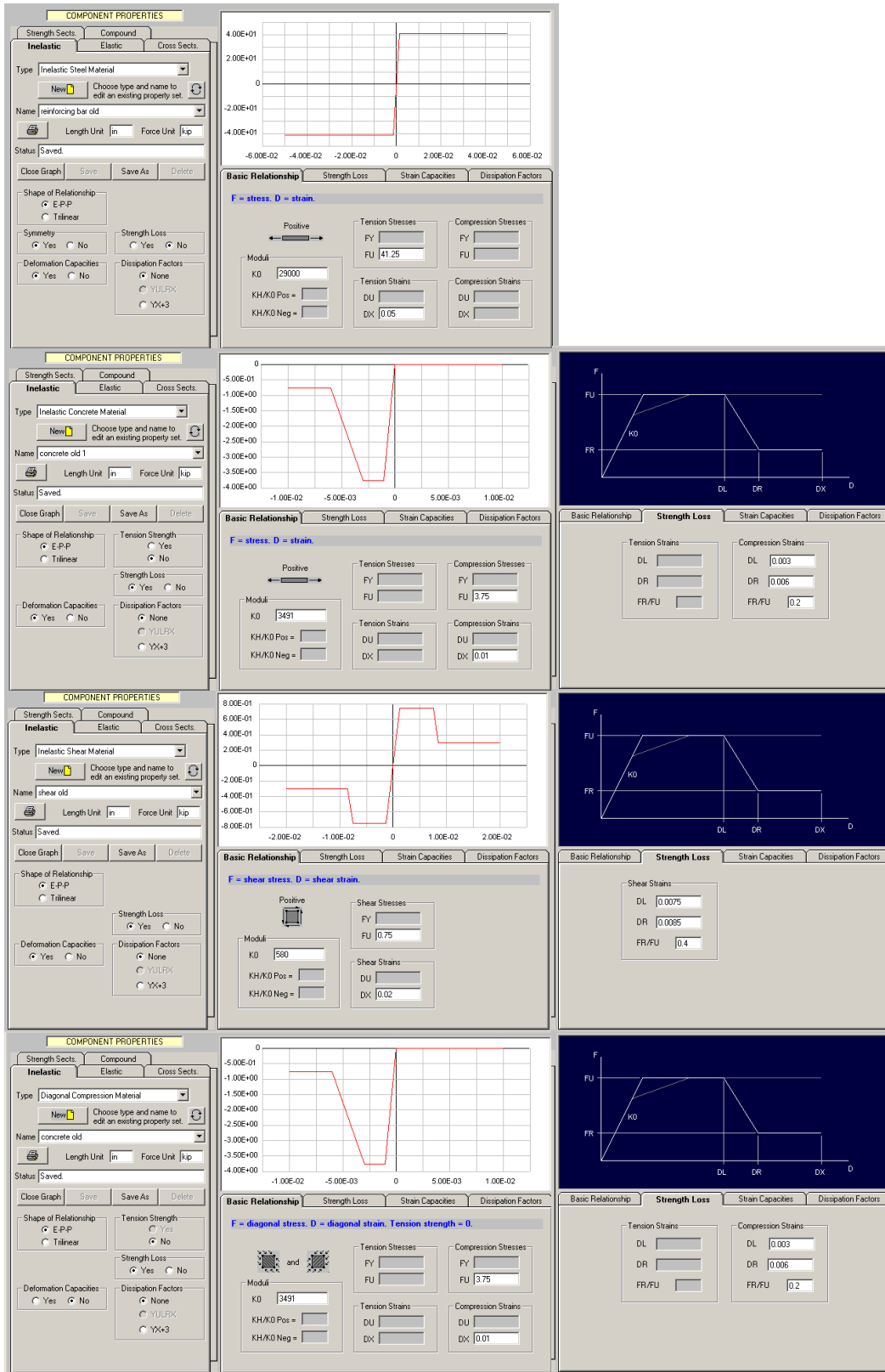
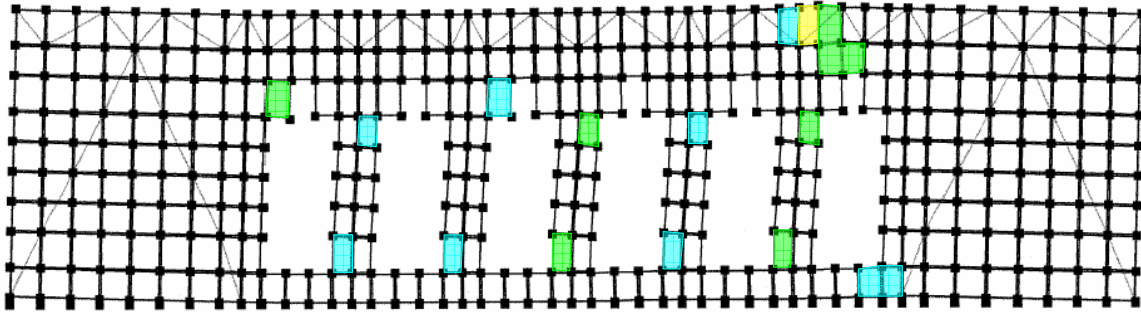


Figure 4.8 Ram Perform input properties for the intact structure



(a)



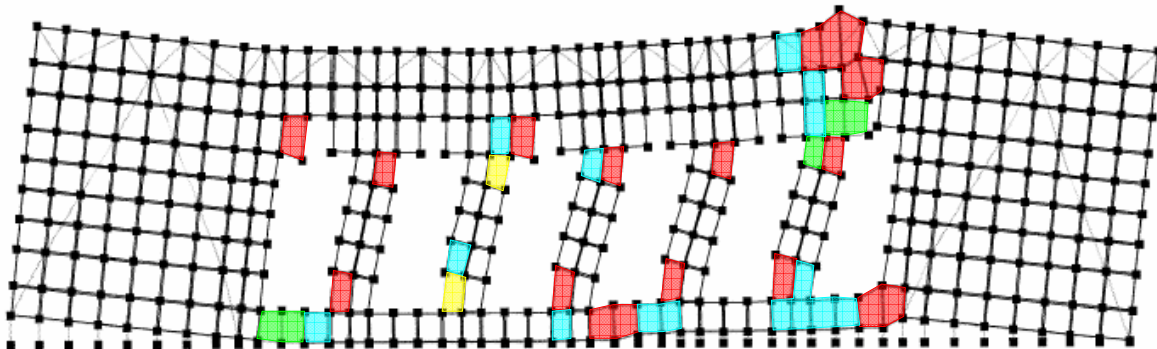
DEFLECTED SHAPE SHOWING USAGE RATIOS

Reference Drift = 0.004958

Limit state group = all deformation states

Minimum usage ratio for each color : 0.0 0.5 1 1.5 2

(b)



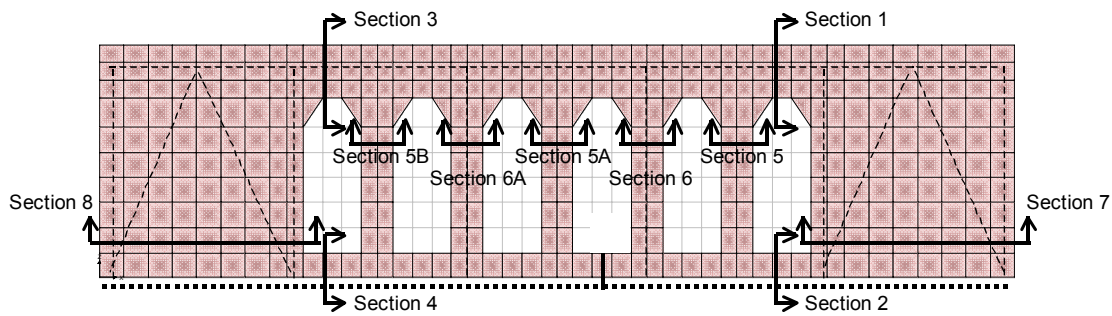
DEFLECTED SHAPE SHOWING USAGE RATIOS

Reference Drift = 0.02027

Limit state group = all deformation states

Minimum usage ratio for each color : 0.0 0.5 1 1.5 2

**Figure 4.9 Nonlinear finite element model using *RAM Perform* at (a) 0.5% roof drift and (b) 2.0% roof drift**



Structural Member	Structure Section	Governed by	Hand Calc	Peak Value from Ram Perform		Roof Drift when Peak Occurs
Peak Vertical Capacity of Roof Spandrel	Section 1	Shear Strength in Diagonal Tension	130 k	210 k		0.30%
Peak Vertical Capacity of Floor Spandrel	Section 2	-	-	149 k		0.90%
Peak Vertical Capacity of Roof Spandrel	Section 3	Shear Strength in Diagonal Tension	130 k	176 k		0.80%
Peak Vertical Capacity of Floor Spandrel	Section 4	-	-	78 k		0.37%
Peak Lateral Capacity of Wall Pier without Steel Column	Section 5	Flexure (Mn) at top and bottom	28 k	Horizontal 41 k 40 k 50 k	Vertical 158 k 145 k 196 k	0.83%
	Section 5A					0.73%
	Section 5B					0.80%
Peak Lateral Capacity of Wall Pier with Steel Column	Section 6	Flexure (Mn) at top and bottom	45 k	61 k		0.45%
	Section 6A			65 k		0.63%
Peak Lateral Capacity of End Wall	Section 7	Foundation Uplift	369 k	571 k		0.31%
Peak Lateral Capacity of End Wall	Section 8	Foundation Uplift	113 k	192 k		0.32%

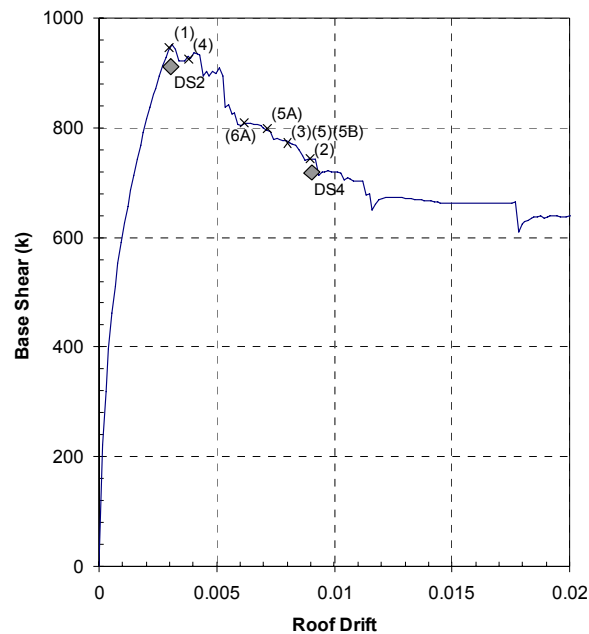


**Figure 4.10 Forces at key structure section cuts, by computer analysis and hand calculation, and points on the force-displacement curve when peak strength of each section is reached**

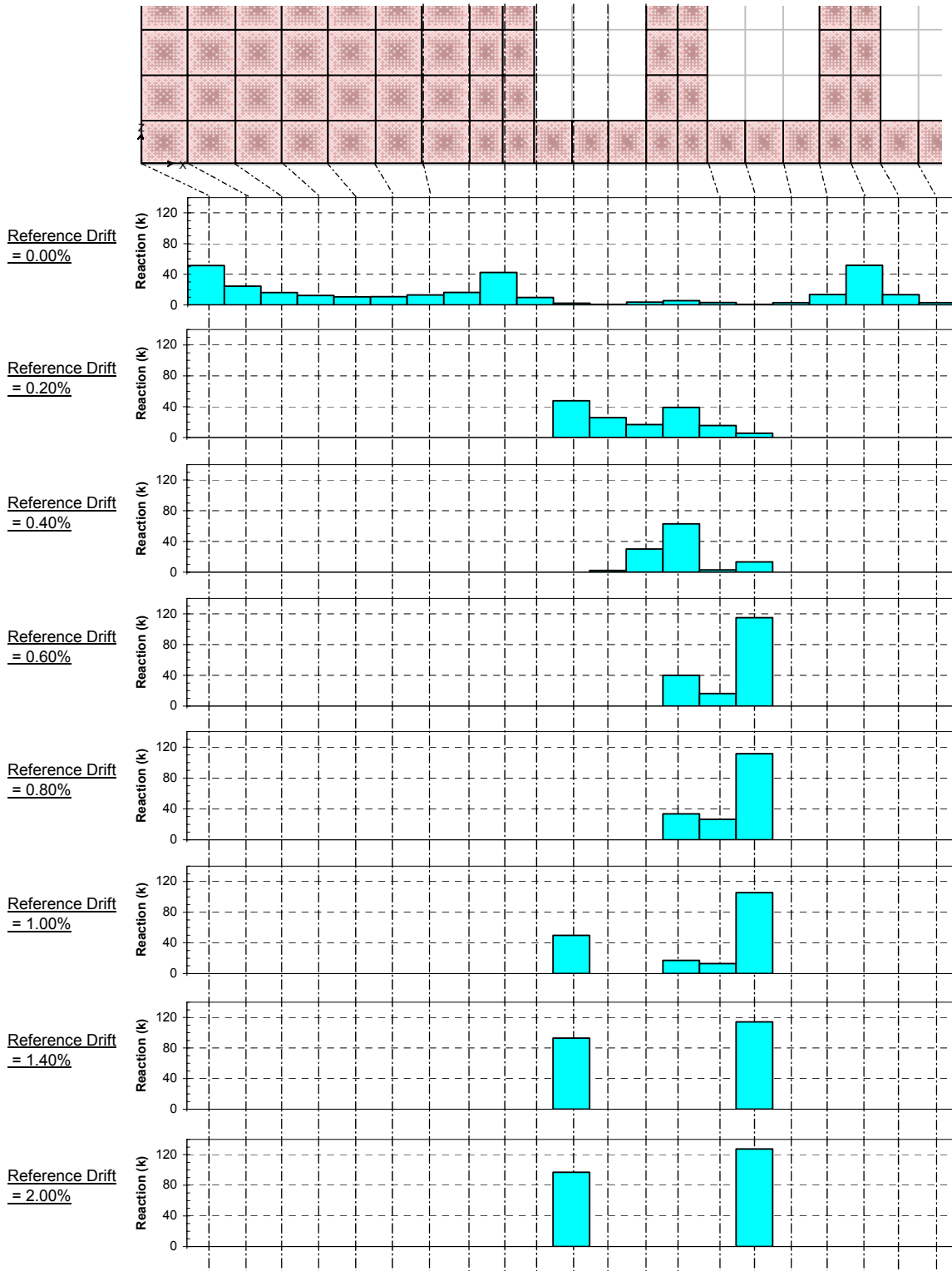


Figure 4.11 Foundation reaction forces from *RAM Perform* nonlinear static model

### 4.3 SEISMIC EVALUATION OF THE DAMAGED STRUCTURE

Using the methodology of the *Guidelines*, damage states are defined at various roof drifts, labeled “DS2” and “DS4” on the intact structure force-displacement curve of Figure 4.10. For each damage state, a revised *RAM Perform* model is created by changing the properties of certain structural elements based on the damage they sustain. For example, concrete shear strength degrades at high levels of ductility, as shown in Figure 4.14. Figure 4.15 shows how this degradation translates into a “damaged-component” stress-strain backbone curve applied to concrete in the affected regions. Table 4.4 documents the roof drifts and component damage that define each damage state, and Figure 4.12 depicts the locations of these degraded components.

Damage to components changes the strength and stiffness of the structure. The periods of vibration of the damaged structure are estimated based on the change in initial stiffness, as presented in Table 4.5. Performing nonlinear static analyses on each of the “damaged-structure” models generates damaged-structure force-displacement curves to characterize expected behavior in an aftershock (Fig. 4.13). Figures 4.16–4.18 plot shear force in various elements as a function of global roof drift.

**Table 4.4 Modeling of each damage state in *RAM Perform***

<b>Damage State</b>	<b>Roof Drift</b>	<b>Components modeled with damaged properties</b>
Intact	0	None
DS2	0.3 %	Section 1: Spandrel
DS4	0.9 %	Section 1: Spandrel Section 2: Grade Beam Section 3: Spandrel Section 4: Grade Beam Section 5, 5A, 5B: Wall Pier without Steel Column Section 6, 6A: Wall Pier with Steel Column Section 9: Grade Beam

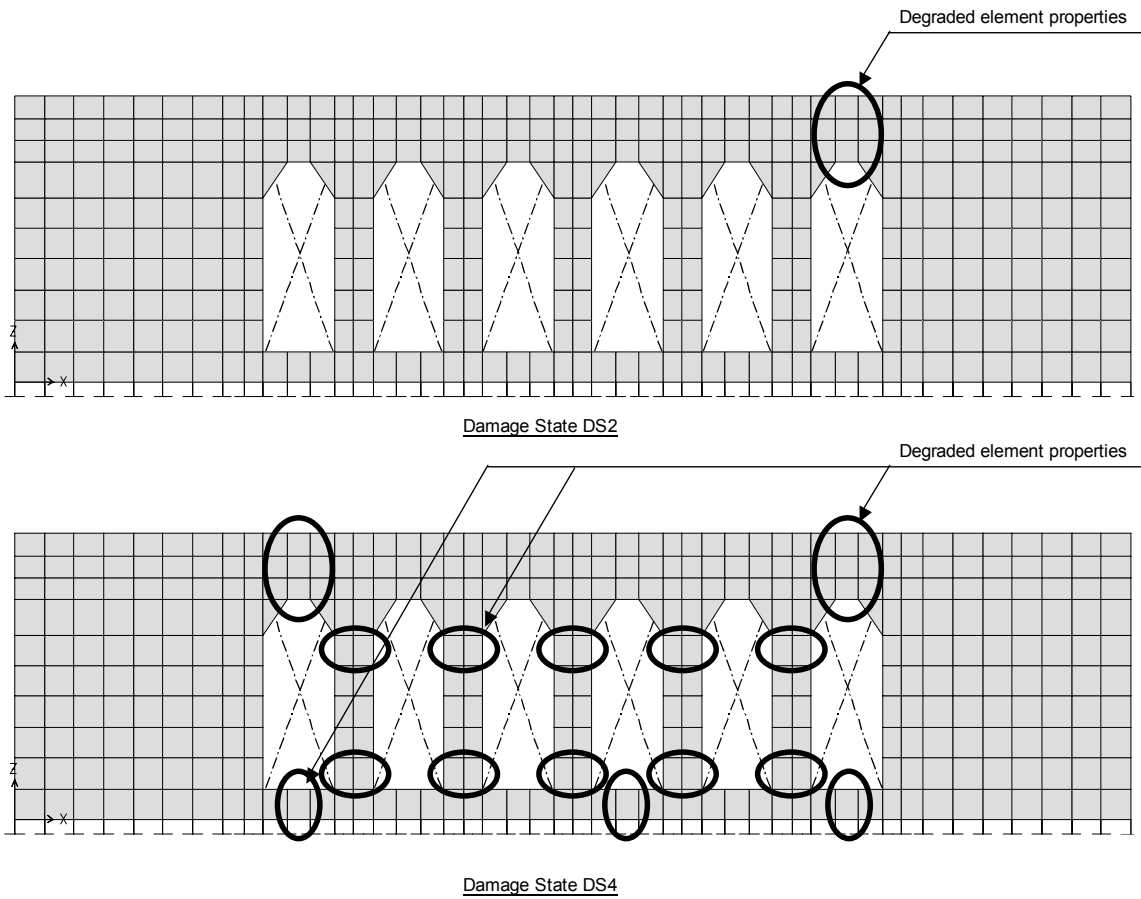


**Figure 4.12 Modeling of each damage state**

**Table 4.5 Assumed fundamental period of vibration**

Damage State	Roof Drift at 400kips Lateral Force	Stiffness/Intact	T (sec)
Intact	0.040%	1.00	0.20
DS2	0.054%	0.74	0.23
DS4	0.069%	0.58	0.26

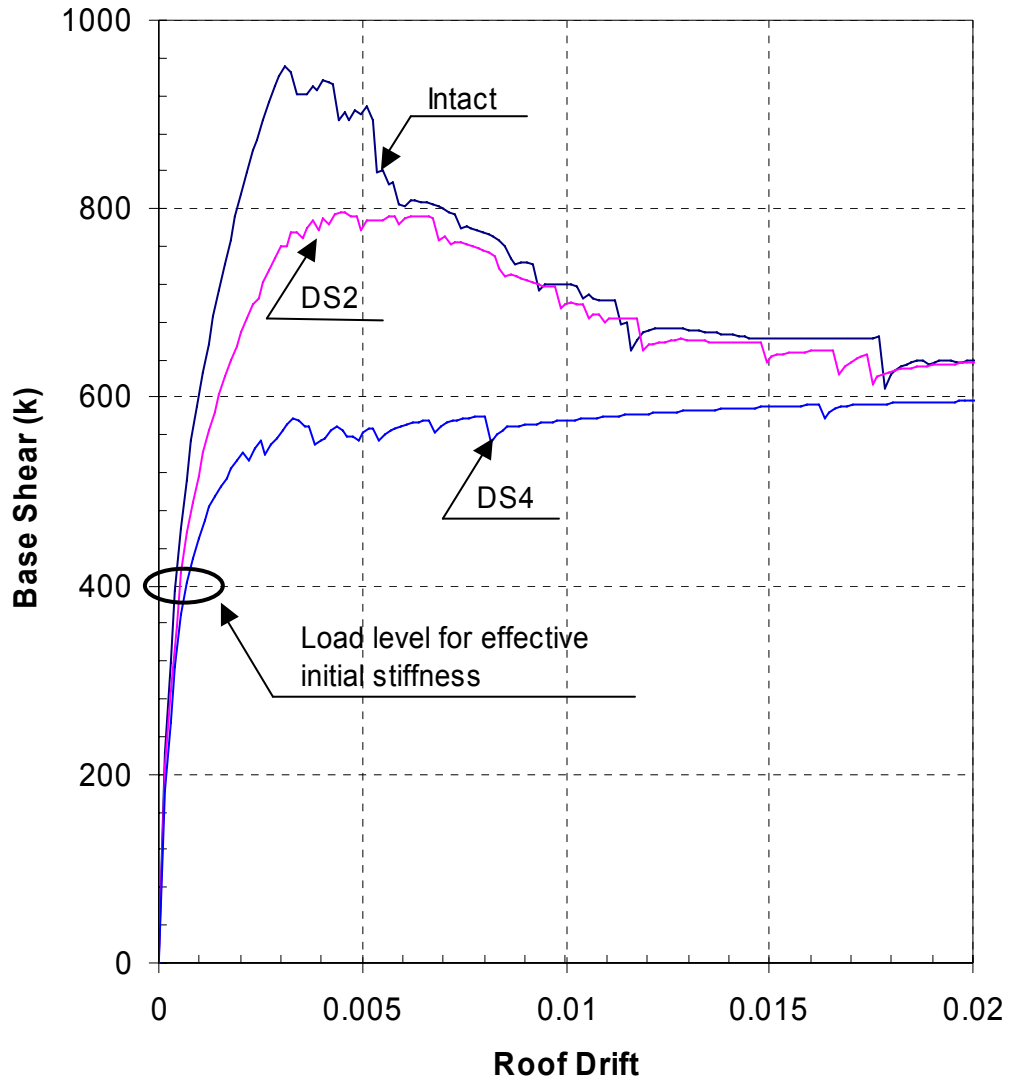


**Figure 4.13 Force-displacement curves for the intact structure and for damage states DS2 and DS4**

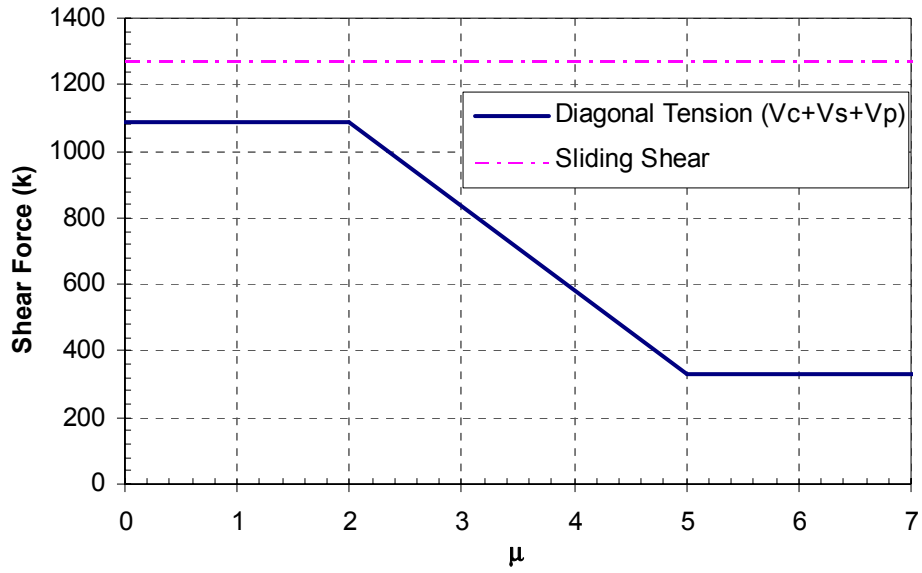


Figure 4.14 Concrete shear strength behavior by FEMA 306

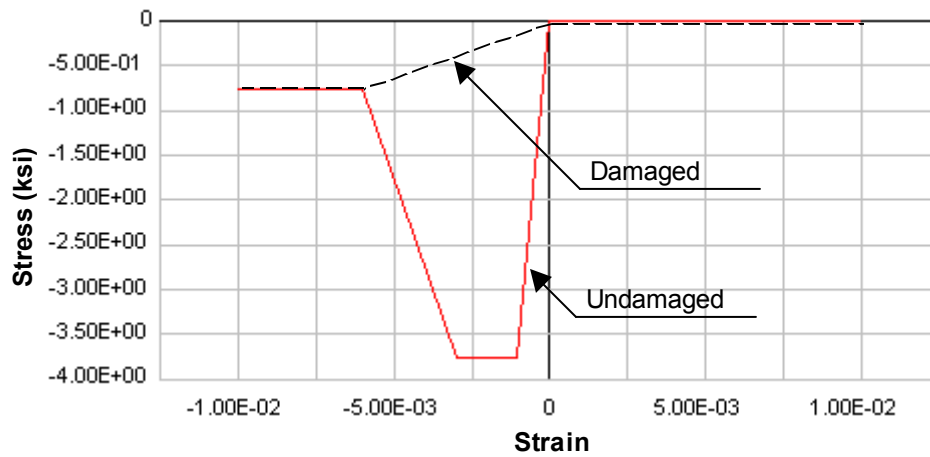
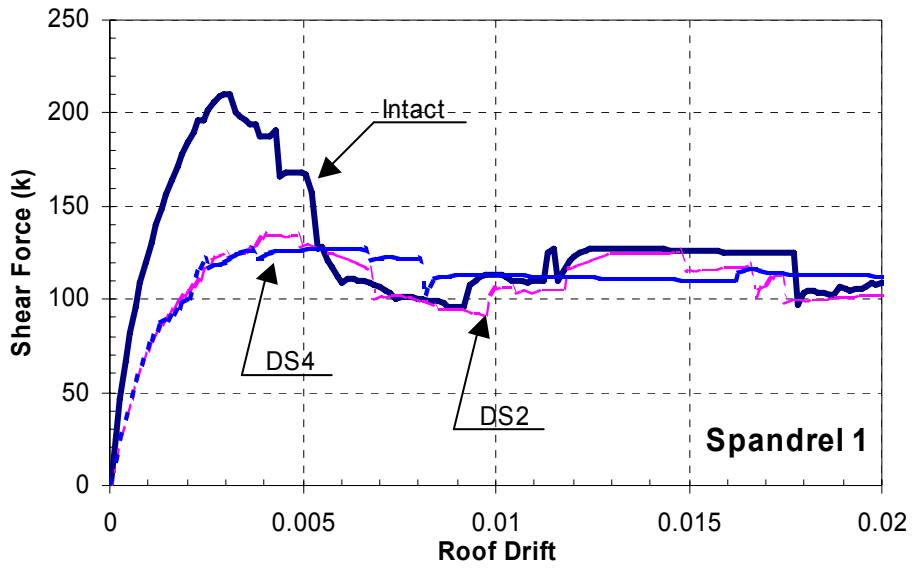
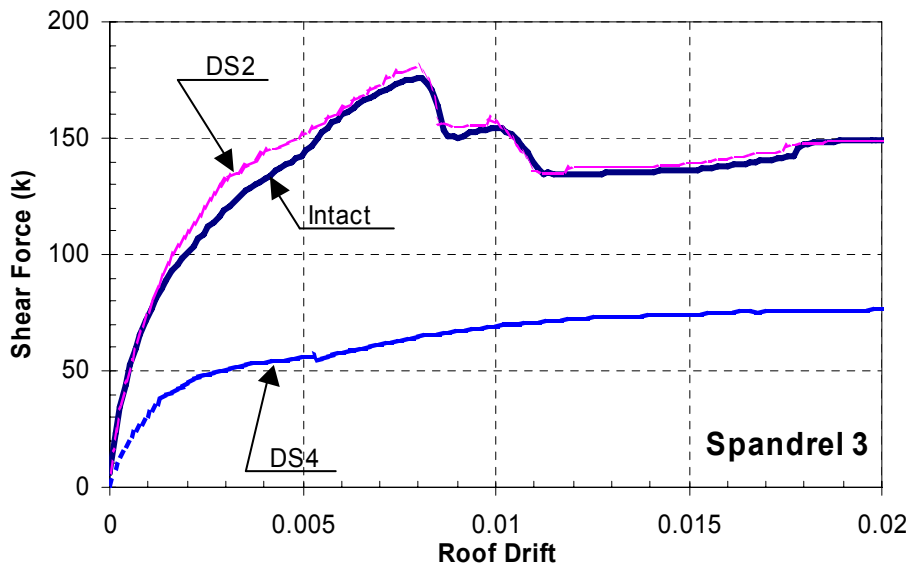


Figure 4.15 Component material properties in *RAM Perform* for undamaged and damaged concrete



**Figure 4.16 Spandrel 1 section strength for the intact structure and for damaged structures DS2 and DS4**



**Figure 4.17 Spandrel 3 section strength for the intact structure and for damaged structures DS2 and DS4**



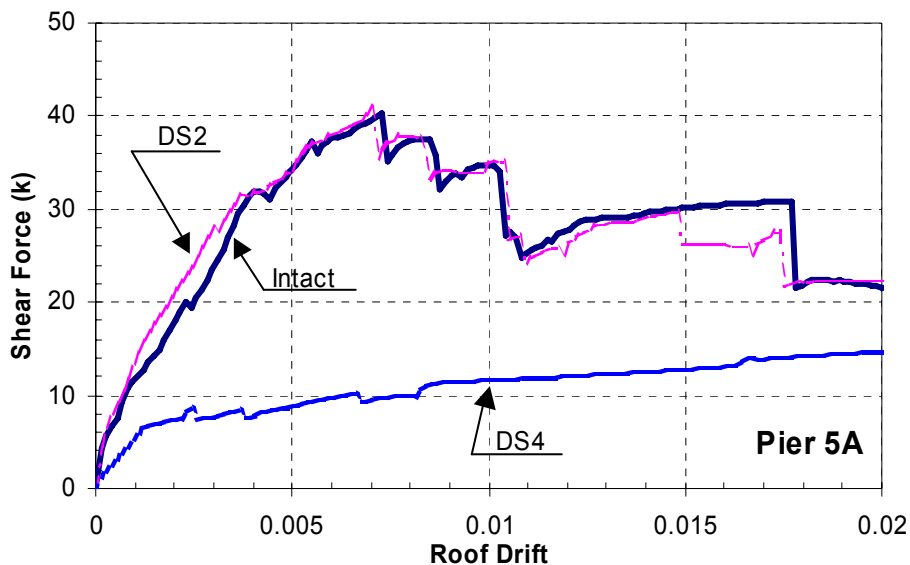


**Figure 4.18 Pier 5A section strength for the intact structure and for damaged structures DS2 and DS4**

#### 4.4 INFERRED DYNAMIC BEHAVIOR (SPO2IDA)

From the nonlinear force-displacement plots of Figure 4.13 the *SPO2IDA* program is used to compute the relationship between spectral acceleration and global ductility demand for each damage state. The *SPO2IDA* program takes as input a fundamental period of vibration and a quadrilinear force-displacement plot of the building's global response. Figure 4.19 displays the quadrilinear approximations of force-displacement response used for input into *SPO2IDA*. Table 4.6 specifies this input numerically.

Figures 4.20–4.22 display the normalized graphical output from *SPO2IDA*, and Figures 4.23–4.25 present the same data in terms of spectral acceleration and roof drift. A comparison of Figures 4.23–25 indicates that for the damage states examined in this example, the DS2 response has similar collapse acceleration to that of the intact structure, and the DS4 response shows collapse at a reduced level of acceleration.

From the intact structure *SPO2IDA* plot, the spectral acceleration expected to cause each damage state (Table 4.7) is determined. The tabulated acceleration values correspond to points

on the median (IDA-50%) curve at which the structure reaches the roof drifts of Table 4.4. Next, from each of the damaged-structure *SPO2IDA* plots, the spectral acceleration expected to cause collapse in an aftershock (Table 4.8) is determined. The values in Table 4.8 form the basis for defining post-earthquake tagging limit states.

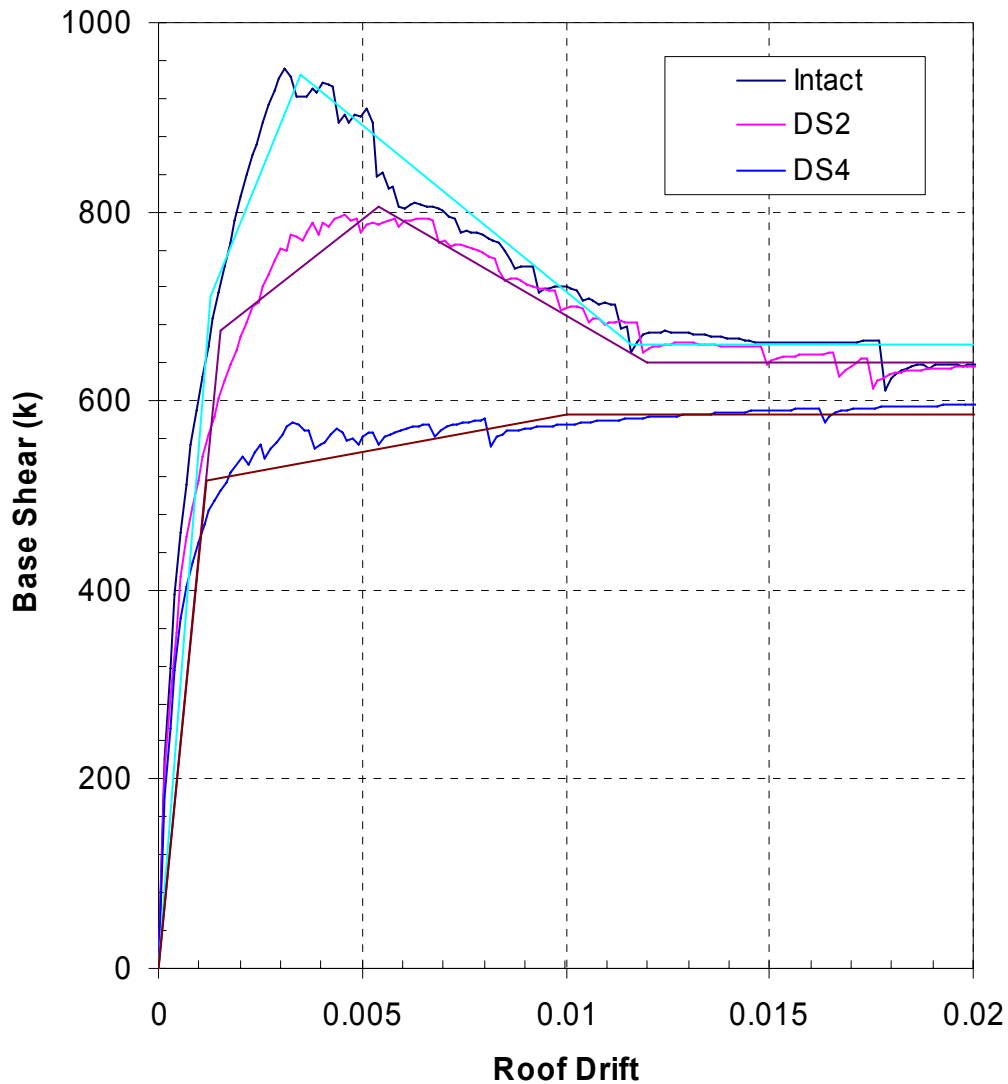


**Figure 4.19 Force-displacement curves and linear approximations for the intact structure and damaged structures DS2 and DS4**

**Table 4.6 SPO2IDA input**

Damage State	Yield Point		Peak Strength		Beginning of Plateau		SPO2IDA Input					Period T
	Roof Drift	V/W	Roof Drift	V/W	Roof Drift	V/W	Hardening $\mu$	Hardening Slope	Softening Slope	Residual Plateau	Fracturing $\mu$	
Intact	0.0013	1.97	0.0035	2.62	0.0116	1.83	2.7	19.5%	-6.4%	0.93	23.1	0.2
DS2	0.0015	1.88	0.0054	2.24	0.0120	1.78	3.6	7.4%	-5.6%	0.95	20.0	0.23
DS4	0.0012	1.43	0.0100	1.63	0.0200	1.63	8.3	1.9%	0.0%	1.14	25.0	0.26

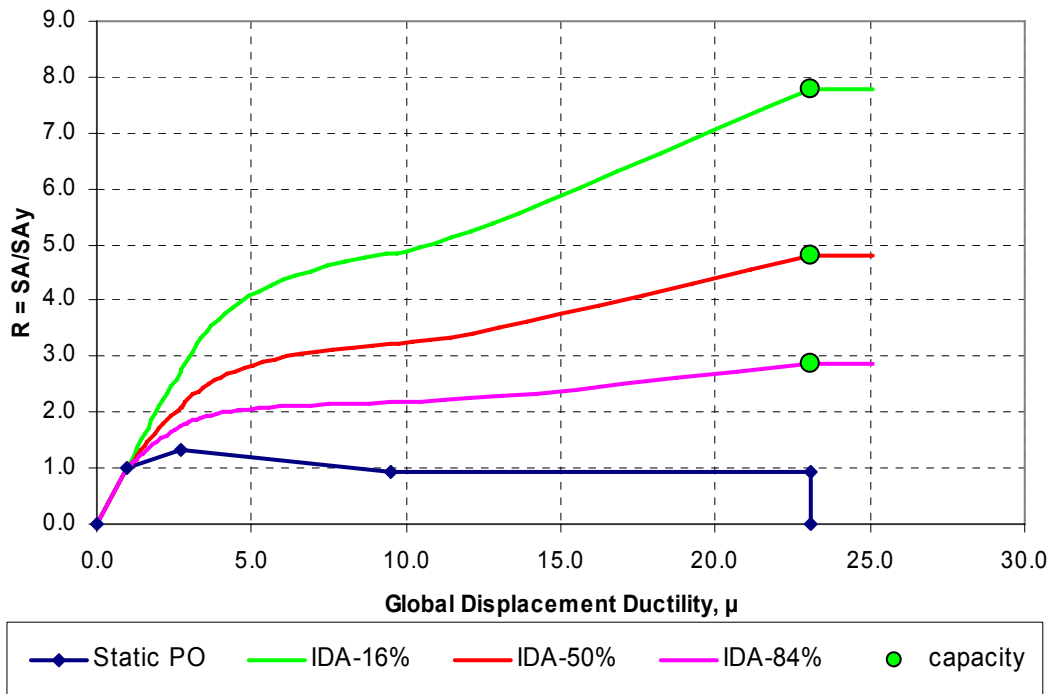


**Figure 4.20 SPO2IDA intact (R vs.  $\mu$ )**

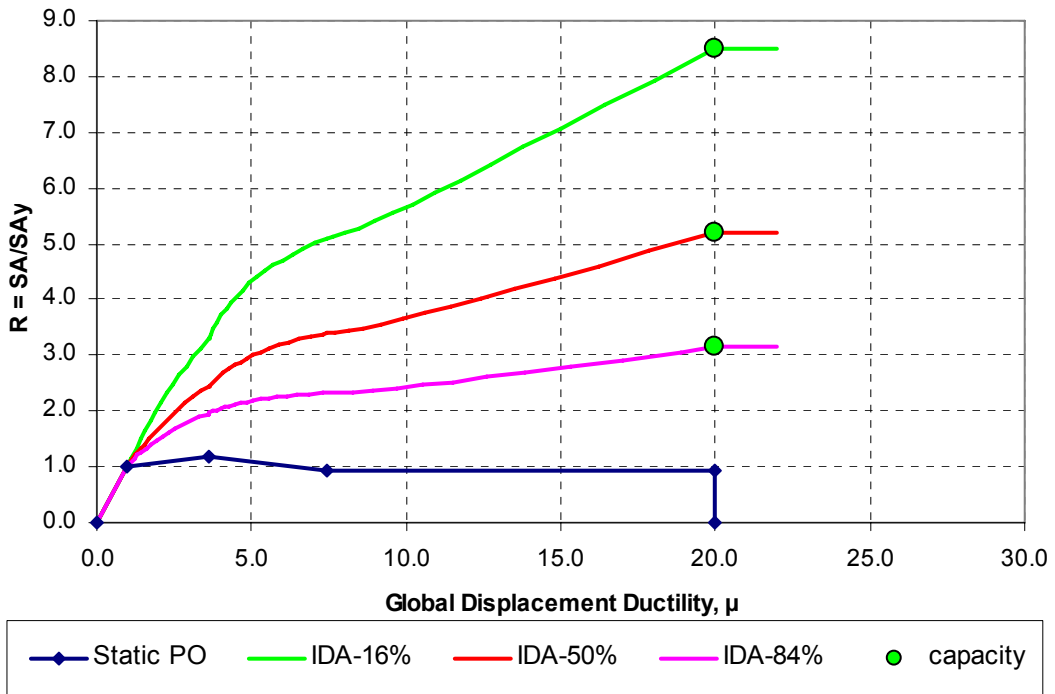


Figure 4.21 *SPO2IDA* DS2 (R vs.  $\mu$ )

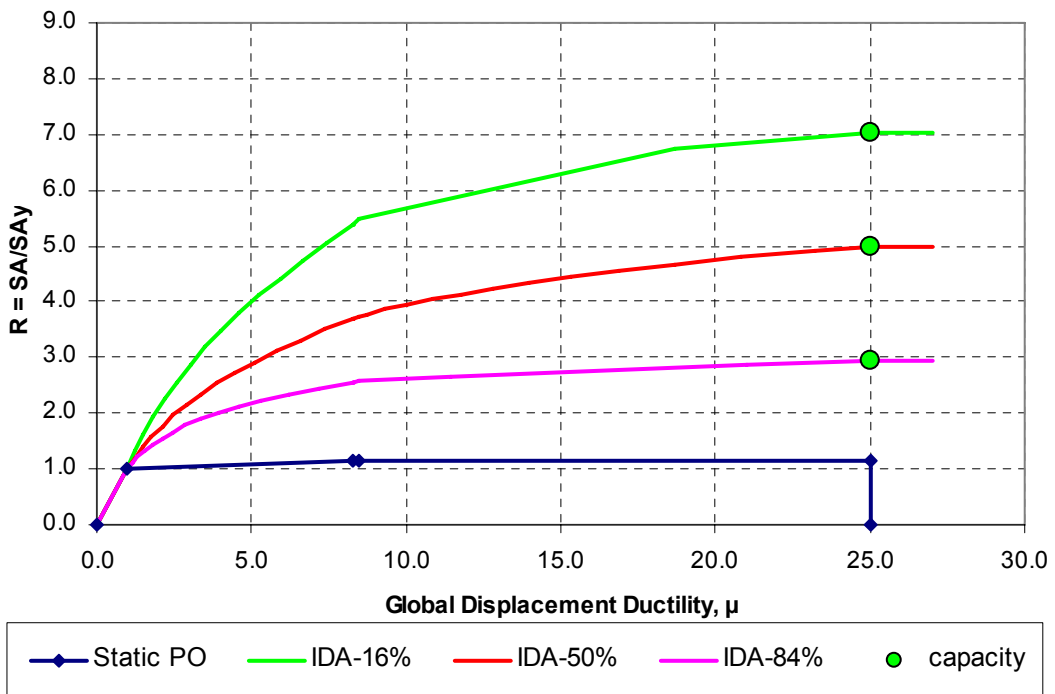


Figure 4.22 *SPO2IDA* DS4 (R vs.  $\mu$ )

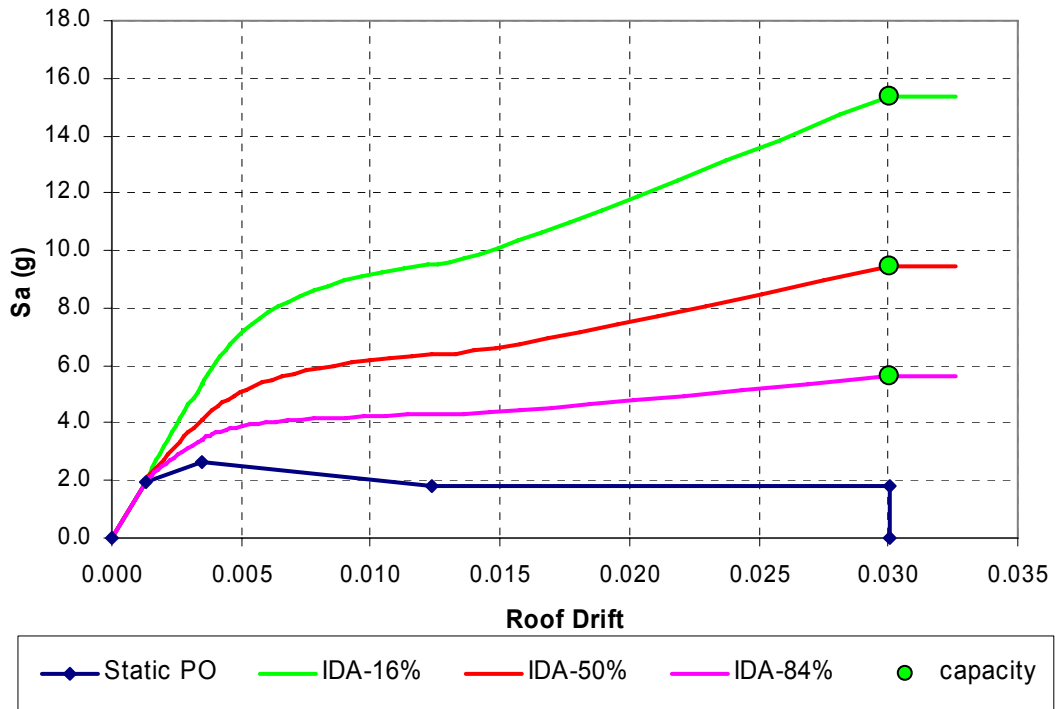


Figure 4.23 *SPO2IDA* intact ( $S_a$  vs. roof drift)

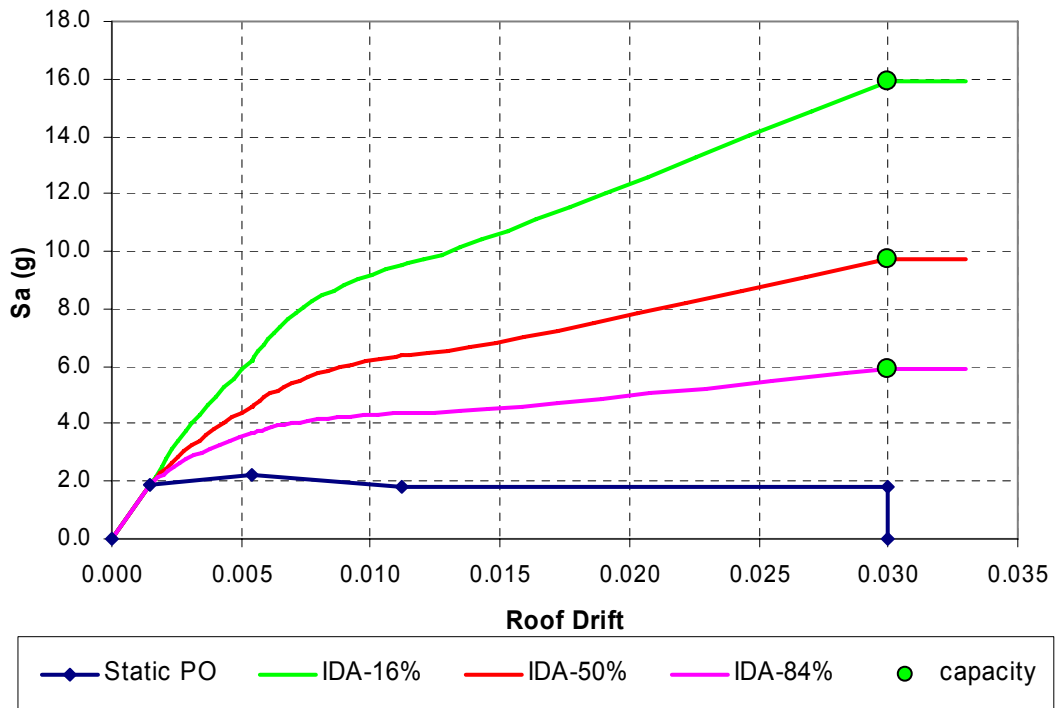


Figure 4.24 *SPO2IDA* DS2 ( $S_a$  vs. roof drift)

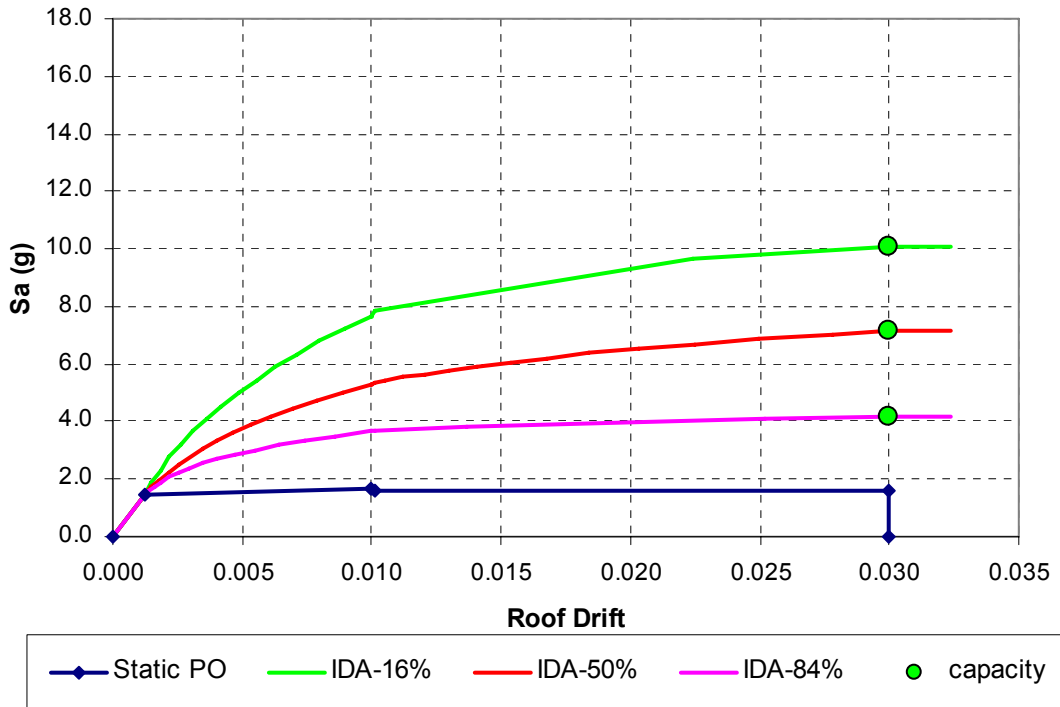


Figure 4.25 *SPO2IDA* DS4 ( $S_a$  vs. roof drift)

Table 4.7 Spectral acceleration to cause each damage state (from Fig. 4.23)

Damage State	$S_a$ (g)
DS2	3.7
DS4	6.1
Collapse	9.5

Table 4.8 Spectral acceleration to collapse the structure in an aftershock

Damage State	IDA 50% $S_a$ (g)	IDA 84% $S_a$ (g)	Source
Intact	9.5	5.6	Figure 4.2
DS2	9.8	5.9	Figure 4.2
DS4	7.2	4.2	Figure 4.2

#### 4.5 POST-EARTHQUAKE TAGGING LIMIT STATES

Plotting the median (IDA-50%) main-shock spectral acceleration to cause each damage state (Table 4.7) versus the aftershock acceleration to collapse the damaged structure (Table 4.8), main-shock spectral accelerations are identified at which different post-earthquake tagging limit

states are expected to occur. Figures 4.26–4.27 depict two different proposed criteria for predicting the onset of yellow tag and the onset of red tag.

Tagging Criteria C (Fig. 4.26) defines the onset of yellow tag as the median main-shock acceleration for which an aftershock of the same acceleration will cause collapse in 50 out of 100 ground motions. The onset of red tag is the median main-shock acceleration for which an aftershock having 75% of this acceleration will cause collapse in 50 out of 100 ground motions.

Tagging Criteria D (Fig. 4.27) is more conservative and defines yellow tag by the same criteria as red tag, except with improved confidence based on variability estimates from the *SPO2IDA* program. Tagging Criteria D defines the onset of red tag as the median main-shock acceleration for which an aftershock of the same acceleration will cause collapse in 50 out of 100 ground motions. (For comparison, this same point defines the onset of yellow tag under Criteria C.) The onset of yellow tag is the median main-shock acceleration for which an aftershock of the same acceleration will cause collapse in 16 out of 100 ground motions.

Both sets of tagging criteria described above use probabilistic methods to define tagging decisions that post-earthquake inspectors will make based on visual evidence. These probabilistic estimates are correlated to structural displacement and response events (which can often be related to visible damage) by marking the onset of yellow tag and onset of red tag on the force-displacement response plot (Fig. 4.28). The marked limit state displacements correspond to main-shock spectral accelerations at points A and B of Figure 4.27 (Tagging Criteria D).

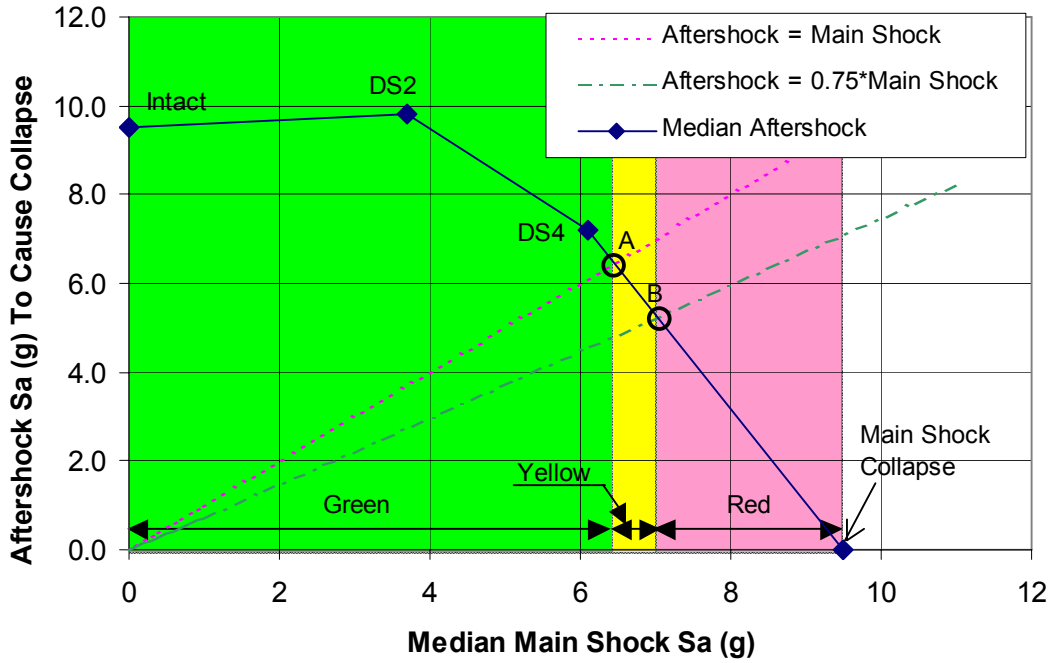


Figure 4.26 Main shock vs. aftershock to cause collapse, Tagging Criteria C

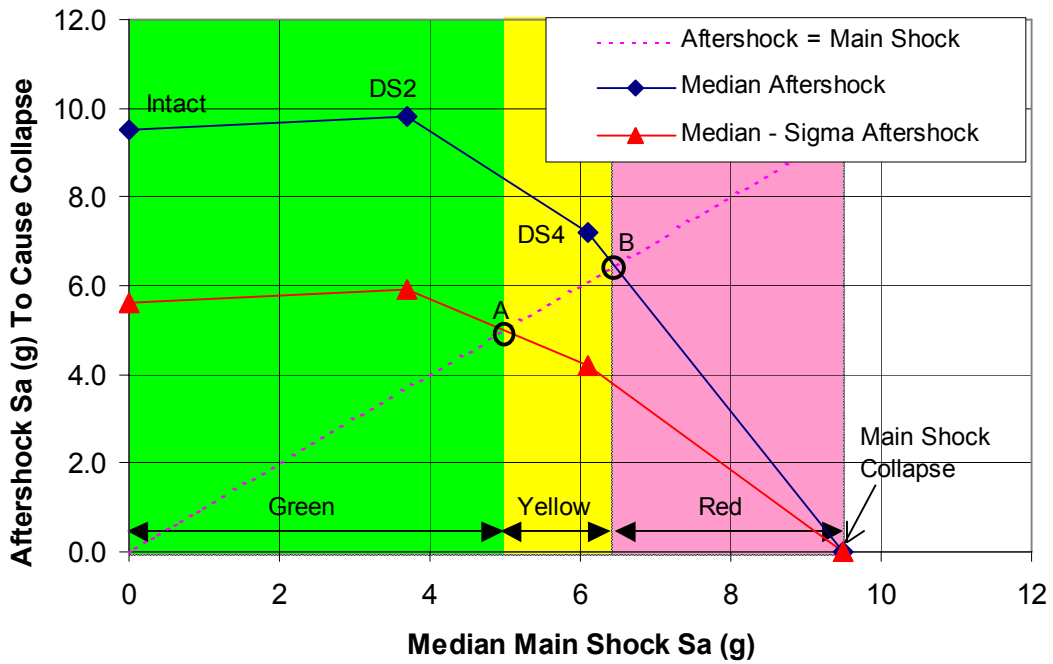
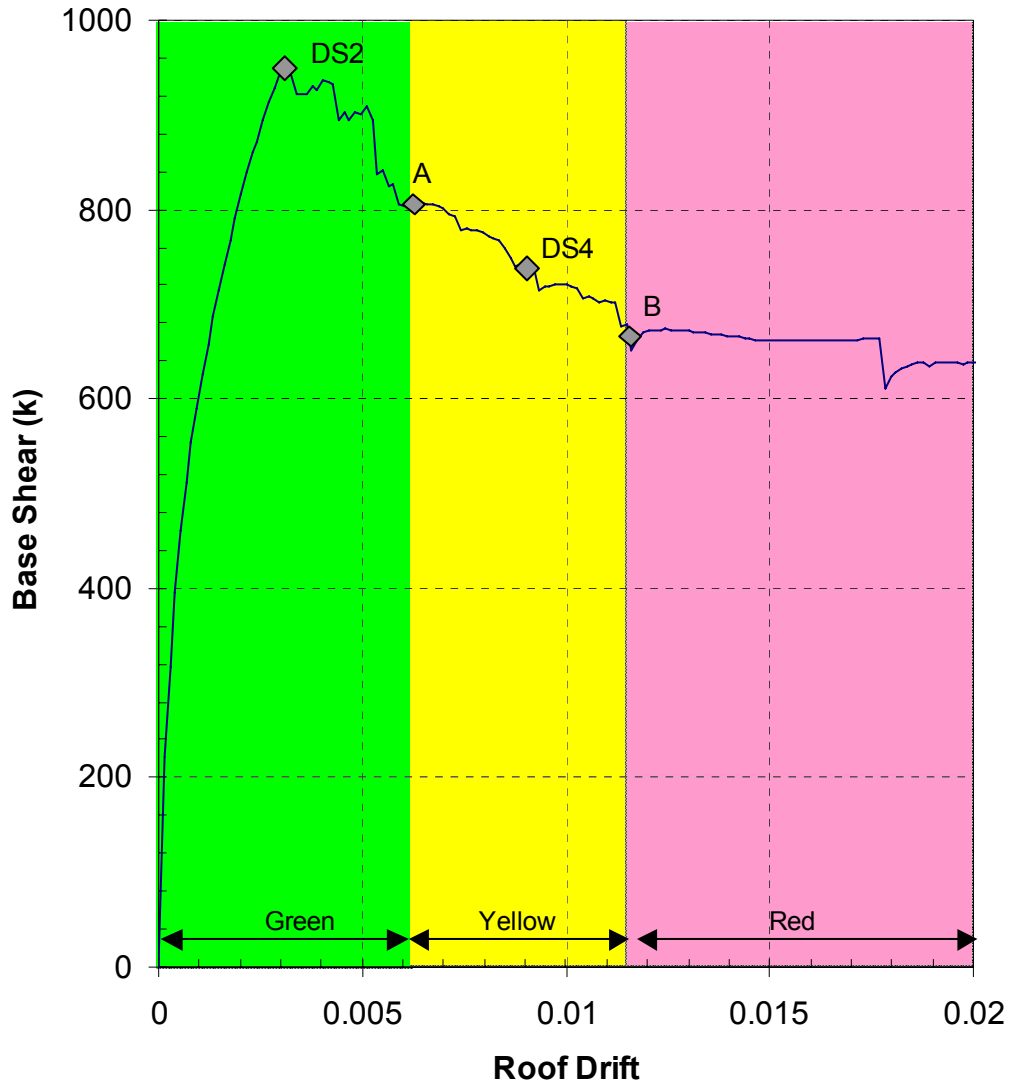


Figure 4.27 Main shock vs. aftershock to cause collapse, Tagging Criteria D





**Figure 4.28 Tagging limit states, per Criteria D, on the force-displacement curve of the intact structure**

## 4.6 FRAGILITY CURVES

Based on uncertainty measures for the randomness of nonlinear response in earthquake ground motions and the uncertainty of structural capacity ( $\beta_R$  and  $\beta_U$  in Tables 4.9–4.10), structure fragility curves (Fig. 4.29) provide a probabilistic assessment of spectral acceleration capacity. For example, from Figure 4.29, in a ground motion with peak spectral acceleration 5.0g, there is a 44% probability that the building will sustain at least enough damage to receive a yellow tag (56% probability of green tag). For the same peak spectral acceleration, there is a 37% probability that it will reach the onset of red tag, and there is a 21% probability that it will exceed the assumed collapse displacement. This information is also provided in Table 4.11, which indicates that for this example the onset of yellow tag will be exceeded with 5% probability if spectral acceleration exceeds 1.79g, with 25% probability if spectral acceleration exceeds 3.49g, with 50% probability if spectral acceleration exceeds 5.51g, and so on. The evaluation indicates that the structure will suffer significant damage only at very high accelerations. The structure meets PG&E’s performance goals without retrofitting in the building longitudinal direction.

**Table 4.9  $\beta_R$  values taken from the intact structure SPO2IDA results, and  $S_{a(cap)}$  values**

Damage State	Roof Drift	$\mu$	$\beta_R$	$S_{a(cap)}$ (g)
Onset of Damage	0.003	2.31	0.16	3.67
Yellow	0.006	4.81	0.32	5.51
Red	0.012	8.85	0.39	6.35
Collapse	0.030	23.1	0.52	9.45

**Table 4.10 Uncertainty values for fragility curves**

Uncertainty Value	Onset of Damage	Onset of Yellow	Onset of Red	Collapse	Basis
$\beta_U$	0.40	0.60	0.60	0.60	Mill-type building, improved (Bazzurro 2003)
$\beta_R$	0.16	0.32	0.39	0.52	From SPO2IDA
$\beta$	0.43	0.68	0.72	0.79	SRSS of $\beta_U$ and $\beta_R$

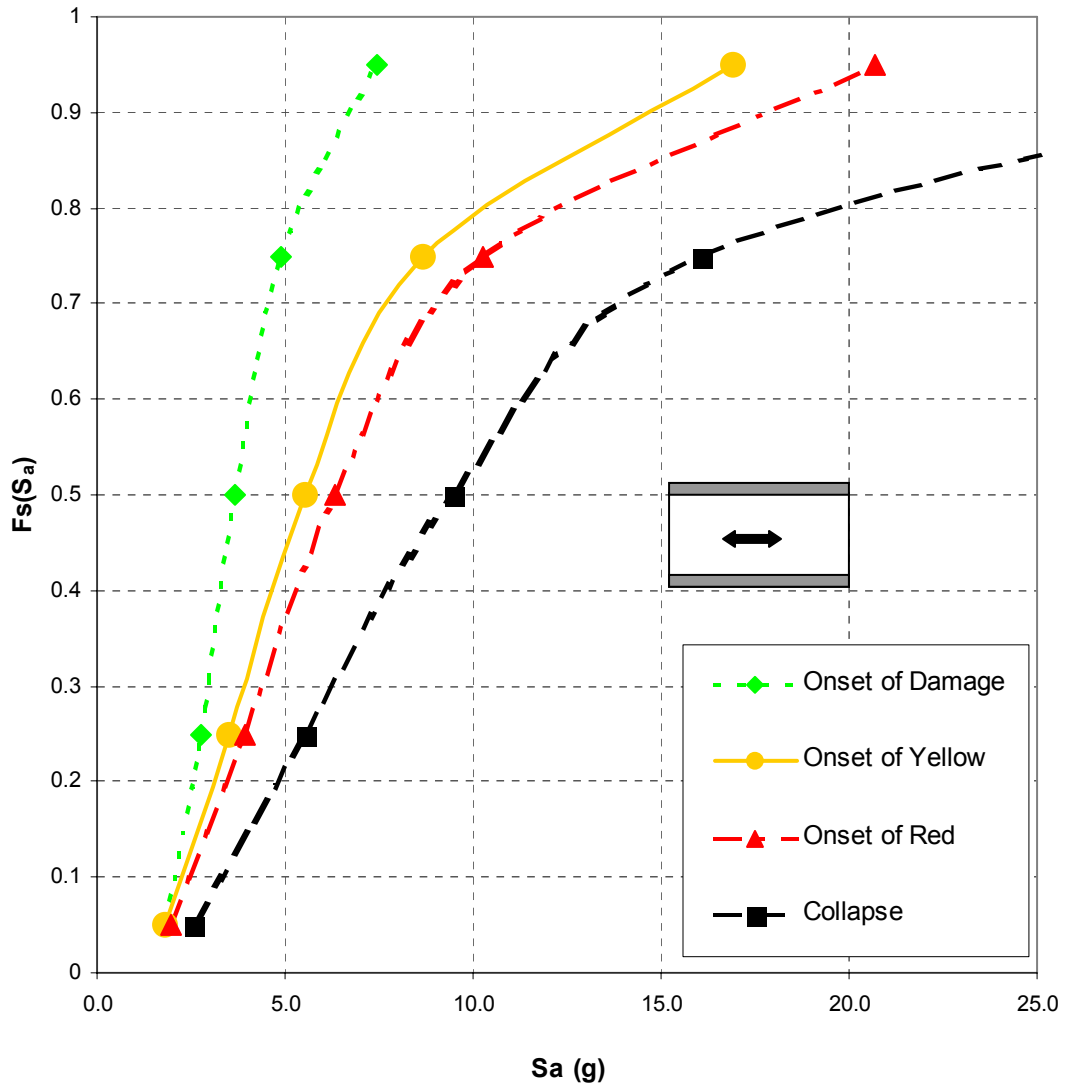


Figure 4.29 Fragility curves

Table 4.11 Spectral acceleration values (g) for fragility curves

$F_S(S_a)$	$x$	Onset of Damage	Onset of Yellow	Onset of Red	Collapse
0.05	-1.65	1.80	1.79	1.95	2.55
0.25	-0.67	2.75	3.49	3.93	5.55
0.5	0	3.67	5.51	6.35	9.45
0.75	0.67	4.90	8.69	10.26	16.09
0.95	1.65	7.47	16.92	20.68	35.03

## **5 Study of the Finite Element Modeling Assumptions for Test Application 2**

A key step in the Advanced Seismic Assessment procedure is the assembly of individual building components into a model that reflects overall building performance. Computer modeling represents one method for achieving this. Ideally, for nonlinear static analysis, modeled behavior should match true structural behavior in terms of initial stiffness, peak strength, strength degradation, and failure mode. (For nonlinear dynamic analysis, a match of hysteresis loop shape is also desirable.) This section examines finite element properties in the *RAM Perform* computer analysis program used in Test Application 2 and attempts to replicate performance observed in an experimental test of a reinforced concrete wall.

### **5.1 ATTEMPTED CALIBRATION OF FINITE ELEMENT MODEL**

To evaluate the accuracy of current state-of-the-art computer modeling tools, an applicable test specimen is selected, and an attempt to model its behavior is carried out using a computer structural analysis program. The behavior mode being examined, in-plane wall shear failure, is one that is considered particularly difficult to model (Dr. Graham Powell pers. comm. 2004). The modeling techniques evaluated here are similar to those used in the mill building structural analysis of Section 4. The modeling parameters are varied to assess their effects on the accuracy of the model's initial behavior as well as the model's damaged-structure behavior.

#### **5.1.1 Test Specimen**

Barda (1976) tested a reinforced concrete wall subjected to cyclic static in-plane lateral loading (Fig. 5.2). The wall aspect ratio is square, with clear height and clear length of 75 inches each.

Floor slabs and flanged boundary elements confine the wall in-plane on all edges. The wall is 4 inches thick with two curtains of #3 reinforcement at approximately 11 inches on center in each direction. Barda tested the specimen to a final lateral displacement of 3.0 inches, or 4% drift. Figure 5.3(a) shows the visual condition of the specimen at ultimate load and at the conclusion of loading. Figure 5.2 plots the envelope of hysteresis loops from the test.

### 5.1.2 Computer Analysis Model

The computer analysis model (Fig. 5.1) uses the program *RAM Perform* to attempt to replicate the performance of the test specimen. In the analysis, multi-layer finite elements represent inelastic steel (reinforcing) material, inelastic concrete material, inelastic shear material, and diagonal compression material in the wall. Bar elements along the top and sides represent the floor slab and boundary elements confining the specimen. Nodes along the bottom edge of the model are all fixed against translation.

Table 5.1 summarizes the input properties for 12 different analysis runs using the *RAM Perform* model. Figure 5.4 graphically displays the material input properties used in one of the analysis runs. Properties for the concrete material are specified and adjusted considering research recommendations such as those shown in Figure 5.5.

The last four rows of Table 5.1 indicate our comparison between computer analysis output and test specimen results. For example, in Figure 5.3 colored areas denote damaged finite elements from Run 4 for comparison with the failure pattern in the test specimen photo above. Figure 5.2 plots hysteresis loops from the same analysis run overlaid on the envelope of test specimen hysteresis loops. From the hysteresis loops the model's initial stiffness, peak strength, and strength degradation are compared to those of the test specimen.

### 5.1.3 Results and Recommendations

Of the analysis runs presented in Table 5.1 no single run closely matches all four categories of specimen performance. For example, Run 4 exhibits reasonable matches of initial stiffness and peak strength, and a fair match of strength degradation, but the pattern of failure is nearly the opposite of that exhibited in the test specimen.

This degree of modeling accuracy is sufficient for limited purposes. For example, for the computational purposes of the Advanced Seismic Assessment method, matching failure patterns within walls is not necessarily critical to the analysis, as long as the resulting envelope of hysteresis loops or force-displacement curves accurately reflect the elements' structural performance. However, achieving accurate output through inaccurate means in one particular wall model does not guarantee that a model of a different wall would achieve comparably accurate output.

The engineering research and structural software communities should perform further studies of this type to calibrate computer structural analysis programs used in practice to experimental results.

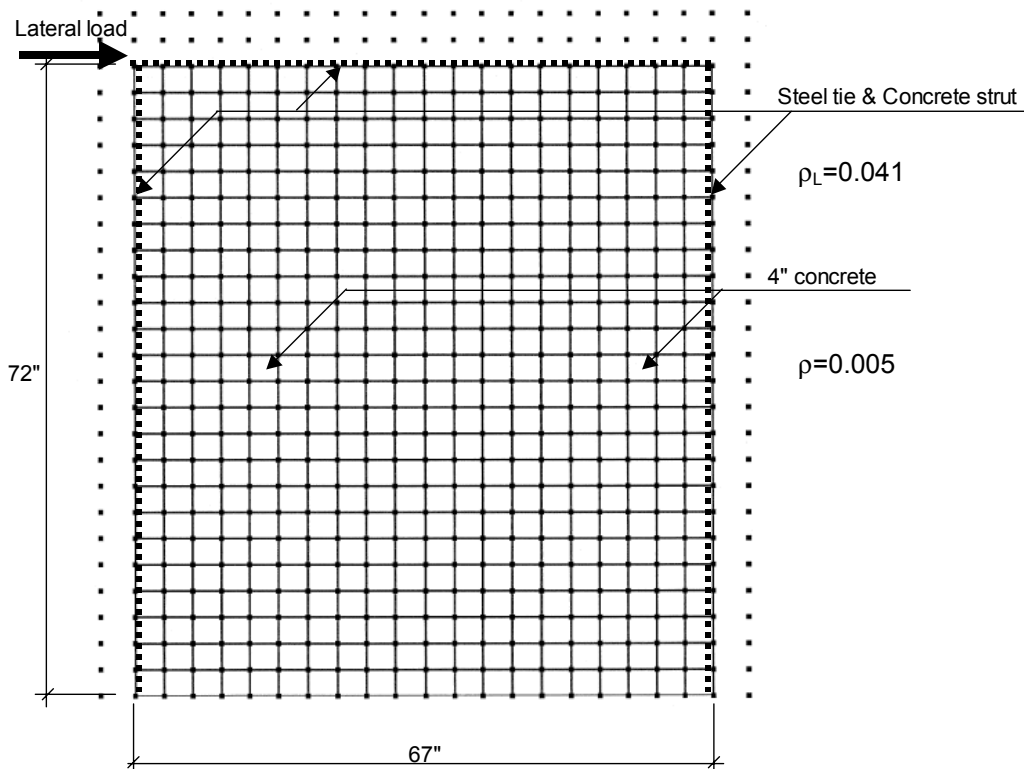
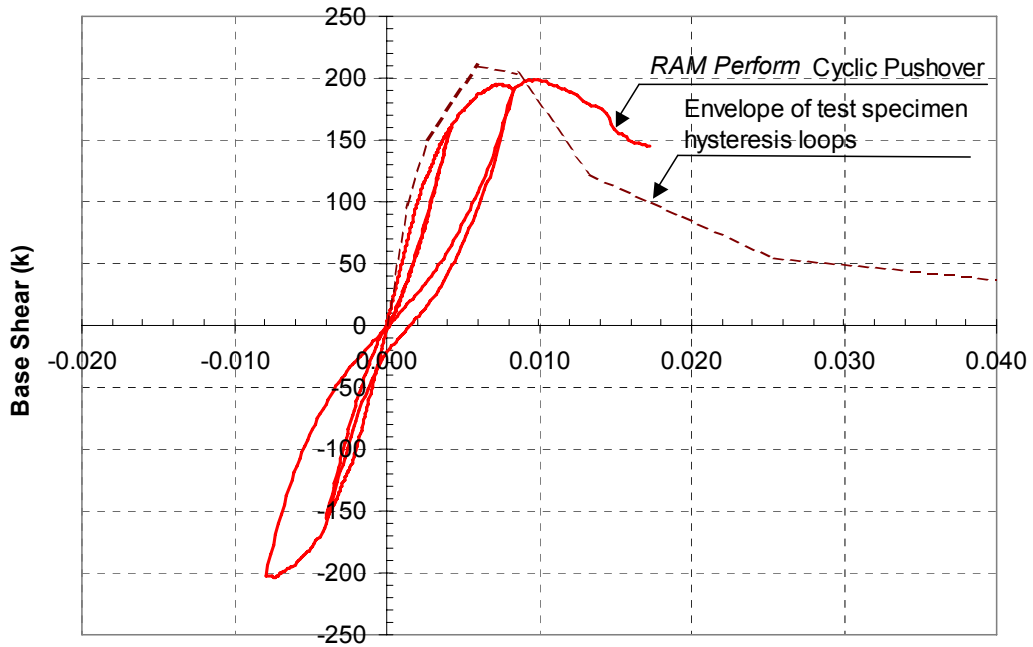


**Figure 5.1 Calibration to concrete wall test specimen, *RAM Perform* analysis model**



Roof Drift

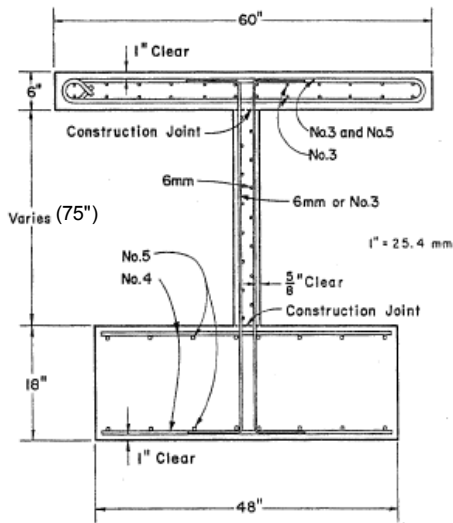


Fig. 3. Representative vertical section.

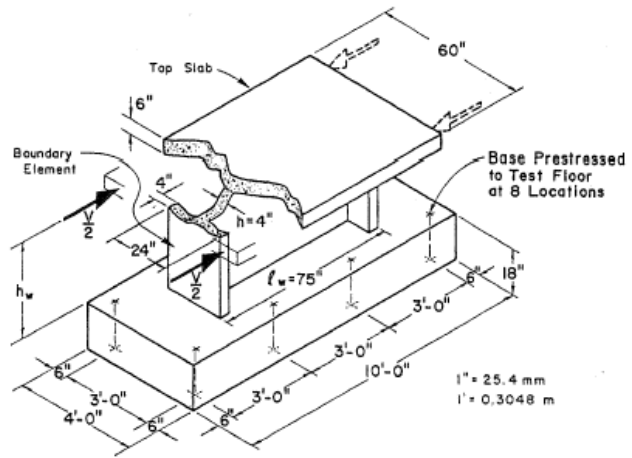
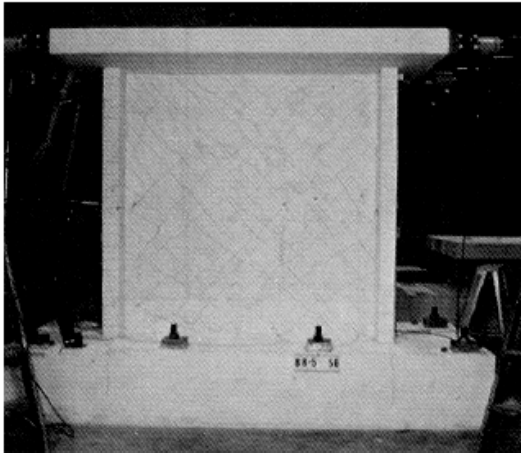


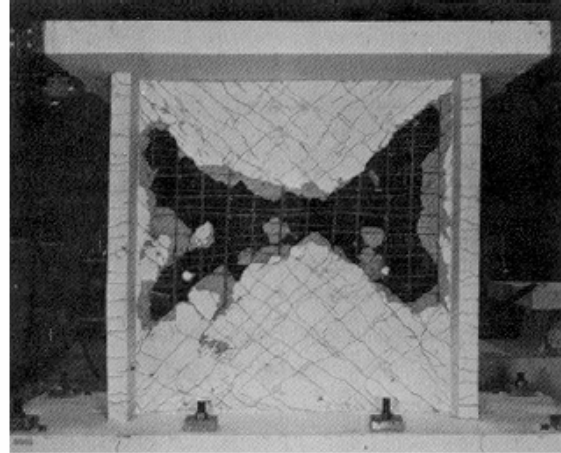
Fig. 1. Test specimen indicating application of load.

Figure 5.2 Concrete wall test specimen (Barda 1976) and calibration of *RAM Perform* cyclic pushover (Run 4)

(a)

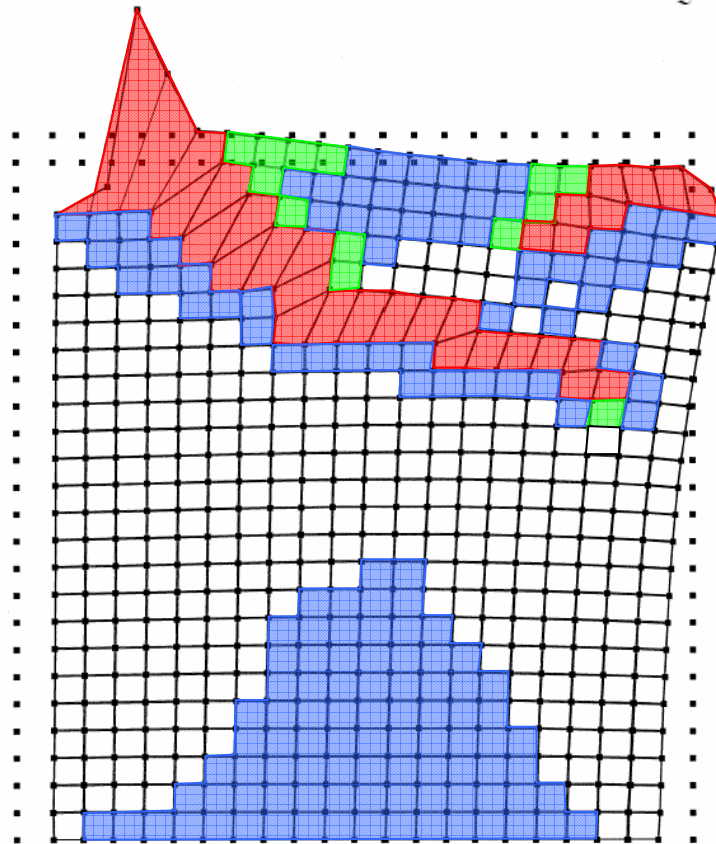


Test specimen at ultimate load  
 $\Delta = 0.2$  in  $\Delta/h_w = 0.005$   $\lambda_Q = 1.0$



Test specimen at conclusion of loading  
 $\Delta = 3.0$  in  $\Delta/h_w = 0.040$   $\lambda_Q = 0.2$

(b)



DEFLECTED SHAPE SHOWING USAGE RATIOS

Structure = exp-2 (yn)

Analysis Series = test-c (test-c)

Load Case = [6] = [5] + push3

Reference Drift = 0.01724

Limit state group = all deformation states

Minimum usage ratio for each color : 0.0 0.5 1 1.5 2

Figure 5.3 (a) Photo of damaged test specimen (Barda 1976); (b) finite element model (Run 4)



**Table 5.1 Concrete wall calibration to test specimen: *RAM Perform* input properties**

	Run #	0	1	2	3	4	5	6	7	8	9	10	11	Note	
Inelastic Steel Material	Shape	E-P-P	E-P-P	E-P-P	E-P-P	E-P-P	E-P-P	E-P-P	E-P-P	Trilinear	Trilinear	Trilinear	Trilinear	E-P-P	$29000 = E_s$ $71 = F_y$ $92.3 = 1.3 F_y$ $81.7 = 1.15 F_y$
	$K_0$ (ksi)	29000	29000	29000	29000	29000	29000	29000	29000	29000	29000	29000	29000	29000	
	$F_R$ (ksi)	71	71	71	71	71	71	71	71	71	71	71	71	71	
	$F_U$ (ksi)	-	-	-	-	-	-	-	-	92.3	92.3	92.3	81.7	-	
	$D_U$	-	-	-	-	-	-	-	-	0.05	0.05	0.05	0.03	-	
	$D_L$	0.1	0.1	0.1	0.1	0.1	-	-	-	0.033	0.033	0.033	0.033	-	
	$D_R$	0.11	0.11	0.11	0.11	0.11	-	-	-	0.036	0.036	0.036	0.036	-	
	$F_R/F_U$	0.05	0.05	0.05	0.05	0.05	-	-	-	0.05	0.05	0.05	0.05	-	
Inelastic Concrete Material	$K_0$ (ksi)	3300	3300	3300	3300	3300	3300	3300	2310	2310	2310	2310	2310	3300	$2310 = 2/3 E_c$ $3.4 = f'_c, 4.08 = 1.2 f'_c$ See note 1
	$F_U$ (ksi)	4.08	4.08	4.08	4.08	4.08	4.08	4.08	3.4	3.4	3.4	3.4	4.08	3.4	
	$D_L$	0.003	0.003	0.003	0.003	0.003	0.003	0.003	0.002	0.002	0.002	0.002	0.002	0.003	
	$D_R$	0.006	0.006	0.006	0.006	0.006	0.006	0.006	0.006	0.006	0.006	0.006	0.006	0.006	
	$F_R/F_U$	0.1	0.1	0.1	0.1	0.1	0.1	0.1	0.01	0.01	0.01	0.01	0.01	0.2	
Inelastic Shear Material	$K_0$ (ksi)	50	50	50	50	50	50	50	50	50	145	145	145	560	$145 = \rho E_s$ $0.204 = 3.5 \sqrt{f'_c}$ $0.17 = 0.6/3.5$ (FEMA 306)
	$F_U$ (ksi)	0.64	0.64	0.64	0.64	0.64	0.64	0.64	0.64	0.64	0.204	0.204	0.7	0.71	
	$D_L$	0.0256	0.0256	0.0154	0.0154	0.0154	0.0154	0.0154	0.0154	0.0154	0.003	0.003	0.005	0.0075	
	$D_R$	0.064	0.064	0.0384	0.032	0.0256	0.0256	0.0256	0.0256	0.0256	0.007	0.007	0.007	0.0085	
	$F_R/F_U$	0.2	0.4	0.4	0.5	0.5	0.5	0.5	0.5	0.5	0.5	0.17	0.17	0.4	
Diagonal Compression Material	$K_0$ (ksi)	3300	3300	3300	3300	3300	3300	3300	(Same as Inelastic Concrete Material)	(Same as Inelastic Concrete Material)	(Same as Inelastic Concrete Material)	(Same as Inelastic Concrete Material)	(Same as Inelastic Concrete Material)	(Same as Inelastic Concrete Material)	
	$F_U$ (ksi)	4.08	4.08	4.08	4.08	4.08	4.08	4.08							
	$D_L$	-	-	-	-	-	-	-							
	$D_R$	-	-	-	-	-	-	-							
	$F_R/F_U$	-	-	-	-	-	-	-							
Match of Initial Stiffness		OK	OK	OK	OK	OK	OK	OK	Fair	Fair	Good	Good	Good	Poor	
Match of Peak Strength		OK	Good	OK	OK	OK	OK	OK	Fair	Fair	Poor	Poor	Poor	Fair	
Match of Strength Degradation		OK	Poor	Fair	OK	Fair	Poor	Poor	Poor	Poor	Poor	Poor	Fair	Poor	
Match of Failure Pattern		-	-	-	-	Poor	Fair	Fair	OK	OK	Fair	Fair	Poor	Poor	

**Note 1: Value of  $D_L=0.002$  and  $D_R=0.006$  corresponded to Park and Pauley (1975)**

The image displays the RAM Perform software interface for defining material properties and relationships for a calibration test specimen. The interface is organized into several main sections:

- Component Properties:** This section defines the material type and name for different components.
  - Reinforcing Bar Old:** Type: Inelastic Steel Material. Name: reinforcing bar old. Modulus (K0): 29000. Tension Strength (FY): 71. Compression Strength (FY): 71. Tension Strain (DX): 1.0. Dispensation Factors: None.
  - Concrete Old 1:** Type: Inelastic Concrete Material. Name: concrete old 1. Modulus (K0): 3300. Tension Strength (FY): 4.08. Compression Strength (FY): 4.08. Tension Strain (DX): 0.02. Dispensation Factors: None.
  - Shear Old:** Type: Inelastic Shear Material. Name: shear old. Modulus (K0): 50. Shear Strength (FY): 0.64. Shear Strain (DX): 0.5. Dispensation Factors: None.
- Basic Relationship:** This section defines the relationship between stress (F) and strain (D).
  - Reinforcing Bar Old:** F = stress, D = strain. Shows a bilinear stress-strain relationship with a yield plateau.
  - Concrete Old 1:** F = stress, D = strain. Shows a stress-strain relationship with a peak followed by a softening branch.
  - Shear Old:** F = shear stress, D = shear strain. Shows a bilinear stress-strain relationship.
- Strength Loss:** This section defines the strength loss parameters for the materials.
  - Concrete Old 1:** DL: 0.003, DR: 0.006, FR/FU: 0.1.
  - Shear Old:** DL: 0.0154, DR: 0.0256, FR/FU: 0.5.
- Strain Capacities:** This section defines the strain capacities for the materials.
  - Concrete Old 1:** DL: 0.003, DR: 0.006, FR/FU: 0.1.
  - Shear Old:** DL: 0.0154, DR: 0.0256, FR/FU: 0.5.
- Dispensation Factors:** This section defines the dispersion factors for the materials.
  - Concrete Old 1:** DL: 0.003, DR: 0.006, FR/FU: 0.1.
  - Shear Old:** DL: 0.0154, DR: 0.0256, FR/FU: 0.5.
- Fibers:** This section defines the fiber properties for the concrete.
  - Concrete:** Material name: concrete old 1. Wall thickness: 4. No. of fibers: 4.
  - Steel:** Material name: reinforcing bar old. Area, as PERCENT of concrete area: 0.5. No. of fibers: 4.
  - Monitored Fibers:** Monitored fibers are used in limit states.
    - Concrete:** Material name: concrete old 1. No. of fibers: 0 (Max = 2).
    - Steel:** Material name: reinforcing bar old. No. of fibers: 2 (Max = 2).
- Basic Components:** This section defines the basic components for the test specimen.
  - Vertical Axis/Bending Component:** Type: Fiber Section for a General Wall. Name: wall old.
  - Horizontal Axis/Bending Component:** Type: Fiber Section for a General Wall. Name: wall old.
  - Shear Components:** Wall thickness for concrete shear (0 = none): 4. Shear material name: shear old. Wall thickness for diagonal compression (0 = none): 4. Diagonal material name: concrete old. Diagonal layer active for gravity? Yes.

Figure 5.4 RAM Perform input properties for calibration to test specimen (Run 4)

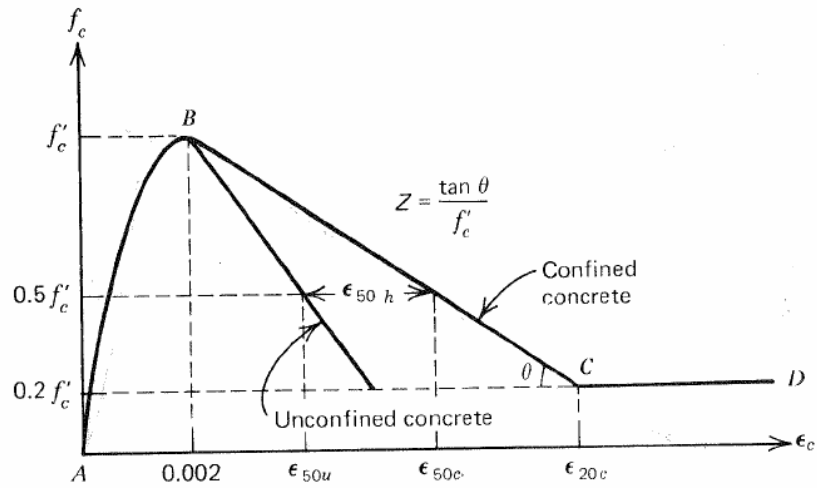


**Figure 5.5 Stress-strain curve for concrete confined by rectangular hoops (Park and Paulay 1975)**

## 6 Other Applications of the Guidelines

In addition to the two test application buildings included in the original scope of this project, Rutherford & Chekene has applied the evaluation methodology of the *Guidelines* to several other buildings. Pacific Gas & Electric engaged R&C and SGH to apply the methodology to an eight-story steel moment-frame building, and PG&E engaged R&C to apply the methodology to four additional buildings. The buildings are listed in Table 6.1. For each building summarized in this section, the reference listed in Table 6.1 provides further information on the seismic assessment. These examples demonstrate the variety of structures and analysis approaches that can be used with the *Guidelines*. Depending on the characteristics and expected nonlinear behavior of each building, a suitable analysis approach is selected and applied within the context of the *Guidelines*. This section discusses unique aspects associated with the application of the *Guidelines* to each of these buildings.

### 6.1 EIGHT-STORY STEEL MOMENT-FRAME BUILDING

The application of the *Guidelines* to an eight-story steel moment-frame building differs from the first two test applications not only in terms of the height of structure analyzed but also in terms of the analysis method employed. While the first two test applications use nonlinear static analyses and the *SPO2IDA* program to produce plots of spectral acceleration versus roof drift, this application uses actual nonlinear response history analyses to perform incremental dynamic analyses of the intact structure and the damaged structure. Higher mode effects may influence the building's dynamic behavior in ways that the *SPO2IDA* program does not capture. Nonlinear static analyses are performed and the *SPO2IDA* program is used to compare the results of the two analysis procedures.

**Table 6.1 Applications of the Advanced Seismic Assessment Guidelines**

<b>Building description (primary reference)</b>	<b>Section</b>	<b>Key behaviors</b>	<b>Analysis method(s)</b>
3-story steel moment frame (this report)	2	Beam-column connection fracture	2-D nonlinear static with frame elements; elastic analyses of damaged structure to estimate re-loading stiffness; <i>SPO2IDA</i>
1-story mill building (this report)	4	Wall and spandrel shear	2-D nonlinear static with finite elements using sequential elastic analyses
			Also, 2-D nonlinear static with finite elements; adjustment of nonlinear properties of concrete in the damaged structure; <i>SPO2IDA</i>
8-story steel moment frame (R&C, SGH 2004)	6.1	Beam-column connection fracture	2-D nonlinear response history with frame elements; modeled cyclic behavior of beam-column connections with fracturing; incremental dynamic analysis
			Also, 2-D nonlinear static with frame elements; <i>SPO2IDA</i>
1-story mill building with 2-story rear portion (R&C 2005a)	6.2	Discontinuous wall, wall shear	2-D nonlinear static for each wall line using plastic mechanism spreadsheet and force levels from tributary mass; <i>SPO2IDA</i>
3-story pier-and-spandrel building with concrete frame (R&C 2005b)	6.3	Wall pier and spandrel shear, interior column shear, diaphragm expansion joint opening	2-D nonlinear static using plastic mechanism spreadsheet; <i>SPO2IDA</i>
			Also, 3-D nonlinear static with frame elements (stiffness calibrated to equivalent shell element models) and semi-rigid diaphragm; <i>SPO2IDA</i>
1-story plus basement and mezzanine with steel frame and concrete walls (R&C 2006a)	6.4	Precast concrete panel connections, diaphragm shear, discontinuous walls	2-D elastic dynamic to obtain vertical distribution of earthquake forces; 2-D (plan) nonlinear static using spreadsheet sequential elastic analyses; <i>SPO2IDA</i>
1-story mill building with flat roof and skylights (R&C 2006b)	6.5	Diaphragm shear, wall shear	2-D (plan) nonlinear static with finite element diaphragm and nonlinear horizontal springs at wall locations; <i>SPO2IDA</i>

### 6.1.1 Building Description

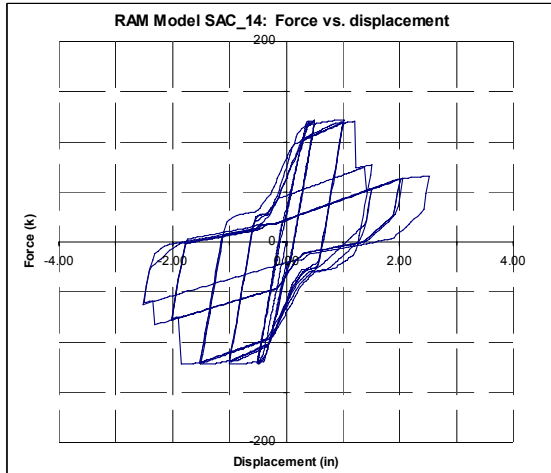
The eight-story welded steel moment-frame building was constructed in 1974. As in the first test application building, the steel moment frames are designed and specified to “pre-Northridge” standards, meaning that the beam-column connections may be susceptible to fracture near the welds of beam flanges to columns. Lightweight precast concrete panels clad the perimeter steel frames as shown in Figure 6.1.



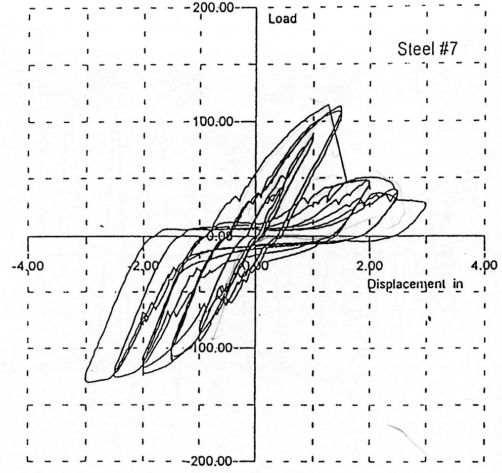
**Figure 6.1 Eight-story moment-frame building (R&C, SGH 2004)**

### **6.1.2 Computer Analysis Model**

A key aspect of modeling the dynamic behavior of this “pre-Northridge” steel moment-frame structure is the modeling of nonlinear hysteretic component properties of beam-to-column connections. In order to accurately represent expected component behavior, each beam-to-column connection in the model includes a group of fiber elements that capture the effects of beam yielding, column panel zone yielding, and connection fracture. The properties of these fiber elements are calibrated to match the hysteretic performance of an experimental test specimen of a pre-Northridge-type steel moment-frame connection tested as part of the SAC program (Anderson 1995). Figure 6.2 compares hysteretic behavior of the connection as modeled to that of the test specimen. Applicable laboratory tests were halted after flanges fractured but before gravity collapse by shear tab failure. Based on engineering judgment, gravity collapse is assumed to occur at a drift of 7% as shown in Figure 6.3. Figure 6.4 displays an example of how this detailed component modeling technique facilitates monitoring damage within the structure.



a. Model behavior



b. Test behavior

**Figure 6.2 Hysteretic behavior of model component (a) and test specimen (b) of beam-column connections (R&C, SGH 2004)**

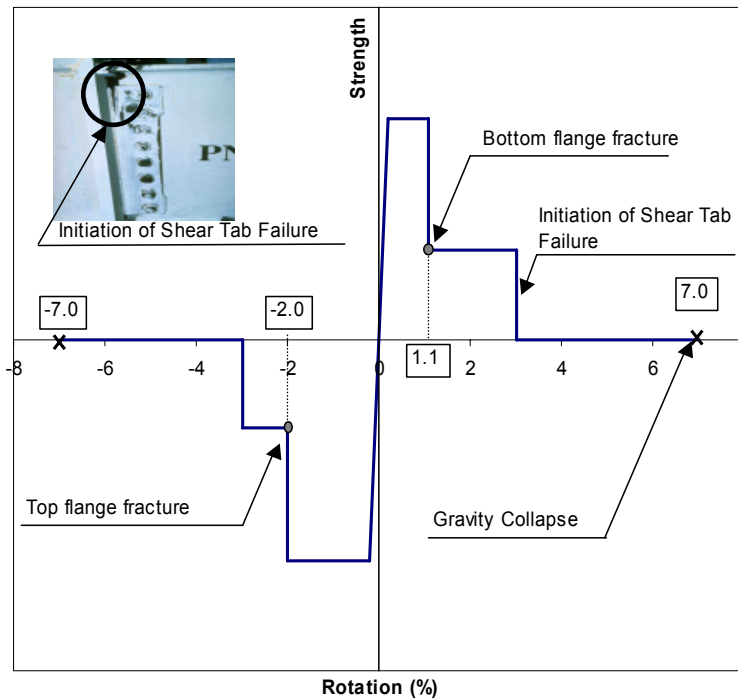


**Figure 6.3 Assumed force-deformation relationship for beam-to-column connections (R&C, SGH 2004) (Photo courtesy of David Bonowitz and taken from SAC Program UC BPN3 test (Popov et al., 1996))**

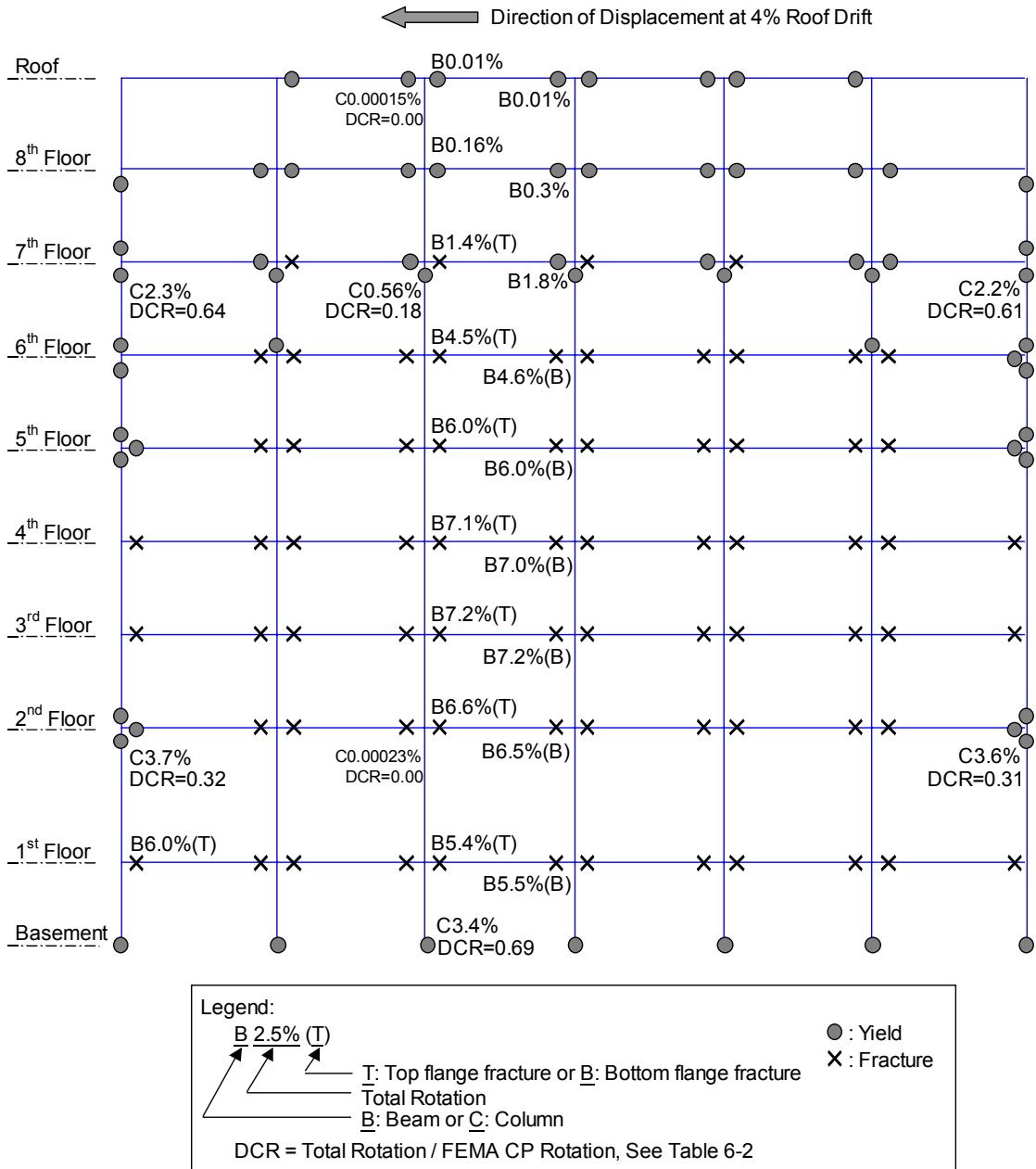


**Figure 6.4 Selected member rotations for damage state DS4 (FN-L-3x0.75) at 4% roof drift during aftershock +FN-S-2x1.5 (R&C, SGH 2004)**



### 6.1.3 Incremental Dynamic Analysis

An incremental dynamic analysis of the intact structure is performed to simulate damage caused by a main-shock earthquake. Then three damage states are defined and incremental dynamic analyses are performed for each of the damage states to simulate response in an aftershock.

Each incremental dynamic analysis consists of a series of nonlinear response history analyses using five different earthquake records. Each of these earthquake records is run at four different scales and the drifts caused by each scaling are recorded. Figure 6.6 displays the resulting IDA curves for the intact structure. For main-shock analysis of the intact structure, a suite of five ground motions is applied with a 2,500-year recurrence interval, and each ground motion is incrementally scaled to amplitudes of 60%, 75%, 100%, and 125% of the 2,500-year hazard; for aftershock analysis of the damaged structure, a different suite of five ground motions is applied with a 200-year recurrence interval, and each ground motion is incrementally scaled to amplitudes of 50%, 100%, 125%, and 150% of the 200-year hazard. If, at a certain scaling, the roof drift exceeds 10% or the analysis becomes unstable, it is determined that that particular ground motion and scaling will cause collapse.

For each nonlinear response history analysis within the aftershock IDA, two sequential ground motions are run: a main-shock ground motion and an aftershock ground motion. Figure 6.5 displays several example response histories for damage state DS4. One main-shock ground motion is selected to run for all damage states, but that ground motion is scaled differently for each damage state such that the main shock causes the amount of damage that characterizes the damage state in question. Within each damage state IDA, a constant main-shock scaling is maintained while incrementally increasing the aftershock scale, as described above. Since the direction of residual drift caused by the main shock may affect aftershock response, each aftershock record is run in both the positive and negative directions.

### 6.1.4 Results

As an example of output data, Figure 6.5 depicts roof drift response histories for the main shock to cause damage state DS4 followed by several examples of incrementally scaled aftershocks in each direction. This plot, analyzed in conjunction with output and comparable plots for other

damage states, illustrates several points regarding results of the main shock plus aftershock incremental dynamic analyses:

- Within the ten aftershocks (and even within the five in one direction), there is a large variability between the record with the lowest scale factor needed to cause collapse and the record with the highest scale factor.
- The applied direction of the aftershock is critical.
- There is a consistent relationship between maximum roof drift and maximum beam rotation.
- For the low levels of damage such as DS2, large aftershocks are necessary in order to cause collapse.

### 6.1.5 Comparison of IDA and SPO2IDA

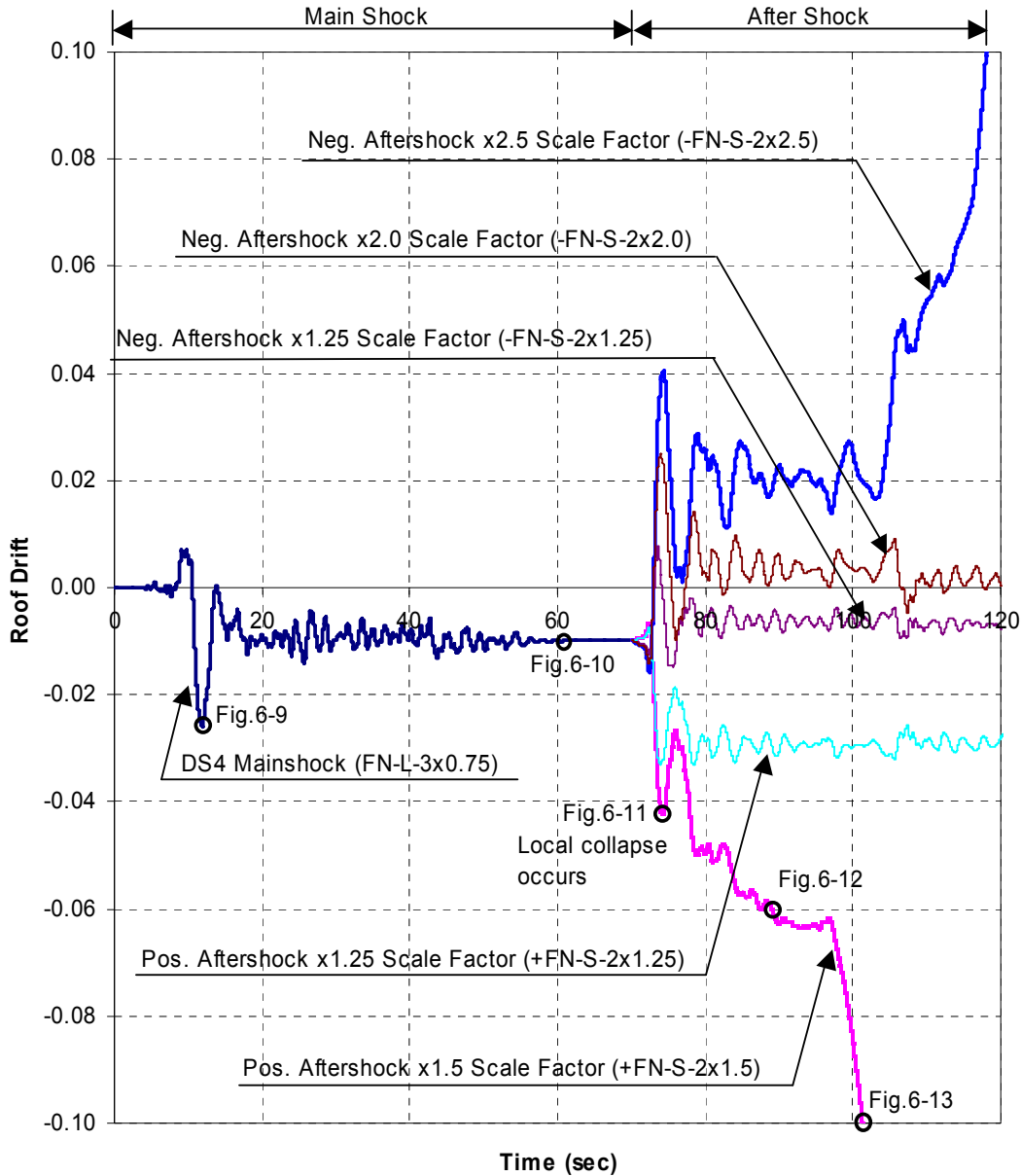
For comparison of analysis methods, nonlinear static analyses of the damaged structure are also performed, and the *SPO2IDA* program is used to generate IDA curves. To reach each damage state, the structure is first subjected to the same main-shock record, scaled as in the incremental dynamic analysis of the damaged structure. Then nonlinear static (pushover) loading is applied, force-displacement curves are generated, and these curves are input into *SPO2IDA*.

Table 6.2 compares IDA and *SPO2IDA* results of spectral accelerations required to cause each damage state. Figure 6.7 depicts this information graphically, where the median IDA curve from Figure 6.6 is shown on the same plot with the *SPO2IDA* results. Compared to the response history results, *SPO2IDA* predicts lower spectral accelerations to achieve the same roof drift.

Table 6.3 compares IDA and *SPO2IDA* results of spectral accelerations required to collapse the damaged structure. Again, the *SPO2IDA* predicts lower spectral acceleration values than do the response history runs. As mentioned above, this discrepancy may be partially due to the fact that higher mode effects can influence the response of an eight-story building in ways that *SPO2IDA* does not necessarily capture.

Figure 6.8 applies Tagging Criteria D to the *SPO2IDA* results to calculate spectral accelerations to cause the onset of yellow- and red-tag classifications. Table 6.4 presents the spectral accelerations and roof drifts expected to cause each limit state. Roof drifts at each limit state are similar for IDA and *SPO2IDA* results. However, as a result of the difference between

intact IDA curves shown in Figure 6.7, the *SPO2IDA* method predicts lower spectral accelerations to cause these roof drifts.



**Figure 6.5 Roof drift vs. time, damage state DS4 main shock + aftershocks (R&C, SGH 2004)**

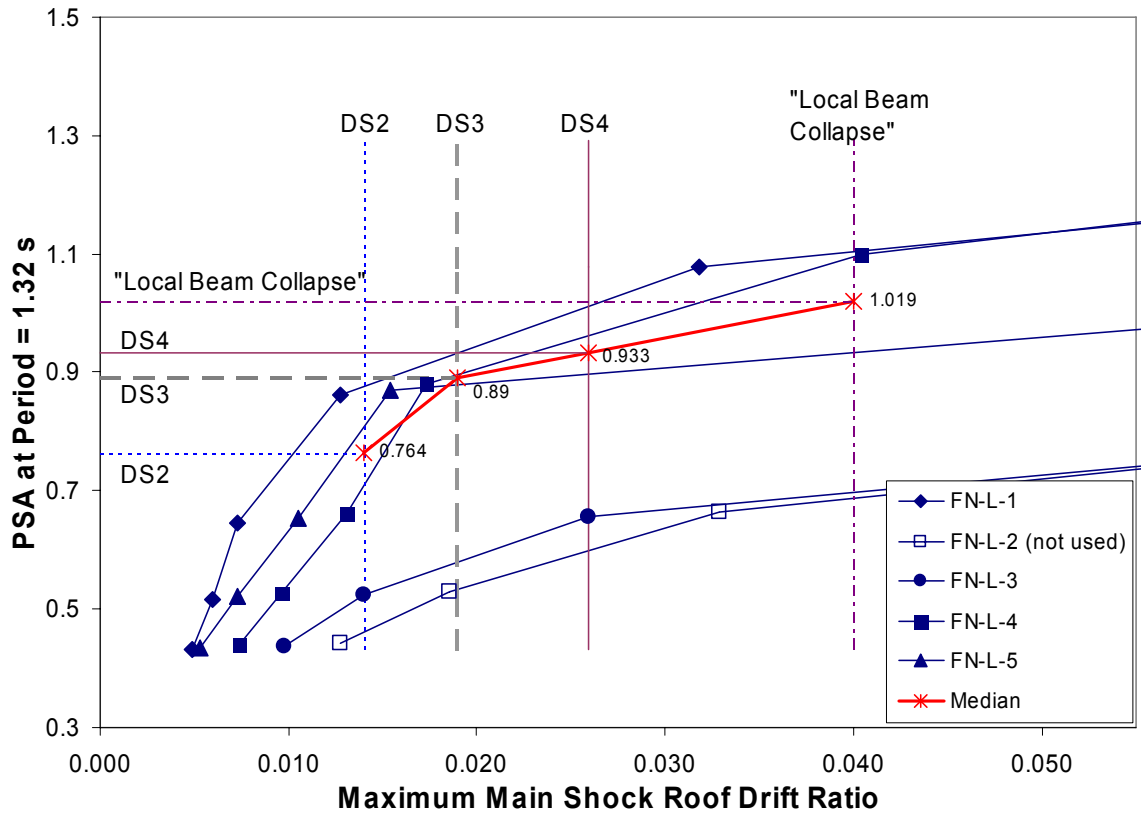


Figure 6.6 IDA from nonlinear response history analyses for intact structure (R&C, SGH 2004)

Table 6.2 Spectral acceleration (g) to cause each damage state, comparison of *SPO2IDA* and nonlinear response history estimates (R&C, SGH 2004)

Damage State	Median of 4 Nonlinear Response Histories	Median SPO2IDA
DS2	0.76	0.39
DS3	0.89	0.54
DS4	0.93	0.72
Collapse	1.02	0.93

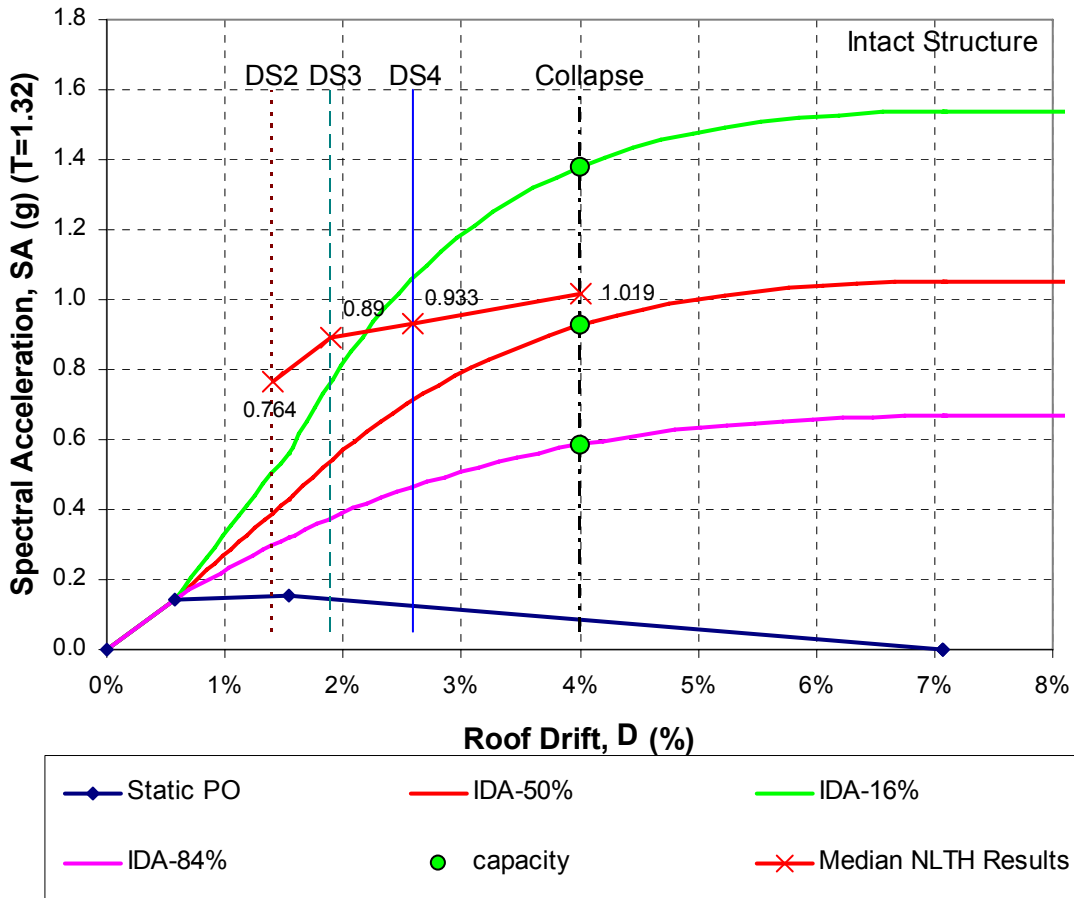


Figure 6.7 *SPO2IDA* for intact structure (R&C, SGH 2004)

Table 6.3 Spectral acceleration (g) to cause collapse in an aftershock, comparison of nonlinear response history and *SPO2IDA* estimates (R&C, SGH 2004)

Damage State	Nonlinear Response History			SPO2IDA		
	Median – Std. Dev.	Median	Median + Std. Dev.	Median – Std. Dev.	Median	Median + Std. Dev.
Intact	—	1.03*	—	0.59	0.93	1.38
DS2	0.78	1.15	1.46	0.52	0.87	1.33
DS3	0.67	0.99	1.49	0.44	0.78	1.20
DS4	0.55	0.83	1.50	0.36	0.62	0.95

\*Spectral acceleration is that at T=1.32 seconds. For the intact structure response history run, this is based on the 2500-year suite of records; for the other response history runs, it is based on the 200-year suite.

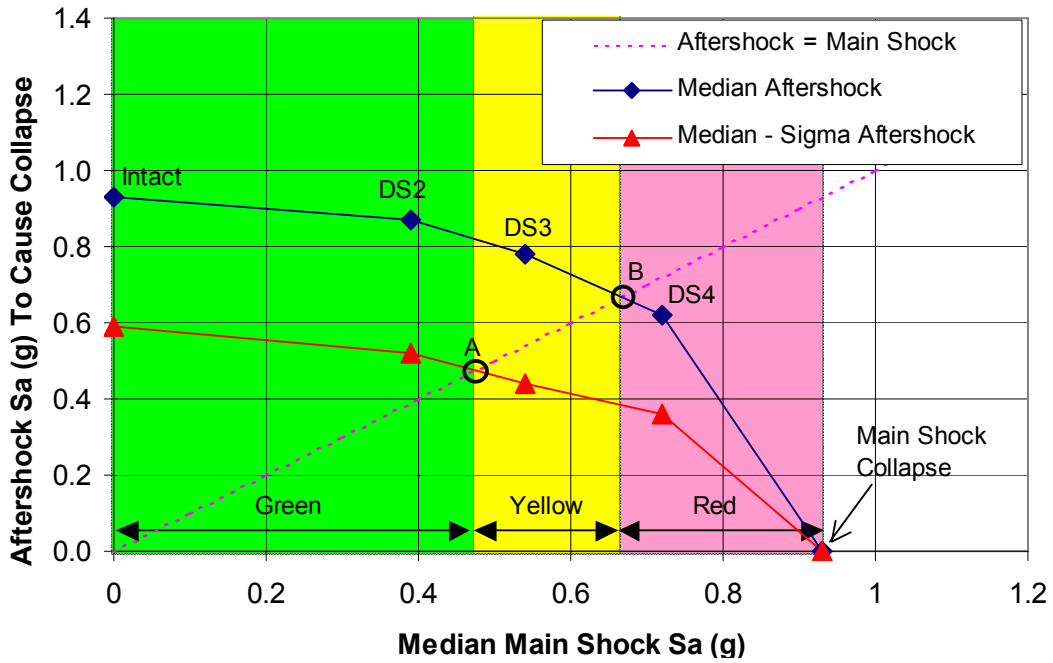


Figure 6.8 Main shock vs. aftershock to cause collapse, Tagging Criteria D using *SPO2IDA* results (R&C, SGH 2004)

Table 6.4 Tagging limit states, comparison of *SPO2IDA* and nonlinear response history analysis (R&C, SGH 2004)

Damage State	NLRH		SPO2IDA	
	Spectral Acceleration	Roof Drift	Spectral Acceleration	Roof Drift
Onset of Yellow	0.76	1.4%	0.48	1.7%
Onset of Red	0.89	2.2%	0.67	2.4%
Collapse	1.02	4.0%	0.93	4.0%

## 6.2 ONE-STORY MILL BUILDING WITH TWO-STORY REAR PORTION

The mill building shown in Figure 6.9 has a steel frame, concrete walls, and a concrete roof supported by steel trusses. The front of the building is a single-story high-bay portion with a hipped roof, and the rear is a shorter two-story portion with a flat roof. Both the front and back portions are rectangular in plan, but the back portion is slightly smaller in plan than the front. Each wall line has a unique configuration of solid walls, piers, and columns.

The building's geometry lends itself to a case-by-case analysis of each wall line. Figure 6.10 displays the estimated nonlinear force-displacement behavior at each wall line. The elastic stiffness of each wall line is estimated using hand and spreadsheet calculations, and it is assumed that roof and floor diaphragms distribute lateral forces to walls according to tributary mass. Spreadsheets are used to perform plastic mechanism analyses in order to determine the lateral strength and governing mode of failure for each wall line. Based on the governing mode of failure, post-yield behavior is estimated such that modeled component behavior is consistent with applicable research results. From the force-displacement relationships of Figure 6.10, *SPO2IDA* is used to compute the relationship between spectral acceleration and ductility demand.

The results of our analysis indicate that retrofitting to mitigate a discontinuous shear wall on Line B in the two-story rear portion will allow the building to achieve PG&E's desired seismic performance goals. This represents a reduced scope of retrofitting compared to that required by a FEMA 356 analysis of the building.



**Figure 6.9 One-story mill building with two-story rear portion (R&C 2005a)**

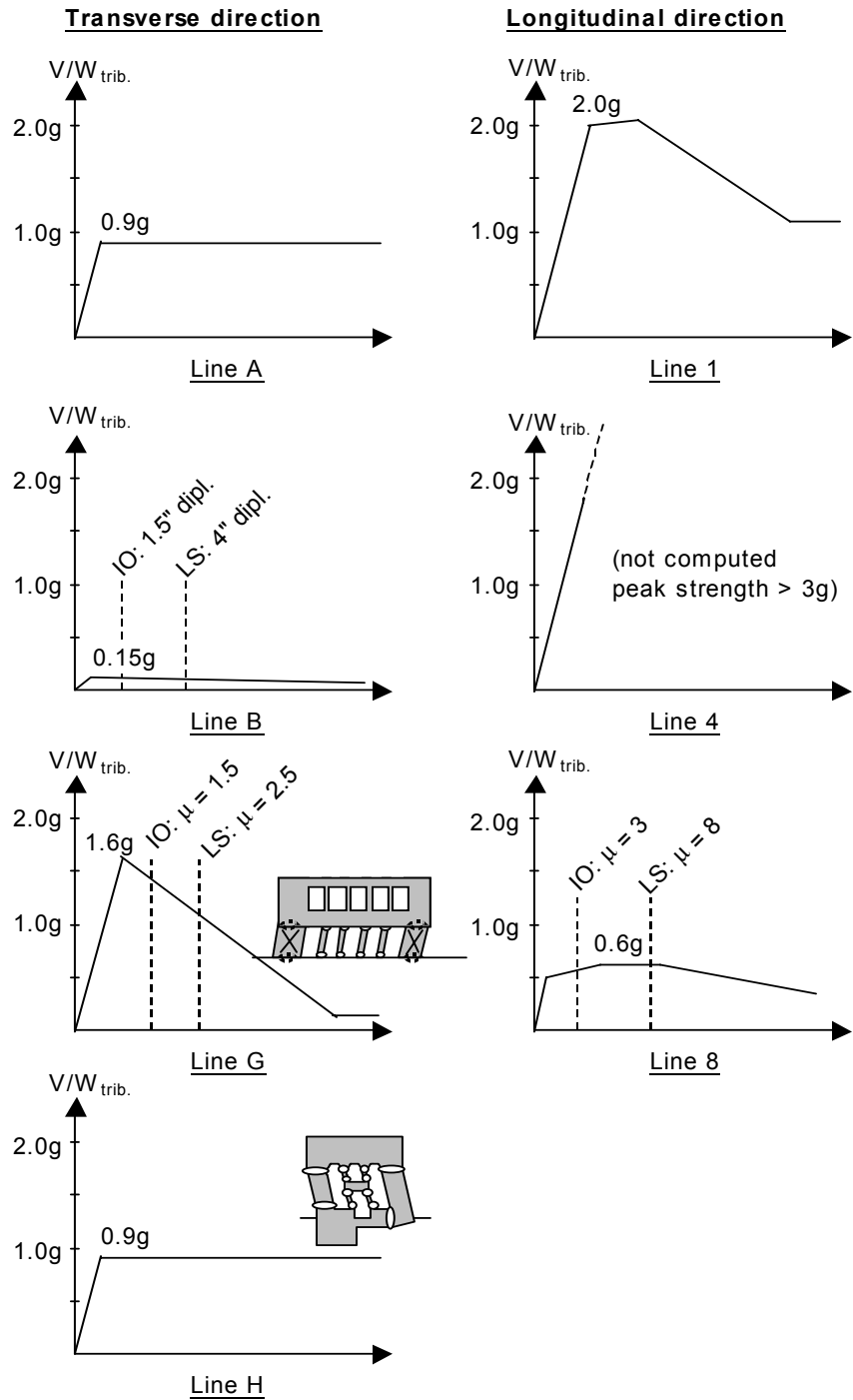


**Figure 6.10 Summary of estimated nonlinear force-displacement behavior at each wall line (R&C 2005a)**



### 6.3 THREE-STORY PIER-AND-SPANDREL BUILDING WITH CONCRETE FRAME

The three-story structure shown in Figure 6.11 has a concrete pier-and-spandrel system around the entire perimeter and an interior grid of concrete columns, beams, and girders. The building is L-shaped in plan, and expansion joints in two plan locations on each floor level have been retrofitted in the past to provide some lateral force transfer between diaphragms on either side of the joints.

Two complementary analyses of this structure are performed: a two-dimensional plastic mechanism analysis using spreadsheets and a three-dimensional nonlinear static analysis using the program *SAP 2000*. The spreadsheet analysis determines likely behavior modes for typical pier-spandrel and beam-column configurations. It allows quick manipulation of member properties to investigate how different retrofit schemes affect the governing mode of nonlinear response. It assumes rigid diaphragm behavior and neglects plan torsion. The computer analysis model shown in Figure 6.12 captures initial stiffness, plan torsion, force demands at diaphragm expansion joints, and variations in pier-spandrel and beam-column configurations. Frame elements are used to represent all piers, spandrels, beams, and columns, but the pier-and-spandrel frame element stiffness properties are first calibrated to match those of a shell element model of the same pier-and-spandrel configuration as shown in Figure 6.13. The 3-D model is used to perform nonlinear static analyses in each plan direction of the building, and the resulting force-displacement response curves are input into *SPO2IDA* to compute the relationship between spectral acceleration and ductility demand.

The results of these analyses demonstrate that a retrofit scheme consisting of fiber-composite column jacketing, strengthened concrete wall piers, and steel gravity supports will allow the building to achieve PG&E's seismic performance goals. This represents a reduced scope of retrofitting compared to previous design proposals.



Figure 6.11 Three-story pier-and-spandrel building with concrete frame (R&C 2005b)

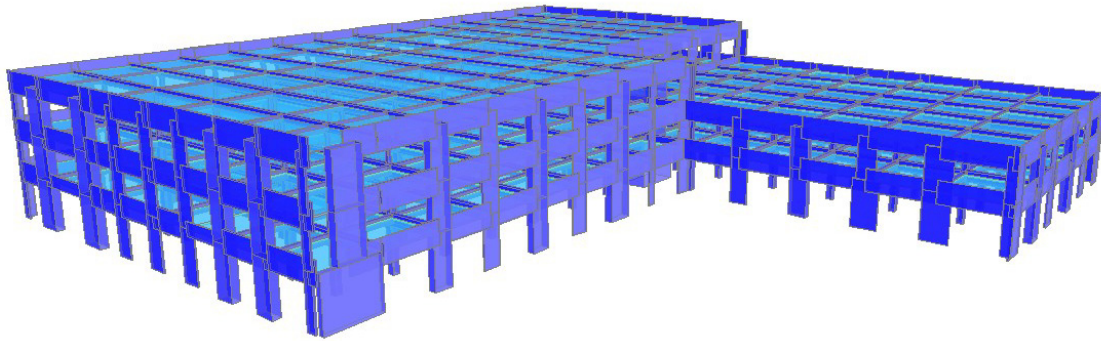


Figure 6.12 3-D computer structural analysis model (R&C 2005b)

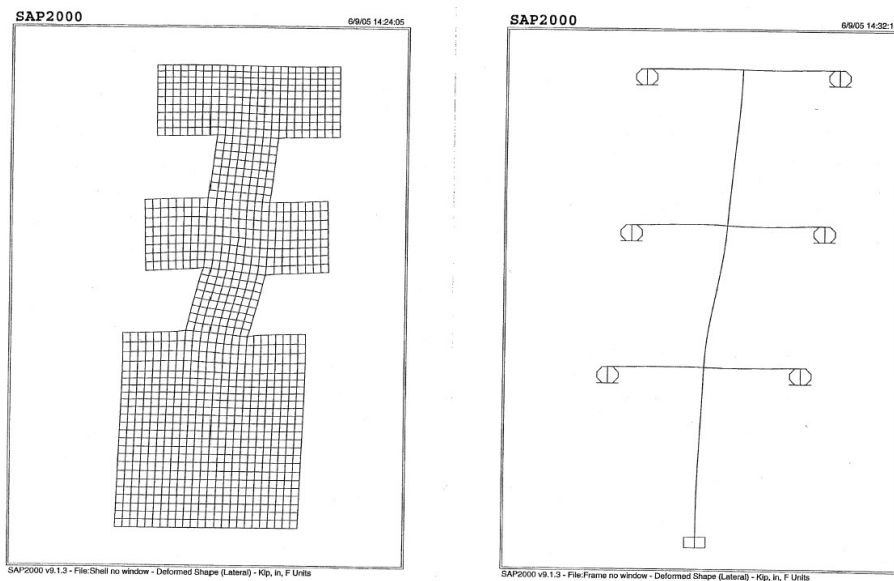


Figure 6.13 Calibration of frame elements in structural analysis model to match shell element properties (R&C 2005b)

## 6.4 ONE-STORY PLUS BASEMENT AND MEZZANINE CONCRETE AND STEEL BUILDING

The building shown in Figure 6.14 is rectangular in plan and consists of a basement, ground floor, mezzanine level, low roof level, and a high roof level. Reinforced concrete beams and columns support the ground floor. Above the ground floor, steel framing encased in concrete and plaster fireproofing supports the mezzanine and roof levels. Cast-in-place concrete walls provide lateral force resistance. Some of these walls are discontinuous from the ground floor to the basement, and some walls do not connect directly to the roof diaphragm above. Precast concrete panels clad the building exterior.

To address the building's irregular configuration and connection details, the structure is analyzed using a spreadsheet analysis to calculate elastic force demands at a given base shear and then create nonlinear force-displacement response curves based on element force capacities, connection force capacities, and expected ductility capacities. For each of the two plan directions of the building, a simplified two-dimensional computer structural analysis model (Fig. 6.15) calculates the existing building's initial stiffness, fundamental period of vibration, and pattern of lateral-force distribution over the building's height. (R&C 2006a)

Two potential retrofit schemes that differ in cost, disruption, and seismic performance are considered. Nonlinear static force-displacement relationships are estimated for each retrofit scheme, and *SPO2IDA* is used to calculate the relationship between spectral acceleration and ductility demand. Using Tagging Criteria D, accelerations expected to cause each tagging limit state are then computed. Figure 6.16 overlays expected tagging limit states for each of the two considered retrofit schemes on the site specific response spectra for the building.



Figure 6.14 One-story plus basement and mezzanine composite building (R&C 2006a)

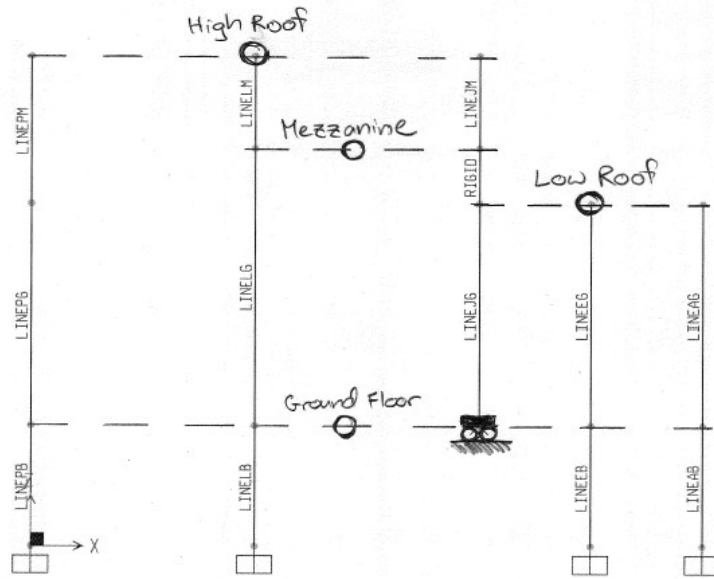


Figure 6.15 2-D computer structural analysis model, longitudinal plan direction (R&C 2006a)

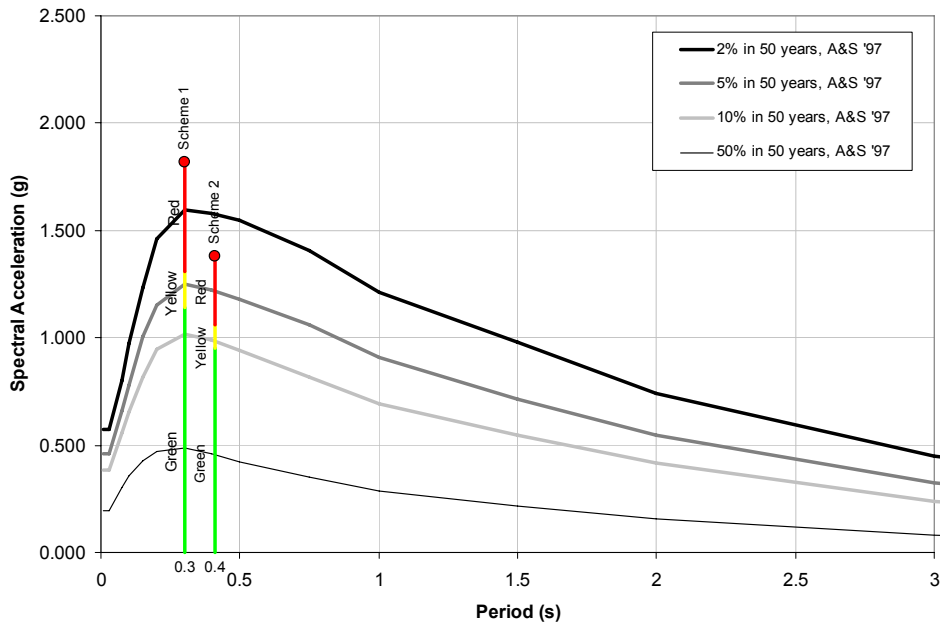


Figure 6.16 Median spectral accelerations to cause each tagging limit state; results for two different retrofit schemes overlain on site-specific response spectra (R&C 2006a)

## 6.5 ONE-STORY MILL BUILDING WITH FLAT ROOF AND SKYLIGHTS

The one-story mill building shown in Figure 6.17 is rectangular in plan with a steel frame, concrete walls, and a flat concrete roof supported by steel trusses. The roof diaphragm contains several large openings for skylights, vents, and mechanical ducts. As in the mill building of Section 6.2, each wall line has a unique configuration of solid walls, piers, and columns. Original structural drawings for the building and field investigations indicate the presence of little to no continuous reinforcement connecting the roof to walls or the walls to foundations for in-plane lateral force transfer.

The building's perforated roof diaphragm necessitates a detailed examination of the stress distribution in this element and its ability to transfer lateral forces to walls below. A two-dimensional model of the roof diaphragm is created using shell elements in the program *SAP 2000* as shown in Figure 6.18. The strength and stiffness of each wall line are calculated by hand, and nonlinear horizontal springs are added to the diaphragm model to represent these walls. Therefore, the two-dimensional diaphragm model effectively represents the three-dimensional behavior of the one-story building. Nonlinear hinges in the horizontal spring elements model the post-yield behavior of each wall line according to the line's governing mechanism: overturning, flexure, diagonal shear cracking, sliding shear at the roof-to-wall interface, or sliding shear at the wall-to-foundation interface. Nonlinear force-displacement curves are generated for the structure using the nonlinear static computer output in conjunction with engineering judgment based on the elastic stresses in the roof diaphragm shell elements. Using *SPO2IDA*, the relationship between spectral acceleration and ductility demand is calculated.

The results of this analysis demonstrate that PG&E's seismic performance goals can be achieved through a reduced scope of retrofitting compared to those prescribed by older evaluation methods.



**Figure 6.17 One-story mill building with flat roof and skylights (R&C 2006b)**

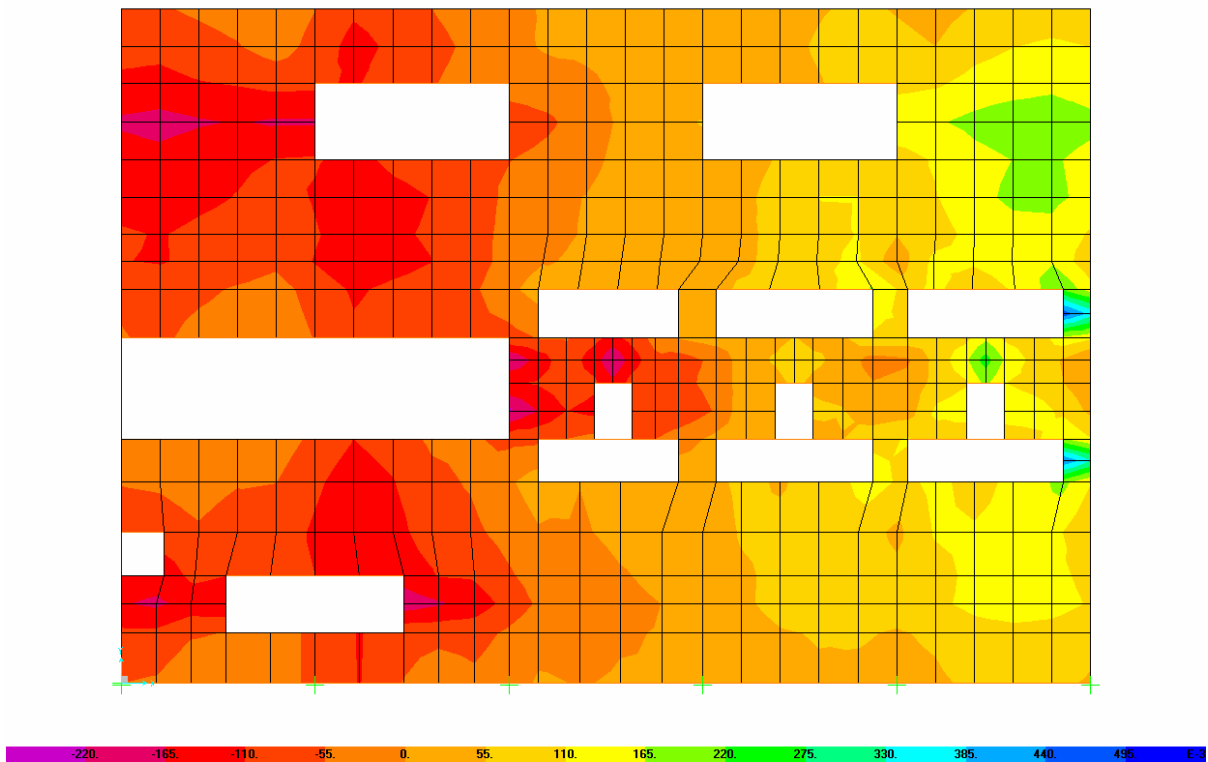


**Figure 6.18 2-D computer structural analysis diaphragm model (R&C 2006b)**

## 7 Key Technical Issues

In applying the *Guidelines* to the example buildings, Rutherford & Chekene recognized two key areas for which further examination and definition of procedures would be useful: (1) residual drift and (2) criteria for defining post-earthquake occupancy (or tagging) limits.

### 7.1 RESIDUAL DRIFT

In assessing the seismic performance of a damaged structure, residual drift or deformation in the building can be an important parameter. The amount of residual drift in a building after a damaging ground motion is unpredictable. It depends on the particular ground motion and the building's inelastic response to it. On average though, residual drift is affected by the amount of peak plastic drift and the shape of the hysteresis loops of force-displacement response. Only the plastic portion of peak drift is relevant to residual drift because a building displaced merely in the elastic range has no residual drift. Strength degradation and the re-centering characteristics of the hysteresis loop shape are key parameters affecting residual drift.

For a damaged structure, the effect of residual drift on seismic performance in an aftershock is also unpredictable. The consequence of the residual drift depends on the particular aftershock ground motion, and whether or not that motion tends to push the structure in the same or opposite direction to the residual drift.

This section outlines a framework and procedure for estimating the effects of residual drift on a structure. Specific research (outside the scope of the Task 508 project) is recommended to estimate residual drift and to determine its effect on a structure's subsequent seismic performance. Such research could provide data to improve the parameters  $\gamma_1$  and  $\gamma_2$  that are used in the framework proposed here. Current research on the topic includes that by Luco et al. (2004).

### 7.1.1 Estimating Residual Drift

The following procedure is used in Test Application 1 to estimate residual drift. (See the notation section for the precise definitions of the variables used.)

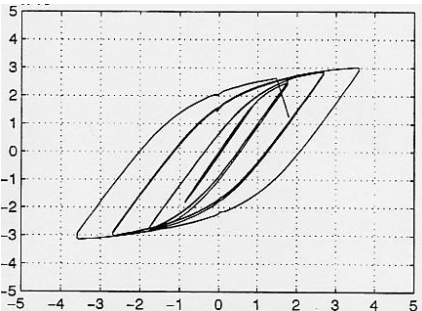
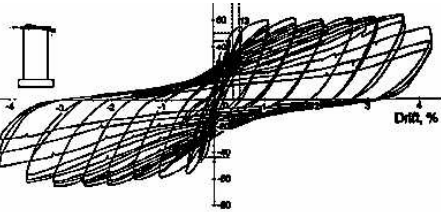
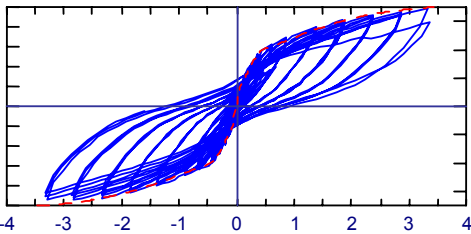
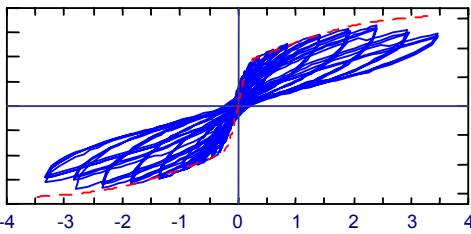
The static residual drift,  $\Delta_{rs}$ , is determined from the static pushover curve and the assumed unloading stiffness, according to the seismic assessment procedure (Fig. 2.12). This static residual drift is a measure of the peak plastic drift that has occurred in the structure.

The actual (dynamic) residual drift,  $\Delta_{rd}$ , cannot be larger than  $\Delta_{rs}$ , and is assumed, on average and for a given hysteresis loop shape, to be proportional to  $\Delta_{rs}$ .

Thus the expected dynamic residual drift,  $\Delta_{rd}$ , is assumed to be a factor  $\gamma_l$  times  $\Delta_{rs}$ . The factor is assumed to depend on the type of seismic-force-resisting system, as it relates to the global hysteresis loop shape of the earthquake response. Specifically, the structural components of the seismic force-resisting system that respond nonlinearly influence the hysteresis loop shape. Hysteresis loop shapes with better displacement restoring characteristics — for example those with a positive slope to the “hysteresis center curve” (MacRae 1995) — are given a smaller value of  $\gamma_l$ . Recommended values of  $\gamma_l$ , as a function of hysteresis loop shape, are shown in Table 7.1.



**Table 7.1 Values of  $\gamma$ , ratio of dynamic to static residual drift**

Example Structure Types	Hysteresis Loop Shapes	$\gamma$
<ul style="list-style-type: none"> <li>• Steel moment frame (with beam flexural hinging)</li> <li>• Steel eccentric braced frame (with link-beam yielding)</li> <li>• Steel buckling-restrained braced frame</li> </ul>		0.5
<ul style="list-style-type: none"> <li>• Flexural plastic hinging in concrete walls or concrete moment frames</li> <li>• Plywood or OSB sheathed walls</li> <li>• Diaphragm-yielding structures (e.g., tilt-ups) with plywood or OSB sheathed diaphragms.</li> <li>• Steel concentric braced frames</li> <li>• Structures not otherwise classified</li> </ul>		0.3
<ul style="list-style-type: none"> <li>• Foundation rocking structures</li> <li>• Other structures with high restoring force from gravity load and rocking-type hysteresis loop shapes</li> </ul>		0.2
<ul style="list-style-type: none"> <li>• Structures specifically designed for minimal residual drift, such as precast hybrid moment frames (FIB 2003)</li> </ul>		0

### 7.1.2 Residual Drift Findings from the Evaluation of an Eight-Story Steel Moment Frame

The evaluation for PG&E of an eight-story steel moment-frame structure with pre-Northridge fracturing beam flange connections (R&C, SGH 2004) provides data on residual drift for this type of structure. The evaluation developed a relatively complete model of the structure's nonlinear hysteretic behavior and subjected that model to numerous ground motions, thus useful data were produced on the potential for the structure to have residual drift. For the eight-story structure, Figures 7.1–7.2 show the relationship between residual roof drift and peak plastic roof drift. Peak plastic roof drift is computed as the peak roof drift minus 0.5%. The value of 0.5% is the estimated roof drift at global yielding of the structure. It is taken from graphically defining an effective initial stiffness on the pushover curve.

If a linear relationship is assumed, Figures 7.1–7.2 show that residual drift equals approximately 0.6 times peak plastic drift. This value of 0.6 can be compared to the  $\gamma_I$  value of 0.5 recommended in Table 7.1. The parabolic trend lines on Figures 6.6–6.7 show that the relationship between residual and peak plastic drift is not truly linear. At least for this structure, the ratio of residual to peak plastic drift increases with increasing drift and deformation. As more beam connections fracture and a greater portion of the response is in the plastic range, residual drift seems to increase parabolically.

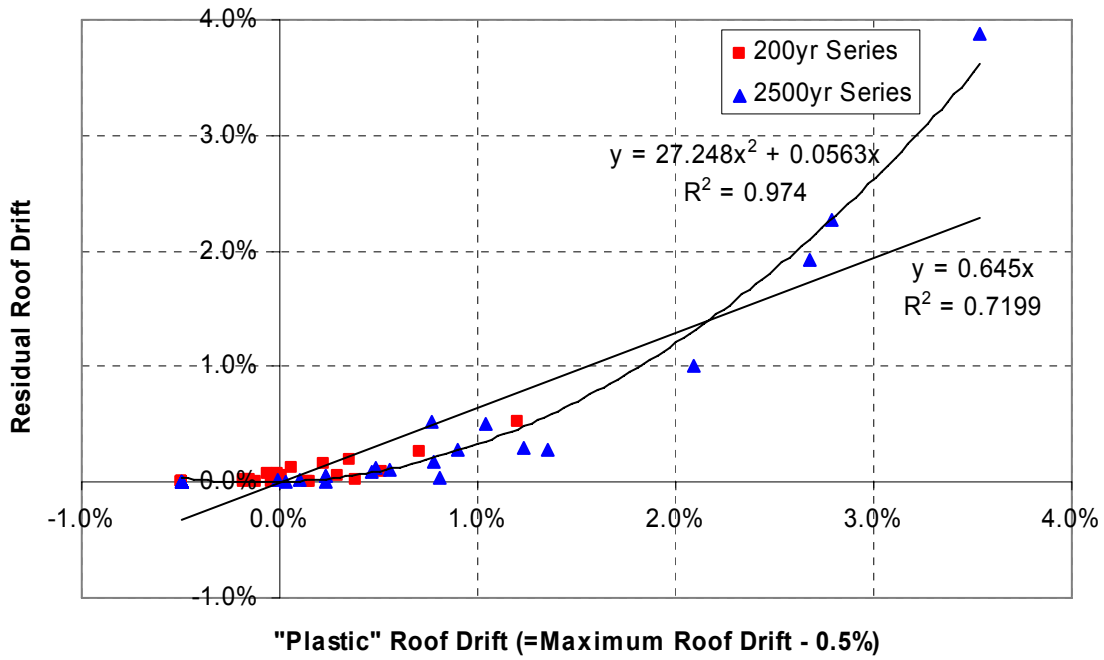


Figure 7.1 Comparison of residual roof drift and maximum roof drift (E-W)

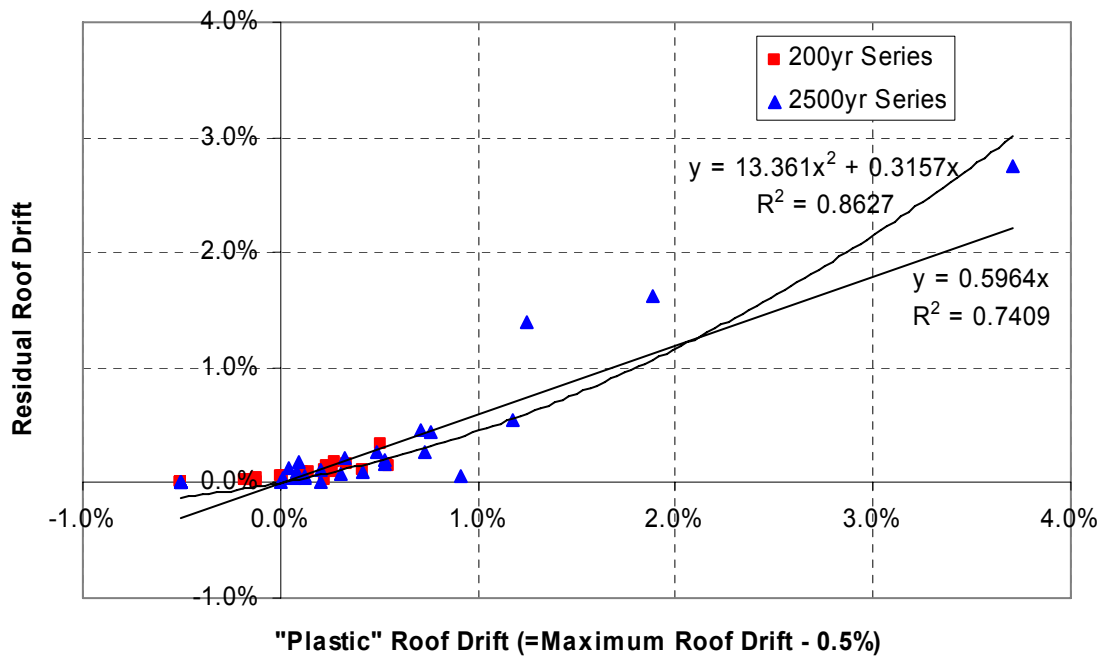


Figure 7.2 Comparison of residual roof drift and maximum roof drift (N-S)

### 7.1.3 Effect of Residual Drift on Seismic Performance

Given a certain amount of residual drift  $\Delta_{rd}$  in a damaged structure, the effect of that residual drift on seismic performance can be considered by reducing in some way the remaining drift capacity of the structure. Under such a framework, the key question is: By how much should drift capacity be reduced? Figure 7.3 conceptually illustrates how the answer to this question is bounded. The figure considers the two-dimensional lateral displacement of a single-degree-of-freedom structure.

Figure 7.3(b) shows the case of the structure with no residual displacement, for which the collapse displacement (displacement capacity) in both the east and west directions is 6 inches. Figure 7.3(c) shows the case for the structure after a damaging ground motion has resulted in a residual displacement of 1 inch to the east. In this case the structure can displace 5 inches to the east or 7 inches to the west before collapsing. The question of interest is: What is the probability of reaching collapse for this structure? The answer can be bounded by observing that the probability of collapse is greater than that for Figure 7.3 (b), but less than that for figure 7.3(d), which shows a structure with a 5-inch displacement capacity in each direction.<sup>1</sup>

Figure 7.3(e) illustrates the definition of  $\Delta_{re}$ , the symmetrical reduction in displacement capacity that would give an equivalent probability of failure to case (c). Based on the bounds observed above, the reduction in global drift capacity  $\Delta_{re}$  must be between zero and  $\Delta_{rd}$ .

---

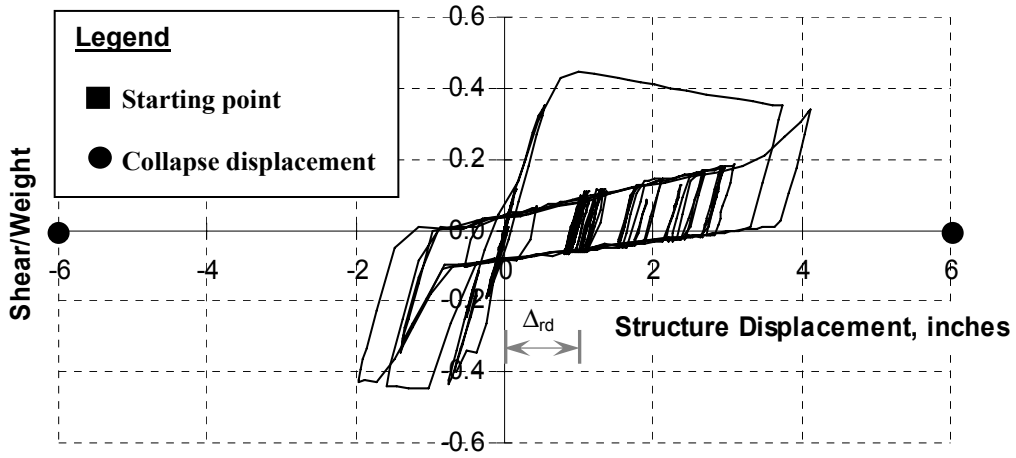
<sup>1</sup>In this observation, it is assumed that (1) the residual displacement affects displacement capacity, not demand, (2) the direction of largest displacement demand is random, and (3) probability of exceedance increases at least linearly with the reduction of displacement demand.

The collapse probability of (c) in Figure 7.3 is less than that for (d) because there will be some percentage of ground motions that push the structure to a westward displacement of between 5 and 7 inches, and an eastward displacement of less than 5 inches, and these will cause collapse for (d) but not for (c). The comparison of case (b) with (c) may be less obvious, but can be proven as indicated below.

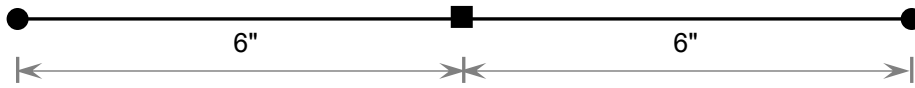
The probability of collapse for (b) is simply the probability that the largest displacement demand in either direction (call this  $\Delta_{d1}$ ) exceeds 6 inches:  $P(\Delta_{d1} > 6")$ . With  $\Delta_{d1}$  equal to the largest displacement demand, and  $\Delta_{d2}$  equal to the maximum displacement demand in the opposite direction, the probability of collapse of (c) can be defined. If  $\Delta_{d1}$  is eastward (a 50% chance) it equals  $P(\Delta_{d1} > 5")$ . If  $\Delta_{d1}$  is westward (also a 50% chance) it equals  $P(\Delta_{d1} > 7")$  plus  $P(\Delta_{d1} < 7") \times P(\Delta_{d2} > 5")$ . The total probability of collapse for (c) is thus  $0.5P(\Delta_{d1} > 5") + 0.5P(\Delta_{d1} > 7") + 0.5P(\Delta_{d1} < 7") \times P(\Delta_{d2} > 5")$ . The sum of the first two terms of this expression equal the average of the probability of reaching a 5" displacement with that of reaching a 7" displacement. Since probability increases at least linearly with the reduction of displacement, the sum of these first two terms alone will always result in a probability of collapse at least equal to that for (b). The addition of the third term, which will never be zero, indicates that the probability of collapse for (c) will always be greater than that for (b).

Thus,  $\Delta_{re}$  is defined to be a factor  $\gamma_2$  times  $\Delta_{rd}$ , where  $\gamma_2$  is between zero and one. The factor  $\gamma_2$  will depend on the particular ground motion, and studies of numerous ground motions applied to structures with residual drift are necessary to determine its average value. Lacking these studies,  $\gamma_2$  is assumed to depend on the strength degradation of the SPO curve, from the observation in nonlinear response that a structure with strength degradation is more likely to ratchet toward a single direction of displacement. The factor  $\gamma_2$  is estimated as a function of strength degradation as shown in Table 7.2.

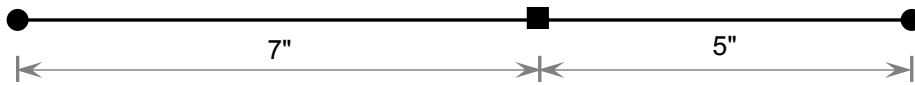
Strength degradation can be classified as high, medium, zero, or strength-increasing by considering the average slope,  $\alpha_i$ , of the SPO between the damage state and the approximate collapse drift. Figure 7.4 shows how  $\alpha_i$  is determined.



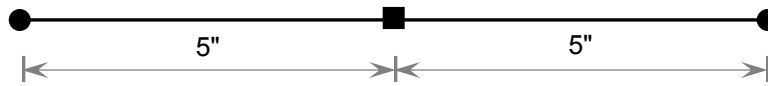
(a) Force-displacement response causing residual displacement of 1 inch



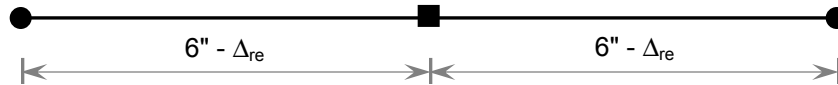
(b) Structure with no residual displacement (intact structure)



(c) Structure with 1 inch residual displacement (damaged structure)



(d) Structure with 5-inch displacement capacity in each direction



(e) Symmetrical reduction in displacement capacity,  $\Delta_{re}$ , calibrated to give the same probability of collapse as in (c)

**Figure 7.3** Diagrams of the relationship between displacement capacity and residual displacement

**Table 7.2 Determining  $\gamma_2$**

Strength Degradation beyond Damage State i	$\gamma_2$
High Degradation	0.9
Moderate Degradation	0.7
Zero Degradation	0.5
Strength Increasing	0.3

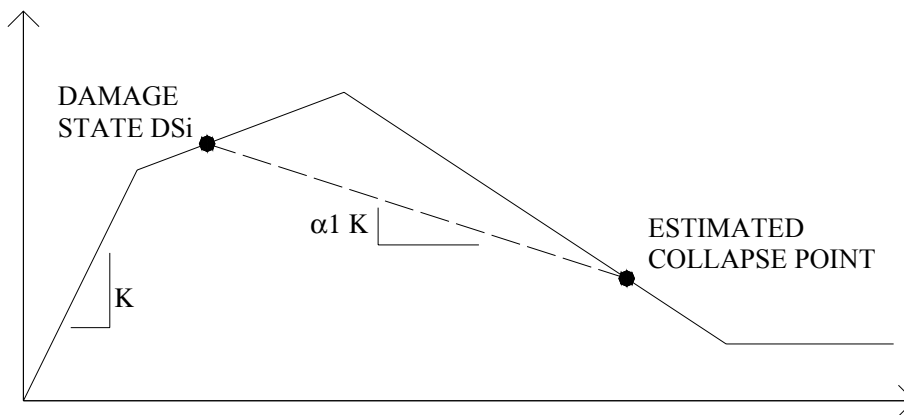


**Figure 7.4 Determining  $\alpha_i$ , slope factor effecting residual drift for  $DS_i$**

## 7.2 TAGGING CRITERIA

The publication of ATC 20 (1989) introduced a common and systematic method of “tagging” buildings immediately following an earthquake to indicate whether or not they should be occupied. The posting of a red tag on the building means that occupancy should not be permitted because it would be unsafe to be in the building in case of an aftershock. The posting of a green tag means that the building is judged to be acceptably safe in an aftershock. The posting of a yellow tag, per ATC-20, means that further investigation is necessary to determine if the building should be posted green or red. In practice, the yellow tag has been used to permit occupancy by a limited number of people or for a limited period of time. For a utility company, such a posting might, for example, permit emergency personnel to briefly access switching equipment.

For different building types, ATC-20 indicates particular damage observations that can be associated with green, yellow, or red tagging. Typically there have been no specific performance criteria, for example, related to aftershock collapse probability, that are defined to correspond to the tagging categories. The FEMA 306 project developed a performance-based framework for evaluating earthquake damage; however the project addressed repair and retrofit decisions and the significance of damage rather than the initial safety assessment with green, yellow, and red tagging. In general terms, ATC-20 states that to receive a green tag, a building should be judged to be able to withstand, without collapse, an aftershock as large as the main shock that struck the building.

For the *Advanced Seismic Assessment Guidelines*, it is necessary to define in seismic performance terms when the tagging limit states are reached. As part of our work in applying the *Guidelines*, four possible tagging criteria are defined. The first is an ideal set of criteria, which would require significant research and consensus judgment before being practically applicable. The remaining three sets of criteria have been applied to test applications of the *Guidelines* as described in Sections 2, 4, and 6. Until such time as Tagging Criteria A are feasible, Tagging Criteria D is recommended.

### **Tagging Criteria A: Based on the probability of collapse for the aftershock seismic hazard**

This option for tagging criteria would be the most technically sophisticated and correct approach, but it requires knowledge of the aftershock<sup>2</sup> seismic hazard and a selection of acceptable collapse probabilities. To date, there has not been much research focused on aftershock seismic hazard. There is the potential that in the near future, more specific data on aftershock seismic hazard could be used in tagging criteria. Research (outside the scope of this project) is recommended in this area. In addition to having a reliable estimate of aftershock seismic hazard, implementation of the criteria requires a consensus judgment of what probability of collapse in an aftershock

---

<sup>2</sup> The terms main shock and aftershock are used throughout this document to mean an initial, damaging ground motion, and then a following ground motion, which can be smaller or larger than the damaging motion. This usage differs from the correct seismological definitions of the terms, which are assigned with certainty only after an earthquake sequence is completed, and for which the terms foreshock, main shock, and aftershock are applied considering the relative magnitude of each earthquake in the sequence.



warrants a yellow or red tag. Calibration to prescriptive tagging guidelines, such as those in ATC-20, could assist in developing this judgment.

**Tagging Criteria B: Based on the probability of collapse of the damaged structure, using the pre-earthquake seismic hazard**

Tagging Criteria B were developed from the idea that for occupancy to be restricted in a building after an earthquake, two conditions should be met. First, the building should have suffered some damage in the earthquake. This condition is based on the ATC-20 practices that only trigger yellow or red tagging based on observing earthquake damage. Second, the building in its post-earthquake condition should be more vulnerable to collapse than is a typical new building designed according to the building code. FEMA 308 (ATC 1999c) uses this concept as a framework for developing triggers and policies for the repair or retrofit of earthquake-damaged buildings.

Tagging Criteria B are explained as *follows*:

*If the increase in probability of collapse is less than 10% ( $P/P_0 < 1.10$ ), then the tagging condition is green.* In other words, if  $P/P_0 < 1.10$ , the ability of the building to survive an earthquake has not been significantly changed by whatever damage has occurred. As is customary in post-earthquake inspection, if a building has not suffered any consequential damage, then it is given a green tag. Even if it is a highly vulnerable building, it is given a green tag because the earthquake did not change its vulnerability.

*If the increase in probability of collapse is greater than 10% ( $P/P_0 > 1.10$ ), then the tagging condition depends on the probability of collapse in an aftershock.* In the absence of aftershock hazard information, this is assumed to correlate to the magnitude of ground shaking, expressed by return period, that would cause collapse. The return period corresponds to the pre-earthquake seismic hazard at the site, i.e., assuming that that hazard has not changed by the occurrence of the damaging earthquake.

*If the return period to cause collapse is greater than 1000 years, then the tagging condition is Green.* For  $RP > 1000$  years, the building has an ability to survive earthquake collapse that is equivalent to or better than that assumed for new structures in conformance with the latest building codes. Therefore, despite the damage sustained, the building is given a green tag.

*If the return period to cause collapse is between 250 and 1000 years, then the tagging condition is yellow.*

*If the return period to cause collapse is less than 250 years, then the tagging condition is red.* A building that has been damaged ( $P/P_0 > 1.10$ ) and will collapse under the relatively small  $RP < 250$  ground motions is considered under enough risk that it warrants a red tag rather than a yellow tag.

For this criteria the trigger values of  $P/P_0 = 1.10$ ,  $RP = 250$ , and  $RP = 1000$  are selected by the judgment of the authors, and could be adjusted as appropriate to calibrate the criteria to past practices or further engineering judgment. In Tagging Criteria B, the size of the main shock affects tagging only in that a larger main shock will cause increased damage. Criteria B do not include the assumption that a larger main shock also correlates to higher aftershock hazard.

### **Tagging Criteria C: Based on the ability to sustain an aftershock proportional to the main shock**

Tagging Criteria C are based on the idea from ATC-20 that a green tagged structure should be able to withstand an aftershock ground motion that could be as large as the main-shock motion. This implies that as the size of the main shock increases, the size of potential aftershocks increases proportionally.

Under this option, the tagging criteria are as follows:

*If the damaged structure can withstand, without collapse, an aftershock with  $S_a$  equal to that of the damaging earthquake, then the tagging condition is green.*

*If the damaged structure collapses under the above test, but can withstand an aftershock with  $S_a$  equal to 0.75 times that of damaging earthquake, then the tagging conditions is Yellow.*

*If the damaged structure collapses under an aftershock with  $S_a$  equal to 0.75 times that of damaging earthquake, then the tagging condition is Red.*

The factor of 0.75 is based on judgment to give a criterion for red tag that corresponds to increased vulnerability compared to the yellow tag. For more conservative criteria, the factors of 1.0 times the damaging ground motion for the onset of yellow tag and 0.75 times the damaging ground motion for the onset of red tag might, for example, be changed, to 1.5 and 1.0, respectively. This latter assumption was found to be more appropriate in the seismic evaluation of an eight-story moment-frame building (R&C, SGH 2004).

In Tagging Criteria C, as the size of the main shock increases, tagging is affected in two ways. First, a larger main shock causes increased damage, and second, a larger main shock requires the damaged structure to be tested by a proportionally larger aftershock.

### **Tagging Criteria D: Refinement of Criteria C based on the variability of structural response**

Tagging Criteria D are a refinement of Tagging Criteria C that makes use of information from the *SPO2IDA* program on the variability of the structural response. The idea, consistent with the ATC-20 framework, is that a yellow tag differs from a red tag principally in the degree of confidence one has that collapse will occur in an aftershock equal in size to the main shock. A red tag means that there is a higher probability of collapse in a given aftershock compared to a yellow tag.

Tagging Criteria D defines the onset of *red tag* as the median main-shock acceleration for which an aftershock of the same acceleration will cause collapse in 50 out of 100 ground motions. The onset of yellow tag is the median main-shock acceleration for which an aftershock of the same acceleration will cause collapse in 16 out of 100 ground motions. The variability being considered in this definition includes only the  $\beta_R$  term, the variability in nonlinear response, which is conveniently provided by the *SPO2IDA* program. The variability of structural deformation capacity is not included in this assessment.

## 8 Conclusions

The project described in this report investigates the practical application and potential of performance-based seismic assessment methods. The project explores issues that may affect the wider application in practice of seismic and structural engineering procedures that use state-of-the-art techniques.

### 8.1 OVERALL FINDINGS

In general, the project finds the following:

- The *Advanced Seismic Assessment Guidelines* are a logical, rational, and technically sound method.
- The *Guidelines* can be implemented in conjunction with a variety of structural analysis approaches, ranging from hand-calculated building response to fully computerized analysis of intact and damaged structures.
- The results of the procedure depend on the technical definition of what collapse potential should correspond to a red-tag, yellow-tag, or green-tag occupancy. This report investigates several options for tagging criteria and generally recommends what is defined as Tagging Criteria D, with correlation to engineering judgment.
- The results of the procedure depend on key assumptions and practices related to evaluating the intact and damaged structure. These practices include the following:
  - Whether the analysis truly identifies and incorporates the structural behavior modes that will govern the seismic response (This is a key aspect of any seismic evaluation procedure.)
  - How degraded components are assumed to respond (This must be based on available research results and technical approaches.)

- Estimating the residual drift in a structure and the relationship between that residual drift and the displacement demand (This report gives recommendations based on a structure's peak plastic drift, hysteresis loop shape, and strength degradation characteristics.)
- For the most effective application of the *Guidelines*, research is needed on the structural response of degraded components, specifically in the following areas:
  - For steel moment-frame structures, tests of beam-column connections are needed, where the tests are taken to displacements beyond flange fracture. (While there have been many tests of such connections, very few have continued testing beyond flange fracture.)
  - For concrete wall structures, a review and assessment of past laboratory testing would be useful, considering behavior modes including flexure, shear, and foundation rocking. (There are a reasonable number of tests available, but appropriate recommendations for seismic evaluation assumptions have not been developed or verified.)
  - Advanced computer models of structural elements — in particular, multi-layer nonlinear finite element models of concrete walls, and nonlinear fiber models of fracturing steel beam connections — should be calibrated to experimental testing.

## 8.2 SPECIFIC RECOMMENDATIONS ON IMPLEMENTATION

In addition to the overall conclusions of the report, the items below summarize some key recommendations to engineers who are using the *Guidelines*, indicating sections of this report that may be especially helpful:

- Engineers using the assessment procedure may find the step-by-step description of applying the *Guidelines*, Section 2.7, to be a useful example.
- A key step for an engineer applying the procedure is the calculation of the SPO of a damaged structure. This report contains examples of different ways that the SPO can be calculated. The procedure for calculating the SPO should be based on:
  - The intact SPO and the damage state  $DS_i$
  - Effective residual deformation,  $\Delta_{re}$

- Reloading initial stiffness,  $K_i$
- Reloading hardening stiffness,  $K_{hi}$

Given this data, the SPO can be graphically constructed. Alternatively, changing material properties using appropriate nonlinear analysis software can be an effective approach.

- For various types of structures, the engineer needs to know how to estimate unloading and reloading global stiffness, and global hardening stiffness as a function of damage state. This report gives recommendations for steel moment frames. Alternatively the engineer can use nonlinear software with appropriate modifications to material properties to account for damage. This report gives an example of this approach, applicable to concrete wall buildings. As shown in Section 5, such analysis approaches need further calibration for degrading behavior modes such as shear failure in concrete walls.
- The engineer must account for the effect of residual deformation on the deformation capacity under subsequent shaking. Section 7.1 of this report gives an approximate approach that attempts to account for the key variables of hysteresis loop shape and strength degradation. Further research is recommended to assess the effects of residual deformation.
- Engineers may find a plot of  $S_d/S_{a10/50}$ , such as that shown in Figure 2.24, helpful as means for comparing the IDAs for different damage states on the same graph.

## REFERENCES

- ACI, 2005, *Building Code Requirements for Structural Concrete (ACI 318-05)*, American Concrete Institute, Detroit, Michigan.
- Anderson, J., 1995, "Post Earthquake Studies of a Damaged Low Rise Office Building," Technical Report SAC 95-07, SAC Joint Venture. Sacramento, CA, December.
- ATC 20, 1989, *Procedures for Postearthquake Safety Evaluation of Buildings*, Applied Technology Council (ATC), ATC: Redwood City, California.
- ATC 20-2, 1995, *Addendum to the ATC-20 Postearthquake Building Safety Evaluation Procedures*, Applied Technology Council (ATC), ATC: Redwood City, California.
- ATC, 1999a, *Evaluation of Earthquake Damaged Concrete and Masonry Wall Buildings, Basic Procedures Manual* prepared by the Applied Technology Council (ATC-43 project) for the Partnership for Response and Recovery, published by the Federal Emergency Management Agency, Report No. *FEMA 306*, Washington D.C.
- ATC, 1999b, *Evaluation of Earthquake Damaged Concrete and Masonry Wall Buildings, Technical Resources*, prepared by the Applied Technology Council (ATC-43 project) for the Partnership for Response and Recovery, published by the Federal Emergency Management Agency, Report No. *FEMA 307*, Washington D.C.
- ATC, 1999c, *Repair of Earthquake Damaged Concrete and Masonry Wall Buildings, Technical Resources*, prepared by the Applied Technology Council (ATC-43 project) for the Partnership for Response and Recovery, published by the Federal Emergency Management Agency, Report No. *FEMA 308*, Washington D.C.
- Barda F., Hanson J.W., and W.G. Corley, "Shear Strength of Low-Rise Walls with Boundary Elements," Research and Development Bulletin RD043.01D, preprinted with permission from ACI Symposium *Reinforced Concrete Structures in Seismic Zones*, American Concrete Institute, by Portland Cement Association, 1976.
- Bazzurro P., Cornell C.A., Menun C., Luco N., and M. Motahari, 2004, *Advanced Seismic Assessment Guidelines*, prepared for Pacific Gas and Electric/PEER, September.
- FEMA, 2000, *Prestandard and Commentary for the Seismic Rehabilitation of Buildings*, Report No. *FEMA 356*, Federal Emergency Management Agency, Washington, D.C., November.
- FIB, 2003, *Seismic Design of Precast Concrete Building Structures*, State-of-the-Art Report prepared by Task Group 7.3, International Federation for Structural Concrete (FIB), Lausanne, Switzerland, October.

- ICBO, 1997, *Uniform Building Code*, Volume 2, Structural Engineering Design Provisions, International Conference of Building Officials, Whittier, California.
- Luco N., Bazzurro P., and C.A. Cornell, 2004, "Dynamic Versus Static Computation of the Residual Capacity of a Mainshock-Damaged Building to Withstand an Aftershock," proceeding of the 13<sup>th</sup> World Conference on Earthquake Engineering, Vancouver, B.C., Canada, August.
- MacRae G.A., 1994, "P- $\Delta$  Effects on Single-Degree-of-Freedom Structures in Earthquakes," *Earthquake Spectra*, Volume 10, Issue 3, pp. 539-568, August.
- Park, R. and T. Paulay, 1975, *Reinforced Concrete Structures*, A Wiley-Interscience Publication, New York.
- Paulay, T. and M. J. N. Priestley, 1992, *Seismic Design of Reinforced Concrete and Masonry Buildings*, John Wiley and Sons, New York
- R&C and SGH, 2004, *Seismic Assessment of the Building Located at 111 Almaden Street, San Jose, California*, prepared for Pacific Gas and Electric Company, Rutherford & Chekene Consulting Engineers, Oakland CA, August.
- R&C, 2005a, *PG&E Vaca-Dixon Substation: Findings from Advanced Seismic Evaluation*, prepared for Pacific Gas and Electric Company, Rutherford & Chekene Consulting Engineers, Oakland CA, June.
- R&C, 2005b, *PG&E San Francisco Central Services Garage: Findings from Advanced Seismic Assessment and Conceptual Retrofit Design*, prepared for Pacific Gas and Electric Company, Rutherford & Chekene Consulting Engineers, Oakland CA, September.
- R&C, 2006a, *PG&E Larkin Substation: Advanced Seismic Assessment and Conceptual Retrofit Design*, prepared for Pacific Gas and Electric Company, Rutherford & Chekene Consulting Engineers, San Francisco CA, draft, April.
- R&C, 2006b, *PG&E Berkeley F Substation: Advanced Seismic Assessment and Conceptual Retrofit Design*, prepared for Pacific Gas and Electric Company, Rutherford & Chekene Consulting Engineers, San Francisco CA, in progress.
- Vamvatsikos, D. and C.A. Cornell, 2002, "Direct Estimation of the Seismic Demand and Capacity of Oscillators with Multi-Linear Static Pushovers through Incremental Dynamic Analysis" *Proceedings of the 7th National Conference on Earthquake Engineering*, Boston, July.



## PEER REPORTS

PEER reports are available from the National Information Service for Earthquake Engineering (NISEE). To order PEER reports, please contact the Pacific Earthquake Engineering Research Center, 1301 South 46<sup>th</sup> Street, Richmond, California 94804-4698. Tel.: (510) 665-3405; Fax: (510) 665-3420.

- PEER 2006/04** *Probabilistic Seismic Evaluation of Reinforced Concrete Structural Components and Systems.* Tae Hyung Lee and Khalid M. Mosalam. August 2006.
- PEER 2006/02** *Pacific Earthquake Engineering Research Center Highway Demonstration Project.* Anne Kiremidjian, James Moore, Yue Yue Fan, Nesrin Basoz, Ozgur Yazali, and Meredith Williams. April 2006.
- PEER 2006/01** *Bracing Berkeley. A Guide to Seismic Safety on the UC Berkeley Campus.* Mary C. Comerio, Stephen Tobriner, and Ariane Fehrenkamp. January 2006.
- PEER 2005/15** *CPT-Based Probabilistic Assessment of Seismic Soil Liquefaction Initiation.* R. E. S. Moss, R. B. Seed, R. E. Kayen, J. P. Stewart, and A. Der Kiureghian. April 2006.
- PEER 2005/14** *Workshop on Modeling of Nonlinear Cyclic Load-Deformation Behavior of Shallow Foundations.* Bruce L. Kutter, Geoffrey Martin, Tara Hutchinson, Chad Harden, Sivapalan Gajan, and Justin Phalen. March 2006.
- PEER 2005/13** *Stochastic Characterization and Decision Bases under Time-Dependent Aftershock Risk in Performance-Based Earthquake Engineering.* Gee Liek Yeo and C. Allin Cornell. July 2005.
- PEER 2005/12** *PEER Testbed Study on a Laboratory Building: Exercising Seismic Performance Assessment.* Mary C. Comerio, editor. November 2005.
- PEER 2005/11** *Van Nuys Hotel Building Testbed Report: Exercising Seismic Performance Assessment.* Helmut Krawinkler, editor. October 2005.
- PEER 2005/10** *First NEES/E-Defense Workshop on Collapse Simulation of Reinforced Concrete Building Structures.* September 2005.
- PEER 2005/09** *Test Applications of Advanced Seismic Assessment Guidelines.* Joe Maffei, Karl Telleen, Danya Mohr, William Holmes, and Yuki Nakayama. August 2006.
- PEER 2005/08** *Damage Accumulation in Lightly Confined Reinforced Concrete Bridge Columns.* R. Tyler Ranf, Jared M. Nelson, Zach Price, Marc O. Eberhard, and John F. Stanton. April 2006.
- PEER 2005/07** *Experimental and Analytical Studies on the Seismic Response of Freestanding and Anchored Laboratory Equipment.* Dimitrios Konstantinidis and Nicos Makris. January 2005.
- PEER 2005/06** *Global Collapse of Frame Structures under Seismic Excitations.* Luis F. Ibarra and Helmut Krawinkler. September 2005.
- PEER 2005/05** *Performance Characterization of Bench- and Shelf-Mounted Equipment.* Samit Ray Chaudhuri and Tara C. Hutchinson. May 2006.
- PEER 2005/04** *Numerical Modeling of the Nonlinear Cyclic Response of Shallow Foundations.* Chad Harden, Tara Hutchinson, Geoffrey R. Martin, and Bruce L. Kutter. August 2005.
- PEER 2005/03** *A Taxonomy of Building Components for Performance-Based Earthquake Engineering.* Keith A. Porter. September 2005.
- PEER 2005/02** *Fragility Basis for California Highway Overpass Bridge Seismic Decision Making.* Kevin R. Mackie and Bozidar Stojadinovic. June 2005.
- PEER 2005/01** *Empirical Characterization of Site Conditions on Strong Ground Motion.* Jonathan P. Stewart, Yoojoong Choi, and Robert W. Graves. June 2005.
- PEER 2004/09** *Electrical Substation Equipment Interaction: Experimental Rigid Conductor Studies.* Christopher Stearns and André Filiatrault. February 2005.
- PEER 2004/08** *Seismic Qualification and Fragility Testing of Line Break 550-kV Disconnect Switches.* Shakhzod M. Takhirov, Gregory L. Fenves, and Eric Fujisaki. January 2005.
- PEER 2004/07** *Ground Motions for Earthquake Simulator Qualification of Electrical Substation Equipment.* Shakhzod M. Takhirov, Gregory L. Fenves, Eric Fujisaki, and Don Clyde. January 2005.

- PEER 2004/06** *Performance-Based Regulation and Regulatory Regimes.* Peter J. May and Chris Koski. September 2004.
- PEER 2004/05** *Performance-Based Seismic Design Concepts and Implementation: Proceedings of an International Workshop.* Peter Fajfar and Helmut Krawinkler, editors. September 2004.
- PEER 2004/04** *Seismic Performance of an Instrumented Tilt-up Wall Building.* James C. Anderson and Vitelmo V. Bertero. July 2004.
- PEER 2004/03** *Evaluation and Application of Concrete Tilt-up Assessment Methodologies.* Timothy Graf and James O. Malley. October 2004.
- PEER 2004/02** *Analytical Investigations of New Methods for Reducing Residual Displacements of Reinforced Concrete Bridge Columns.* Junichi Sakai and Stephen A. Mahin. August 2004.
- PEER 2004/01** *Seismic Performance of Masonry Buildings and Design Implications.* Kerri Anne Taeko Tokoro, James C. Anderson, and Vitelmo V. Bertero. February 2004.
- PEER 2003/18** *Performance Models for Flexural Damage in Reinforced Concrete Columns.* Michael Berry and Marc Eberhard. August 2003.
- PEER 2003/17** *Predicting Earthquake Damage in Older Reinforced Concrete Beam-Column Joints.* Catherine Pagni and Laura Lowes. October 2004.
- PEER 2003/16** *Seismic Demands for Performance-Based Design of Bridges.* Kevin Mackie and Božidar Stojadinovic. August 2003.
- PEER 2003/15** *Seismic Demands for Nondeteriorating Frame Structures and Their Dependence on Ground Motions.* Ricardo Antonio Medina and Helmut Krawinkler. May 2004.
- PEER 2003/14** *Finite Element Reliability and Sensitivity Methods for Performance-Based Earthquake Engineering.* Terje Haukaas and Armen Der Kiureghian. April 2004.
- PEER 2003/13** *Effects of Connection Hysteretic Degradation on the Seismic Behavior of Steel Moment-Resisting Frames.* Janise E. Rodgers and Stephen A. Mahin. March 2004.
- PEER 2003/12** *Implementation Manual for the Seismic Protection of Laboratory Contents: Format and Case Studies.* William T. Holmes and Mary C. Comerio. October 2003.
- PEER 2003/11** *Fifth U.S.-Japan Workshop on Performance-Based Earthquake Engineering Methodology for Reinforced Concrete Building Structures.* February 2004.
- PEER 2003/10** *A Beam-Column Joint Model for Simulating the Earthquake Response of Reinforced Concrete Frames.* Laura N. Lowes, Nilanjan Mitra, and Arash Altoontash. February 2004.
- PEER 2003/09** *Sequencing Repairs after an Earthquake: An Economic Approach.* Marco Casari and Simon J. Wilkie. April 2004.
- PEER 2003/08** *A Technical Framework for Probability-Based Demand and Capacity Factor Design (DCFD) Seismic Formats.* Fatemeh Jalayer and C. Allin Cornell. November 2003.
- PEER 2003/07** *Uncertainty Specification and Propagation for Loss Estimation Using FOSM Methods.* Jack W. Baker and C. Allin Cornell. September 2003.
- PEER 2003/06** *Performance of Circular Reinforced Concrete Bridge Columns under Bidirectional Earthquake Loading.* Mahmoud M. Hachem, Stephen A. Mahin, and Jack P. Moehle. February 2003.
- PEER 2003/05** *Response Assessment for Building-Specific Loss Estimation.* Eduardo Miranda and Shahram Taghavi. September 2003.
- PEER 2003/04** *Experimental Assessment of Columns with Short Lap Splices Subjected to Cyclic Loads.* Murat Melek, John W. Wallace, and Joel Conte. April 2003.
- PEER 2003/03** *Probabilistic Response Assessment for Building-Specific Loss Estimation.* Eduardo Miranda and Hesameddin Aslani. September 2003.
- PEER 2003/02** *Software Framework for Collaborative Development of Nonlinear Dynamic Analysis Program.* Jun Peng and Kincho H. Law. September 2003.
- PEER 2003/01** *Shake Table Tests and Analytical Studies on the Gravity Load Collapse of Reinforced Concrete Frames.* Kenneth John Elwood and Jack P. Moehle. November 2003.

- PEER 2002/24** *Performance of Beam to Column Bridge Joints Subjected to a Large Velocity Pulse.* Natalie Gibson, André Filiatrault, and Scott A. Ashford. April 2002.
- PEER 2002/23** *Effects of Large Velocity Pulses on Reinforced Concrete Bridge Columns.* Greg L. Orozco and Scott A. Ashford. April 2002.
- PEER 2002/22** *Characterization of Large Velocity Pulses for Laboratory Testing.* Kenneth E. Cox and Scott A. Ashford. April 2002.
- PEER 2002/21** *Fourth U.S.-Japan Workshop on Performance-Based Earthquake Engineering Methodology for Reinforced Concrete Building Structures.* December 2002.
- PEER 2002/20** *Barriers to Adoption and Implementation of PBEE Innovations.* Peter J. May. August 2002.
- PEER 2002/19** *Economic-Engineered Integrated Models for Earthquakes: Socioeconomic Impacts.* Peter Gordon, James E. Moore II, and Harry W. Richardson. July 2002.
- PEER 2002/18** *Assessment of Reinforced Concrete Building Exterior Joints with Substandard Details.* Chris P. Pantelides, Jon Hansen, Justin Nadauld, and Lawrence D. Reaveley. May 2002.
- PEER 2002/17** *Structural Characterization and Seismic Response Analysis of a Highway Overcrossing Equipped with Elastomeric Bearings and Fluid Dampers: A Case Study.* Nicos Makris and Jian Zhang. November 2002.
- PEER 2002/16** *Estimation of Uncertainty in Geotechnical Properties for Performance-Based Earthquake Engineering.* Allen L. Jones, Steven L. Kramer, and Pedro Arduino. December 2002.
- PEER 2002/15** *Seismic Behavior of Bridge Columns Subjected to Various Loading Patterns.* Asadollah Esmaeily-Gh. and Yan Xiao. December 2002.
- PEER 2002/14** *Inelastic Seismic Response of Extended Pile Shaft Supported Bridge Structures.* T.C. Hutchinson, R.W. Boulanger, Y.H. Chai, and I.M. Idriss. December 2002.
- PEER 2002/13** *Probabilistic Models and Fragility Estimates for Bridge Components and Systems.* Paolo Gardoni, Armen Der Kiureghian, and Khalid M. Mosalam. June 2002.
- PEER 2002/12** *Effects of Fault Dip and Slip Rake on Near-Source Ground Motions: Why Chi-Chi Was a Relatively Mild M7.6 Earthquake.* Brad T. Aagaard, John F. Hall, and Thomas H. Heaton. December 2002.
- PEER 2002/11** *Analytical and Experimental Study of Fiber-Reinforced Strip Isolators.* James M. Kelly and Shakhzod M. Takhirov. September 2002.
- PEER 2002/10** *Centrifuge Modeling of Settlement and Lateral Spreading with Comparisons to Numerical Analyses.* Sivapalan Gajan and Bruce L. Kutter. January 2003.
- PEER 2002/09** *Documentation and Analysis of Field Case Histories of Seismic Compression during the 1994 Northridge, California, Earthquake.* Jonathan P. Stewart, Patrick M. Smith, Daniel H. Whang, and Jonathan D. Bray. October 2002.
- PEER 2002/08** *Component Testing, Stability Analysis and Characterization of Buckling-Restrained Unbonded Braces™.* Cameron Black, Nicos Makris, and Ian Aiken. September 2002.
- PEER 2002/07** *Seismic Performance of Pile-Wharf Connections.* Charles W. Roeder, Robert Graff, Jennifer Soderstrom, and Jun Han Yoo. December 2001.
- PEER 2002/06** *The Use of Benefit-Cost Analysis for Evaluation of Performance-Based Earthquake Engineering Decisions.* Richard O. Zerbe and Anthony Falit-Baiamonte. September 2001.
- PEER 2002/05** *Guidelines, Specifications, and Seismic Performance Characterization of Nonstructural Building Components and Equipment.* André Filiatrault, Constantin Christopoulos, and Christopher Stearns. September 2001.
- PEER 2002/04** *Consortium of Organizations for Strong-Motion Observation Systems and the Pacific Earthquake Engineering Research Center Lifelines Program: Invited Workshop on Archiving and Web Dissemination of Geotechnical Data, 4–5 October 2001.* September 2002.
- PEER 2002/03** *Investigation of Sensitivity of Building Loss Estimates to Major Uncertain Variables for the Van Nuys Testbed.* Keith A. Porter, James L. Beck, and Rustem V. Shaikhutdinov. August 2002.
- PEER 2002/02** *The Third U.S.-Japan Workshop on Performance-Based Earthquake Engineering Methodology for Reinforced Concrete Building Structures.* July 2002.

- PEER 2002/01** *Nonstructural Loss Estimation: The UC Berkeley Case Study.* Mary C. Comerio and John C. Stallmeyer. December 2001.
- PEER 2001/16** *Statistics of SDF-System Estimate of Roof Displacement for Pushover Analysis of Buildings.* Anil K. Chopra, Rakesh K. Goel, and Chatpan Chintanapakdee. December 2001.
- PEER 2001/15** *Damage to Bridges during the 2001 Nisqually Earthquake.* R. Tyler Ranf, Marc O. Eberhard, and Michael P. Berry. November 2001.
- PEER 2001/14** *Rocking Response of Equipment Anchored to a Base Foundation.* Nicos Makris and Cameron J. Black. September 2001.
- PEER 2001/13** *Modeling Soil Liquefaction Hazards for Performance-Based Earthquake Engineering.* Steven L. Kramer and Ahmed-W. Elgamal. February 2001.
- PEER 2001/12** *Development of Geotechnical Capabilities in OpenSees.* Boris Jeremi . September 2001.
- PEER 2001/11** *Analytical and Experimental Study of Fiber-Reinforced Elastomeric Isolators.* James M. Kelly and Shakhzod M. Takhirov. September 2001.
- PEER 2001/10** *Amplification Factors for Spectral Acceleration in Active Regions.* Jonathan P. Stewart, Andrew H. Liu, Yoojoong Choi, and Mehmet B. Baturay. December 2001.
- PEER 2001/09** *Ground Motion Evaluation Procedures for Performance-Based Design.* Jonathan P. Stewart, Shyh-Jeng Chiou, Jonathan D. Bray, Robert W. Graves, Paul G. Somerville, and Norman A. Abrahamson. September 2001.
- PEER 2001/08** *Experimental and Computational Evaluation of Reinforced Concrete Bridge Beam-Column Connections for Seismic Performance.* Clay J. Naito, Jack P. Moehle, and Khalid M. Mosalam. November 2001.
- PEER 2001/07** *The Rocking Spectrum and the Shortcomings of Design Guidelines.* Nicos Makris and Dimitrios Konstantinidis. August 2001.
- PEER 2001/06** *Development of an Electrical Substation Equipment Performance Database for Evaluation of Equipment Fragilities.* Thalia Agnanos. April 1999.
- PEER 2001/05** *Stiffness Analysis of Fiber-Reinforced Elastomeric Isolators.* Hsiang-Chuan Tsai and James M. Kelly. May 2001.
- PEER 2001/04** *Organizational and Societal Considerations for Performance-Based Earthquake Engineering.* Peter J. May. April 2001.
- PEER 2001/03** *A Modal Pushover Analysis Procedure to Estimate Seismic Demands for Buildings: Theory and Preliminary Evaluation.* Anil K. Chopra and Rakesh K. Goel. January 2001.
- PEER 2001/02** *Seismic Response Analysis of Highway Overcrossings Including Soil-Structure Interaction.* Jian Zhang and Nicos Makris. March 2001.
- PEER 2001/01** *Experimental Study of Large Seismic Steel Beam-to-Column Connections.* Egor P. Popov and Shakhzod M. Takhirov. November 2000.
- PEER 2000/10** *The Second U.S.-Japan Workshop on Performance-Based Earthquake Engineering Methodology for Reinforced Concrete Building Structures.* March 2000.
- PEER 2000/09** *Structural Engineering Reconnaissance of the August 17, 1999 Earthquake: Kocaeli (Izmit), Turkey.* Halil Sezen, Kenneth J. Elwood, Andrew S. Whittaker, Khalid Mosalam, John J. Wallace, and John F. Stanton. December 2000.
- PEER 2000/08** *Behavior of Reinforced Concrete Bridge Columns Having Varying Aspect Ratios and Varying Lengths of Confinement.* Anthony J. Calderone, Dawn E. Lehman, and Jack P. Moehle. January 2001.
- PEER 2000/07** *Cover-Plate and Flange-Plate Reinforced Steel Moment-Resisting Connections.* Taejin Kim, Andrew S. Whittaker, Amir S. Gilani, Vitelmo V. Bertero, and Shakhzod M. Takhirov. September 2000.
- PEER 2000/06** *Seismic Evaluation and Analysis of 230-kV Disconnect Switches.* Amir S. J. Gilani, Andrew S. Whittaker, Gregory L. Fenves, Chun-Hao Chen, Henry Ho, and Eric Fujisaki. July 2000.
- PEER 2000/05** *Performance-Based Evaluation of Exterior Reinforced Concrete Building Joints for Seismic Excitation.* Chandra Clyde, Chris P. Pantelides, and Lawrence D. Reaveley. July 2000.
- PEER 2000/04** *An Evaluation of Seismic Energy Demand: An Attenuation Approach.* Chung-Che Chou and Chia-Ming Uang. July 1999.

- PEER 2000/03** *Framing Earthquake Retrofitting Decisions: The Case of Hillside Homes in Los Angeles.* Detlof von Winterfeldt, Nels Roselund, and Alicia Kitsuse. March 2000.
- PEER 2000/02** *U.S.-Japan Workshop on the Effects of Near-Field Earthquake Shaking.* Andrew Whittaker, ed. July 2000.
- PEER 2000/01** *Further Studies on Seismic Interaction in Interconnected Electrical Substation Equipment.* Armen Der Kiureghian, Kee-Jeung Hong, and Jerome L. Sackman. November 1999.
- PEER 1999/14** *Seismic Evaluation and Retrofit of 230-kV Porcelain Transformer Bushings.* Amir S. Gilani, Andrew S. Whittaker, Gregory L. Fenves, and Eric Fujisaki. December 1999.
- PEER 1999/13** *Building Vulnerability Studies: Modeling and Evaluation of Tilt-up and Steel Reinforced Concrete Buildings.* John W. Wallace, Jonathan P. Stewart, and Andrew S. Whittaker, editors. December 1999.
- PEER 1999/12** *Rehabilitation of Nonductile RC Frame Building Using Encasement Plates and Energy-Dissipating Devices.* Mehrdad Sasaki, Vitelmo V. Bertero, James C. Anderson. December 1999.
- PEER 1999/11** *Performance Evaluation Database for Concrete Bridge Components and Systems under Simulated Seismic Loads.* Yael D. Hose and Frieder Seible. November 1999.
- PEER 1999/10** *U.S.-Japan Workshop on Performance-Based Earthquake Engineering Methodology for Reinforced Concrete Building Structures.* December 1999.
- PEER 1999/09** *Performance Improvement of Long Period Building Structures Subjected to Severe Pulse-Type Ground Motions.* James C. Anderson, Vitelmo V. Bertero, and Raul Bertero. October 1999.
- PEER 1999/08** *Envelopes for Seismic Response Vectors.* Charles Menun and Armen Der Kiureghian. July 1999.
- PEER 1999/07** *Documentation of Strengths and Weaknesses of Current Computer Analysis Methods for Seismic Performance of Reinforced Concrete Members.* William F. Cofer. November 1999.
- PEER 1999/06** *Rocking Response and Overturning of Anchored Equipment under Seismic Excitations.* Nicos Makris and Jian Zhang. November 1999.
- PEER 1999/05** *Seismic Evaluation of 550 kV Porcelain Transformer Bushings.* Amir S. Gilani, Andrew S. Whittaker, Gregory L. Fenves, and Eric Fujisaki. October 1999.
- PEER 1999/04** *Adoption and Enforcement of Earthquake Risk-Reduction Measures.* Peter J. May, Raymond J. Burby, T. Jens Feeley, and Robert Wood.
- PEER 1999/03** *Task 3 Characterization of Site Response General Site Categories.* Adrian Rodriguez-Marek, Jonathan D. Bray, and Norman Abrahamson. February 1999.
- PEER 1999/02** *Capacity-Demand-Diagram Methods for Estimating Seismic Deformation of Inelastic Structures: SDF Systems.* Anil K. Chopra and Rakesh Goel. April 1999.
- PEER 1999/01** *Interaction in Interconnected Electrical Substation Equipment Subjected to Earthquake Ground Motions.* Armen Der Kiureghian, Jerome L. Sackman, and Kee-Jeung Hong. February 1999.
- PEER 1998/08** *Behavior and Failure Analysis of a Multiple-Frame Highway Bridge in the 1994 Northridge Earthquake.* Gregory L. Fenves and Michael Ellery. December 1998.
- PEER 1998/07** *Empirical Evaluation of Inertial Soil-Structure Interaction Effects.* Jonathan P. Stewart, Raymond B. Seed, and Gregory L. Fenves. November 1998.
- PEER 1998/06** *Effect of Damping Mechanisms on the Response of Seismic Isolated Structures.* Nicos Makris and Shih-Po Chang. November 1998.
- PEER 1998/05** *Rocking Response and Overturning of Equipment under Horizontal Pulse-Type Motions.* Nicos Makris and Yiannis Roussos. October 1998.
- PEER 1998/04** *Pacific Earthquake Engineering Research Invitational Workshop Proceedings, May 14-15, 1998: Defining the Links between Planning, Policy Analysis, Economics and Earthquake Engineering.* Mary Comerio and Peter Gordon. September 1998.
- PEER 1998/03** *Repair/Upgrade Procedures for Welded Beam to Column Connections.* James C. Anderson and Xiaojing Duan. May 1998.
- PEER 1998/02** *Seismic Evaluation of 196 kV Porcelain Transformer Bushings.* Amir S. Gilani, Juan W. Chavez, Gregory L. Fenves, and Andrew S. Whittaker. May 1998.

**PEER 1998/01** *Seismic Performance of Well-Confined Concrete Bridge Columns.* Dawn E. Lehman and Jack P. Moehle.  
December 2000.